University of Alberta

NUCLEAR POSITIONING OF TRANSLOCATION-PRONE GENE LOCI IN PATIENTS WITH MULTIPLE MYELOMA

by

Lorri Darlene Martin

A thesis submitted to the Faculty of Graduate Studies and Research
in partial fulfillment of the requirements for the degree of

Doctor of Philosophy

in Experimental Oncology

Department of Oncology

Fall 2011

Edmonton, Alberta.

Your file Votre référence
ISBN: 978-0-494-81253-2
Our file Notre référence
ISBN: 978-0-494-81253-2

Dedication

The dedication of this work is two-fold.

I dedicate this work to the memory of my father,

William George Young (1938-2005).

He instilled in me his love for all things wild, introduced me to the thrill of discovery, and taught me that the view is always worth the climb. When I embarked on this journey, I never imagined that I would not have you here beside me to share in the celebration if its completion.

I dedicate this work with all my love and my deepest gratitude

to my husband and my best friend,

Brian Kirk Martin.

You are my *one true thing.*

Abstract

Accumulating evidence suggests that the non-random nature of spatial genome organization contributes to the formation of chromosomal translocations; specifically, that spatial proximity of potential translocation partners influences translocation potential. Purified subpopulations of non-malignant cells from affected patients have not been studied, or compared to sorted subsets from healthy donors (HD). Proximity of loci in patient-derived normal cells may closely reflect loci positioning for the original cell in which the translocation initially formed, and may favour translocations between proximal loci in a patient-specific manner. In multiple myeloma (MM), recurrent translocations in plasma cells (PC) involve *IGH* and *FGFR3* t(4;14) or *CCND1* t(11;14), or less frequently *c-MAF* t(14;16). Utilizing 3-D FISH and 3-D analysis techniques, we analyzed the radial and relative positioning of translocation-prone and control loci in the nuclei of hematopoietic progenitor cells (HPC) and B-

cells from patients with MM and from HD. The radial and relative positioning was not different among HD HPC, HD B-cells, and HPC from MM patients. On average, in all subsets, *IGH*, *FGFR3*, and *CCND1* are centrally located in the nucleus, while *c-MAF* occupies a more peripheral position. In non-malignant B-cells from t(4;14) and t(11;14) patients, *IGH* and *FGFR3*, or *IGH* and *CCND1* are preferentially positioned in spatial proximity: *IGH* and *c-MAF* are not. This pattern of positioning differs in B-cells from t(14;16) patients or HD: *IGH* is equivalently distal to *FGFR3*, *CCND1*, *c-MAF*, and the control locus, *TGFBR2*. Our results suggest that spatial proximity and radial position in the nucleus influence translocation potential of specific loci, and are specific to some patient subsets. Furthermore, *FGFR3*, and *CCND1* frequently position outside their respective chromosome territories (CTs), but *c-MAF* rarely does. The frequency of extra-territorial positioning (ETP) reflects the clinical frequencies in MM and suggests that ETP may influence translocation

potential. Furthermore, extra-territorial *FGFR3*, and *CCND1* occasionally co-localize with *IGH*. The finding that some translocation-prone gene loci (TPGL) frequently extend beyond their CTs, provides evidence for a previously undocumented mechanism that brings TPGL from different chromosomes into spatial proximity with one another.

Acknowledgements

This work would not have been possible without the guidance, support, and/or assistance of several individuals.

First and foremost, I would like to express my immense gratitude to and my deepest respect for my supervisor and mentor, Dr. Linda Pilarski. Thank you for believing in this project and for your support and enthusiasm as it progressed. You provided a safe and nurturing environment in which to learn to "do science" and then challenged me to "do it" to the best of my abilities. Thank you for providing me with a wonderful role model. I continue to be amazed by your energy, insight, generosity, tenacious spirit, and your capacity to retain enormous amounts of information!

I would like to express a special thank-you to Dr. Andy Belch, our colleague and collaborator. You were a staunch supporter of this work, providing not only uplifting encouragement, but also insightful critical analysis.

I extend my gratitude to our Winnipeg collaborator, Dr. Sabine Mai. Thank you Dr. Mai, for welcoming me into your lab and revealing to me the world of 3-D FISH. Thanks for providing the 3-D analysis software, *Chromoview*, which was vital to this project. Thank-you to Dr. Jana Harizanova, post-doctoral fellow in the Mai Lab and the developer of *Chromoview*, for specifically "tweaking" the program to meet the demands of this study, and for teaching me to use it.

I would like to thank my supervisory committee members, Dr. Mary Hitt and Dr. Heather McDermid, for your support and suggestions over the course of this work.

A big thank-you to Dr. Xuejun Sun for your expert advice and direction on all things confocal. Many of our conversations began with "Sun, do you think I can do this...?", and you would find a way in which I could.

I would like to thank Eva Baigorri, Amanda Warkentin, and Sarah Motz for your expert technical assistance and support in the Pilarski Lab. It was greatly appreciated.

As with many thesis projects, much of this work was spent in the dark, however, I wasn't alone, thanks to two wonderful individuals. Thank you Carina Debes-Marun for sharing the darkness and introducing me to many FISH-y things in the "cave". And thank-you to Gerry Barron, for your expert assistance with the confocal microscope over many dark (cold) hours in the Imaging Facility. Thank-you both for your friendship, and for your many words of encouragement.

Thank-you to George Zhu and Christiaan Righolt for your expert statistical analysis.

My family provided much support and love throughout this process. I want to thank my sons Britt and Brent (and TJ) for understanding when I couldn't attend your motocross races or hockey games. The three of you grew into wonderful young men as this work grew to completion.

I would like to thank my mother, Darlene Young. Thanks Mom, for providing love and encouragement, and for lending a sympathetic ear from 900 km away.

Lastly, I cannot begin to thank my silent and long-suffering collaborator (and husband) Brian, for the role you played to ensure that this work was finished. It is now complete; the house is still intact, the boys are OK, and we have survived. Thank you for your encouragement and unending support that allowed me to realize a dream that was mine alone. The finished product, however, belongs to both of us.

Table of Contents

List of Tables

List of Figures

List of Abbreviations

ABL	Abelson murine leukemia viral oncogene homolog
AID	activation-induced cytidine deaminase
APE-1	Apurinic/apyrimidinic endonuclease 1
AGD	average intergene distance
BAC	bacterial artificial chromosome
BCL2	B-cell CLL/lymphoma2
BCR	breakpoint cluster region
BCR-ABL	breakpoint cluster region-Abelson murine leukemia viral oncogene homolog 1 fusion
BER	break excision repair
BM	bone marrow
CDKN2A	cyclin-dependent kinase inhibitor 2A
CDKN2C	cyclin-dependent kinase inhibitor 2C
CCND1	cyclin D1
CCND3	cyclin D3
CLL	chronic lymphocytic leukemia
c-MAF	v-maf musculoaponeurotic fibrosarcoma oncogene homolog
Ch	chromosome
CpG	C phosphate G
CSR	class switch recombination
CT	chromosome territory
CTs	chromosome territories
der	derivative
D_H	diversity segment (immunoglobulin heavy chain)
D_{JH}	diversity joining segment (immunoglobulin heavy chain)
DNA	deoxyribonucleic acid
DNA-PKcs	DNA dependent protein kinase catalytic subunit

DSB	double strand break
E2A	transcription factor 3 (E-box binding protein 2A)
EBF1	early B-cell factor 1
ETP	extra-territorial positioning
FGFR3	fibroblast growth factor receptor 3
FISH	fluorescent in situ hybridization
FRA16	common fragile site 16
GCs	germinal centers
H2AX	H2A histone family, member X
HMCL	human myeloma cell lines
hMLH1	mutL homolog 1, colon cancer, nonpolyposis type 2
HD	healthy donor
HPC	hematopoietic progenitor cells
HR	homologous recombination
Ig	immunoglobulin
IGH	immunoglobulin heavy chain
IGK	immunoglobulin kappa chain
IGL	immunoglobulin light chain
IGV	immunoglobulin variable region
J_H	joining segment (immunoglobulin heavy chain)
kb	kilobase
KRAS	v-Ki-ras2 Kirsten rat sarcoma viral oncogene homolog
MAFB	v-maf musculoaponeurotic fibrosarcoma oncogene homolog B
MB	mobilized blood
MGUS	monoclonal gammopathy of undetermined significance
MM	multiple myeloma
MMR	mis-match repair
MMSET	multiple myeloma SET domain containing protein
MTC	major translocation cluster

MYC	v-myc myelocytomatosis viral oncogene homolog
MYEOV	myeloma overexpressed [in a subset of t(11;14)
positive	multiple myeloma]
NRAS	neuroblastoma RAS viral (v-ras) oncogene homolog
OCAB	POU2AF1: POU class 2 associating factor 1
PAX	paired box
PB	peripheral blood
PBMC	peripheral blood mononuclear cells
PCL	plasma cell leukemia
PC	plasma cells
PIM-1	pim-1 oncogene
PML	promyelocytic leukemia
PTEN	phosphatase and tensin homolog
RAG-1	recombinase-activating gene 1
RAG-2	recombinase-activating gene 2
RARα	retinoic acid receptor alpha
RB	retinoblastoma
RHOH	ras homolog gene family, member H
RNA	ribonucleic acid
RSS	recombination signal sequences
S	switch
Sα	switch region alpha
Sγ	switch region gamma
Sμ	switch region mu
SHM	somatic hypermutation
TGFBR2	transforming growth factor, beta receptor II
TP53	tumour protein p53
TPGL	translocation-prone gene loci
UNG	uracil DNA glycosylase
V(D)J	variable, diversity, joining

Chapter One: INTRODUCTION

Parts of this introduction (including Figure 1.2) have been published. Martin LD, Belch AR, Pilarski LM. Promiscuity of translocation partners in multiple myeloma. J Cellular Biochemistry. 109(6):1085-94, 2010.

The paper was written by L.D. Martin.

1.1 CHROMOSOMAL TRANSLOCATIONS AND CANCER

A chromosome translocation involves the exchange or rearrangement of chromosome segments between two non-homologous chromosomes. As a result, translocations generate novel chromosomes, known as derivative chromosomes (der). Chromosomal translocations may be reciprocal or non-reciprocal. A reciprocal translocation occurs when parts of two chromosomes are interchanged. A non-reciprocal or *Robertsonian* translocation occurs when the q arms of two acrocentric chromosomes fuse together at a single centromere. The presence of translocated chromosomes in tumor cells was first documented by the Theodor Boveri, who postulated that the unlimited growth in malignant cells was attributable to the presence of these abnormal chromosomes[1]. The majority of chromosomal translocations are evident in hematological malignancies (75%), but they are also present in solid tumours, such as sarcomas and carcinomas (reviewed by[2]).

The consequence of specific chromosome translocations in cancer is often the deregulation or disruption of normal gene function, as chromosome

breakpoints disrupt gene coding sequences or their regulatory components. Two kinds of molecular arrangements have been linked to malignant transformation. Chromosomal translocations can result in the juxtaposition of the promoter/enhancer region of a gene on one chromosome to the coding region of a different gene on a second chromosome, resulting in increased expression of the latter gene. This type of translocation was first described in B-cells from patients with Burkitt's lymphoma, where the translocation involving chromosomes 8 and 14 places the *MYC* oncogene under the control of the immunoglobulin heavy chain (*IGH*) promoter. Alternatively, oncogenic translocations may fuse the coding regions of two genes together to create a chimeric or fusion gene. The first example of this molecular rearrangement was the fusion of the BCR and ABL genes in chronic myelogenous leukemia caused by t(9;22).

1.2 FORMATION OF CHROMOSOMAL TRANSLOCATIONS

The formation of a chromosomal translocation is a multi-step process. A specific translocation requires that three events occur: (i) simultaneous

formation of DNA double strand breaks (DSBs) in specific potential partner loci, (ii) proximal arrangement of DNA broken ends of the partner loci, and (iii) illegitimate joining of the heterologous broken ends[3,4]. The sequence of the first two steps is controversial, as the mechanism by which the broken ends of chromosomes at specific loci come into contact in the nucleus of the cell is not clear. Currently, two hypotheses exist: the "contact-first" model suggests that the interaction of two loci on different chromosomes is the initial step required to produce translocations, and that DNA breakage is a subsequent event[5]. Conversely, the "breakage-first" model proposes that DSBs at specific loci on different chromosomes form at distant sites and that the broken DNA ends can roam the nuclear space to "find" potential partners for translocations[6]. In support of the "contact-first" model, it has recently been demonstrated that the DNA ends at DSBs remain positionally immobile[7], supporting the idea that translocation-prone loci pairs must be in close proximity to undergo translocations.

1.3 NON-RANDOM GENOME ORGANIZATION OF THE INTERPHASE NUCLEUS

1.3.1 Genome positioning in the interphase nucleus

Chromosomes are visible as distinct entities during mitosis. During the formation of the interphase nucleus in higher organisms, each chromosome decondenses. It was first postulated by Karl Rabl in 1885, and later in 1909 by Theodor Boveri that chromosomes in the interphase nucleus occupied distinct territories. This view fell from grace and the prevailing model suggested that the chromosomes decondensed in chromatin threads expanding throughout the entire nuclear space, similar to an enclosed bowl of spaghetti. Microirradiation studies by Cremer and Cremer in 1985 provided evidence that each chromosome occupies a distinct, spatially-limited space, known as a chromosome territory (reviewed by[8]). Fluorescence *in situ* hybridization (FISH) with whole chromosome paints confirmed the existence of unique chromosomal territories (CTs) in the interphase nuclei of higher organisms[9-11]. The spatial organization of both chromosomes and genetic loci is not random, and can be described by their average radial positioning relative to the

center of the nucleus[10-13]. It is generally assumed that the periphery of the nucleus is a transcriptionally inactive area; conversely, the interior of the nucleus is a transcriptionally active area (reviewed by [14]).

1.3.2 Non-random spatial positioning of chromosomes

The radial CT positions within the interphase nucleus correlate with chromosome size as well as with gene density. In human fibroblasts, large chromosomes preferentially localize to the nuclear periphery, while smaller chromosomes localize more centrally, but this phenomenon is not as pronounced in non-adherent cells[15]. In both cell types, gene-rich chromosomes adopt a more central location in the cell nucleus, while gene-poor chromosomes are more peripherally located[16]. In addition, gene-rich and gene-poor regions within individual chromosomes cluster to specific areas within the CT boundary, with gene-rich areas closer to the nuclear center and gene-poor areas closer to the periphery[17,18]. Radial CT positioning according to gene density is evolutionarily conserved in primates[19,20], mice[15], and chickens[21], suggesting a functional role for chromosome positioning in vertebrates[11].

Chromosome positioning is not exclusively characterized by gene density and chromosome size. Proliferation[22,23], differentiation[15,24,25], and tissue-specificity[15,26] have each been shown to influence CT positioning. While gene density and chromosome size remain the same, these examples vary with regard to their gene expression profiles, further suggesting that functional status of each chromosome also plays a part in its positioning[27]. The obvious function would be control of gene expression (reviewed by [28]).

1.3.3 Non-random spatial positioning of genes

Genes are also non-randomly positioned within the nucleus during interphase[29,30]. The localization of various genes is not static, and is dependent upon activity and level of gene expression. Generally, transcriptionally active genes are more internally localized, while inactive genes are more externally located (reviewed by [27,31]). For example, *IGH* and *CD4* localize internally in their active state, and to the nuclear periphery in their inactive state[24,32,33]. *IGH* allelic exclusion, which takes place during B-cell development, results in the unrearranged allele moving to an area of centromeric heterochromatin[34]. In resting splenic B-cells,

mono-allelic recruitment to centromeric heterochromatin also takes place, however, transcriptional silencing is controversial[33] .

In addition to possessing preferred positions within the nucleus, genes also localize to favored locations within their respective CT. Genes have been shown to "loop out" of their respective chromosome territory, correlating with local gene density and transcription[35,36]. It has been postulated that specific positioning of a gene in the cell nucleus is not essential to its function, but contributes to optimizing its activity (reviewed by [37]).

1.4 SPATIAL PROXIMITY OF GENE LOCI AND CONSEQUENCES FOR THE FORMATION OF CHROMOSOMAL TRANSLOCATIONS

A large body of evidence suggests that the non-random nature of genome organization in the interphase nucleus contributes to the formation of chromosomal translocations. Several studies utilizing various models indicate that spatial proximity of potential translocation partners influences translocation potential. Chromosomes 12, 14, and 15 participate in

various combinations of translocations in murine lymphomas[38]. Positional mapping of these chromosomes in the interphase nucleus of normal murine lymphocytes revealed spatial proximity in non-random clusters[39]. A similar study of normal mouse hepatocytes reported spatial proximity of chromosomes 5 and 6, which are translocated in murine hepatomas[26]. The clinical frequency that *MYC* is involved in translocations with three potential partners correlates with spatial proximity to *MYC* in a normal B-cell line[29].

Spatial proximity of translocation partners has been shown to vary among different tissues, and vary among cells at different stages of differentiation. In murine models, chromosomes 12 and 15, which participate in translocations in lymphoma, are frequently found in close proximity in lymphocytes, but not in hepatocytes where they do not translocate[38]. Chromosomes 5 and 6, which frequently translocate in murine hepatomas and are spatially proximal in hepatocytes, are not proximal in lymphocytes[26]. The genes PML and RARα which participate in t(15;17) of acute promyelocytic leukemia and the genes ABL and BCR, which participate in t(9;22) of chronic myelogenous leukemia, demonstrate

spatial proximity in a heterogenous population of hematopoietic precursors more frequently than they do in differentiated lymphocytes[40].

1.5 MULTIPLE MYELOMA: PATHOLOGY AND EPIDEMIOLOGY

MM is a fatal, malignant tumor of terminally differentiated B-lineage hematopoietic cells. The pathology of the disease is mediated by the infiltration and clonal expansion of malignant plasma cells (PC) in the bone marrow (BM). The replacement of normal BM cells by malignant PC results in anemia, cytopenia, and subsequent immune failure. The abnormal accumulation of PC is associated with the production of monoclonal immunoglobulin (Ig) that is detectable in the serum and urine and can lead to renal failure. Hypercalcemia, osteoporosis, fractures, spinal cord compression, and painful osteolytic bone lesions are direct consequences of the interaction of malignant PC with the bone marrow microenvironment (reviewed by [41]). The development of MM in a patient is believed to be a multi-step process, whereby MM is preceded by a premalignant condition known as monoclonal gammopathy of undetermined significance (MGUS), progressing to smouldering MM, and

ultimately to intramedullary MM and finally in many patients, to plasma cell leukemia[42]. MGUS is present in 1% of adults, and progresses to malignant MM at a rate of 1% per year[42].

Canadian Cancer Statistics 2010 estimates that the total new cases of multiple myeloma in Canada in 2010 is 2,300 (males 1250; females 1000)[43]. This represents 1.8% of the total new cases of cancer in women, and 1.2% of the total new cases of cancer in men. It is estimated that 650 women and 780 men will die from MM in Canada in 2010. Median survival following the conventional combination therapy of melphalan and prednisone is 3-4 years. The current front-line treatment of MM involves new biological modifiers (e.g. bortezomib, lenalidomide) followed by autologous stem cell transplant, but despite various treatment regimens and development of new therapeutic agents, only 10% of patients remain alive 10 years after diagnosis. MM is a disease of older adults. The average age of onset is 68 years, and only 1% of newly diagnosed cases involve individuals under the age of forty[44].

MM tumor cells can be identified by a mutated V(D)J, immunoglobulin heavy chain (*IGH*) gene rearrangement which provides a clonal molecular

signature[45,46]. The involvement of B-cell progenitors and earlier stage cells in MM has been documented by molecular, phenotypic and functional studies, with the rearranged *IGH* variable, diversity, and joining [V(D)J] genes providing a unique clonal marker to identify cells within the myeloma clone[47-52]. A considerable body of evidence implicates B-cells as generative compartments of the multiple myeloma clone cell[49,50,52-54], including a 3-D culture model of reconstructed bone marrow which suggests that the malignant clone in multiple myeloma arises from a CD20+ B-cell[51].

1.6 CYTOGENETIC ABNORMALITIES IN MULTIPLE MYELOMA

MM is characterized by karyotypic instability, resulting in a highly heterogeneous group of cytogenetic abnormalities in tumor cells. MM can be categorized into two distinct groups according to abnormalities in the number of chromosomes present in malignant cells: hyperdiploid and non-hyperdiploid[55]. Malignant cells in the non-hyperdiploid category that also display t(4;14), complete or partial loss of chromosome 13, and partial loss of chromosome 17 (p53) are associated with reduced life span[56].

Conversely, MM cells categorized as hyperdiploid (characterized by multiple trisomies of chromosomes 3, 5, 7, 9, 11, 15, and 19), or cells that demonstrate t(11;14) are associated with longer survival times[56].

Abnormal genetic events in the progression of MM are considered to be primary, early onset events (such as translocations involving the *IGH* locus), or secondary, late onset events[57]. Secondary events include complex translocations involving *MYC*, activation of *NRAS* and *KRAS*, mutations and deletions of *TP53*, *RB*, and *PTEN*, and inactivation of *CDKN2A* and *CDKN2C*.

1.7 *IGH* TRANSLOCATIONS IN MULTIPLE MYELOMA

Chromosomal translocations in MM most frequently involve the *IGH* locus at 14q32, as with many B-cell malignancies[58,](reviewed by [59]). Translocations involving the *IGH* locus are present in 60% of PC from MM patients, and in 90% of human myeloma cell lines (HMCL), suggesting that the prevalence of *IGH* translocations may increase with disease progression.

The effect of the resulting translocation is likely to be deregulation (increased expression in the case of MM) of an oncogene, as it is repositioned near one or more of the strong *IGH* enhancers (reviewed by [42]). Whereas many other B-cell malignancies harbor a single, specific *IGH* translocation partner (reviewed by [60]), myeloma cells display a promiscuity of translocation partners. There are five primary recurrent partner loci harboring the following oncogenes, with the indicated approximate frequencies:

- 4p16 (*MMSET* and usually *FGFR3*) 15-20%
- 6p21 (*CCND3*) 3%
- 11q13 (*CCND1*) 20%
- 16q23 (*c-MAF*) 5%
- 20q12(*MAF-B*) 2%.

The biology and clinical implications of the three most common translocations [t(4;14), t(11;14), and t(14;16)] will be discussed. The chromosome locations of the four involved loci are depicted in Figure 1-1.

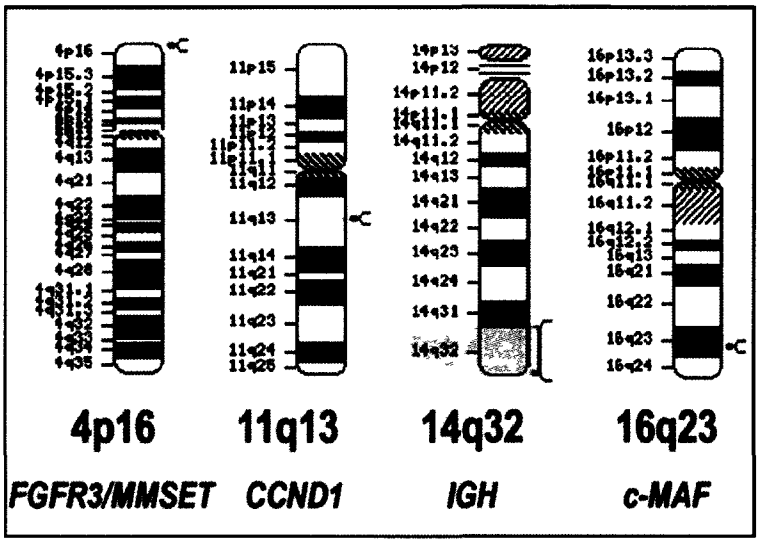

Figure 1-1: Chromosome locations of the translocation-prone gene loci (TPGL) involved in the three most common MM *IGH* translocations. Ideograms sourced from: http://www.ncbi.nlm.nih.gov/projects/mapview/

1.7.1 t(4;14)

The fusion products of chromosomes 4 and 14 results in overexpression of *MMSET* and *FGFR3*. *MMSET* is upregulated on der(4) through the action of the *IGH* enhancer Eμ. *MMSET* is a histone methyltransferase, and recent studies demonstrate that it is a major epigenetic regulator in t(4;14) MM. Loss of *MMSET* expression suppresses cell growth,

decreases adhesion, and induces apoptosis [61]. Upregulation of *FGFR3* on der(14), is driven by *IGH* 3' Eα enhancer. *FGFR3* is a high-affinity tyrosine receptor kinase which activates the anti-apoptotic STAT-3 signalling pathway. Inhibition of *FGFR3* by small molecules results in tumour cell growth arrest and apoptosis. Approximately 25% of patient samples, however, do not express *FGFR3* presumably due to a loss of der(14) [62], suggesting that overexpression of *MMSET* may be the transforming event in t(4;14). Presence of the t(4;14) translocation in patients predicts for a poor response to first-line chemotherapy and poor survival, irrespective of *FGFR3* expression [62].

1.7.2 t(11;14)

The t(11;14) translocation juxtaposes one of the *IGH* enhancers from chromosome 14 to *CCND1* from chromosome 11, resulting in dysregulation of *CCND1*. The oncogenic role of *CCND1* in MM is unclear as MM cells overexpressing *CCND1* do not display increased proliferation over non-expressing cells[63]. Patients with t(11;14) experience a longer survival relative to patients with t(4;14)[64].

1.7.3 t(14;16)

The consequence of the t(14;16) translocation is the overexpression of *c-MAF*[65], a basic -leucine zipper transcription factor which increases MM cell adhesion to bone marrow stromal cells and promotes MM cell proliferation[66]. As mentioned, t(14;16) accounts for ~ 5% of *IGH* translocations in MM; however, the prevalence increases in PCL and in HMCLs[67]. Originally considered to be a poor prognostic indicator, a retrospective study has recently shown that t(14;16) is not prognostic, and that patients with t(14;16) show no difference in overall survival when compared to patients lacking t(14;16)[68].

The *IGH* translocations present in MM are believed to be mediated by errors in *IGH* modification processes necessary for generating antibody diversity. An overview of those processes and their contributions to the formation of *IGH* translocations in MM will be discussed below.

1.8 *IGH* RECOMBINATION: IMPLICATIONS FOR *IGH* TRANSLOCATIONS

1.8.1 Diversification of the *IGH* locus

The *IGH* locus at 14q32 is composed of 44 functional variable (V_H), 27 diversity (D_H), 6 joining (J_H), and 8 constant (C_H) gene segments[69]. To generate the antibody diversity necessary for the unique specificity of the humoral response, the *IGH* locus in B-cells undergoes three DNA modification processes during B-cell development: (i) variable-diversity-joining [V(D)J] recombination; (ii) *IGH* class switch recombination (CSR); and (iii) somatic hypermutation (SHM). All three processes have the potential to produce DSBs within the *IGH* locus.

1.8.2 V(D)J recombination

Prior to antigen exposure, developing B-cells in the BM undergo germline V(D)J recombination of the *IGH* which results in the production of a primary arsenal of antibody specificities. The process is initiated by the recombinase-activating gene (RAG) -1 and -2 proteins (reviewed by [70]). These two proteins form an endonuclease complex which induces site-directed DSBs at recombination signal sequences (RSS) flanking each

gene segment within the V_H, D_H, and J_H regions of *IGH,* and the V_L and J_L regions of the immunoglobulin light chain (*IGL).* Within the *IGH* locus, the D_H to J_H regions recombine first, followed by the V_H to DJ_H. After recombination, the DSBs are rejoined by the non-homologous end-joining pathway (NHEJ), which ligates DNA ends with little or no stretches of homology. The resulting IgM antibodies are of low affinity but high avidity, providing a first line adaptive defense against pathogens and their products. B-cells can also undergo a second round of *IGL* recombination at later stages. This recombination is termed "receptor editing" and its purpose is to ablate autoreactivity.

1.8.3 Somatic hypermutation

Once stimulated by antigen, mature B-cells are directed to proliferate, differentiate, and migrate to the germinal centers (GCs) of the secondary lymphoid organs, such as lymph nodes, tonsils, and spleen[71]. In GCs, the activated B-cells undergo SHM of the $V(D)J_H$ region. By mechanisms that are not fully understood, it is believed that SHM is generated either by direct replication or by error-prone repair systems resolving $V(D)J_H$ region DNA lesions (including DSBs[72,73]), triggered directly or indirectly by the enzyme, activation-induced cytidine deaminase (AID). During high rates

of transcription, AID deaminates cytosine residues to generate U:G mismatches on single-stranded DNA[74,75]. The resulting point mutations create changes in the coding sequence necessary for affinity maturation and antibody specificity (reviewed by [76]). The variety of base substitutions generated is dependent upon the normally error-free pathways used to process the U:G lesions: (i) general replication, (ii) uracil DNA glycosylase (UNG) followed by base excision repair (BER), or (iii) mis-match repair (MMR). In GC B-cells, BER and MMR are redirected from their normal roles of preserving genome integrity to processing U:G mismatches in an error-prone manner to generate the *IGV* diversification necessary for the humoral response (reviewed by [77]). Error-prone polymerases recruited by MMR also induce transition and tranversion mutations at A:T bases[77]. It is interesting to note that V(D)J_H rearrangements in MM contain more mutations than in any other B-cell malignancy (reviewed by [78]).

1.8.4 Class switch recombination (CSR)

Activated B-cells also undergo CSR in GCs. This process is required to change the effector functions of antibodies involved in the humoral response (reviewed by [79]). The process of CSR exchanges the exon coding for the μ constant domain of *IGH* with one of the downstream

exons coding for α, δ, ε, γ1, γ2a, γ2b, or γ3[80]. Directed DSBs are produced through recognition by and action of AID at specialized switch (S) regions located upstream of the exons encoding the various constant regions of *IGH*. Switch regions consist of tandem repeats that are unique to each isotype, although all contain the "hotspot" motif WRC/GYW; where W=A or T, R=G or A, and Y=C or T[81]. During switch region transcription, the enzyme deaminates cytosine residues on single-stranded DNA to produce U:G mismatches. The mismatches are converted into abasic sites, through uracil excision by uracil DNA glycosylase (UNG). Apurinic/apyrimidinic endonuclease 1 (APE-1) nicks the phosphodiester backbone at the abasic site[82]. CSR works on both transient single-strands exposed during transcription, resulting in DSBs. AID-dependent DSBs are introduced and repaired in the G1 phase of the cell cycle[81]. Similar to V(D)J recombination, the DSBs are repaired by the NHEJ pathway, as the nature of S region sequences (lack of long stretches of perfect homology between switch regions) would not support homologous recombination (HR) (reviewed by [83]). The result is a hypermutated, function-specific antibody. MM displays the following distribution for *IGH* expression: 60% IgG, 24% IgA, 3% IgD, and 2% biclonal or other isotypes, including IgE and IgM. The remaining 11% of myelomas produce light chains only

(reviewed by [78]). Although pre-switch clonotypic MM cells are detectable in most patients[49], the presence of a single, unchanging clonotypic switch junction in MM plasma cells suggests that myeloma progenitors reside in the post-switch population[84].

1.9 TRANSLOCATION BREAKPOINTS WITHIN THE *IGH* LOCUS IN MM

Most translocations in myeloma appear to involve DSBs located in or near the switch regions. It has been shown, however, that most studies detecting and cloning breakpoints in myeloma have relied on molecular methods which significantly bias the results towards identifying translocations which occur in or near switch regions. Translocations involving breakpoints in the J_H region have been reported in patients displaying t(4;14), and in as many as 50% of the t(11;14) (reviewed by [57]), suggesting a recombination event outside the switch region. The location of a breakpoint in the *IGH* locus has functional implications for the predicted expression of oncogenes on the derivative chromosomes (Figure 1-2). V(D)J recombination and SHM may generate breakpoints upstream of Eμ, maintaining Eμ and the Eα enhancers on der(14). CSR

mediates breakage in or near switch regions, and causes segregation of the Eα enhancers on der(14), but Eμ is recruited to the other derivative chromosome. The former break can dysregulate a single oncogene on der(14) alone, whereas the latter break has the potential to upregulate two oncogenes; one on each derivative chromosome. The breakpoints in the three most common translocations in myeloma will be discussed.

1.9.1 *IGH* breakpoints in t(4;14)

The translocation event involved in t(4;14) involves 14q32 and 4p16, and displays a prevalence of ~15-20% among myeloma patients[62,85]. The t(4;14) is karyotypically cryptic; however, the breakpoints in this translocation have been heavily documented through the identification of illegitimate switch recombination fragments. The majority of t(4;14) breakpoints recorded thus far in tumours or human myeloma cell lines involve *IGH* switch regions (Figure 1-2A: orange arrowheads)[62,](reviewed by [86,87,88]) Following breakage, the 5' *IGH* fragments localize to der(4). Approximately two-thirds of the 5' *IGH* breakpoints occur at Sμ (Figure 1-2A: first orange arrowhead), with the remainder occurring within the recombined hybrid Sμ/Sγ (Figure 1-2B: yellow arrowhead) or Sμ/Sα regions. The 3' *IGH* fragments localize to der(14), with the 3' *IGH*

breakpoints localizing to Sμ, Sγ, or Sα regions with similar frequencies, and occasionally to hybrid-switch regions Sμ/Sγ, Sμ/Sα, Sα/Sγ· (reviewed by [57]). There is one report of a non-switched IgM myeloma with t(4;14)[89].

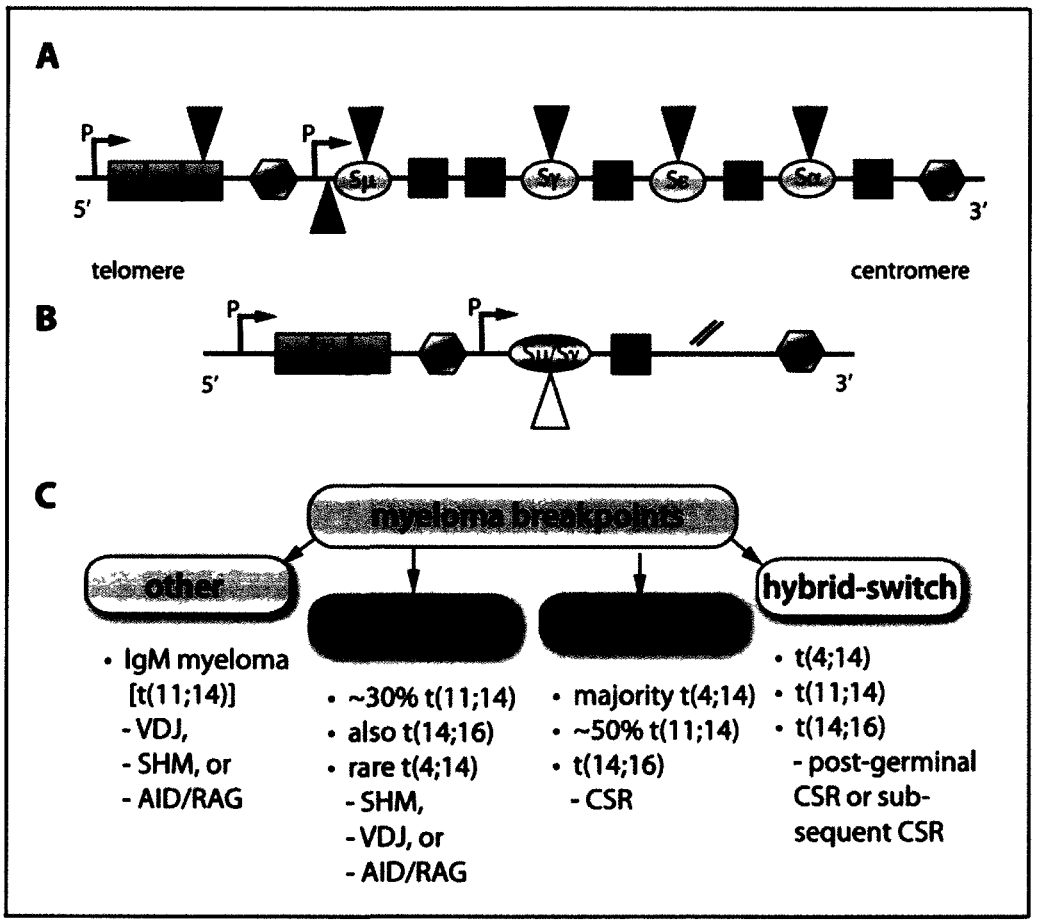

Figure 1-2: Possible aberrant recombination events responsible for primary translocations in multiple myeloma. (A) The clonal V(D)J pre-switch *IGH* locus at 14q32. Breakpoints mediated by aberrant V(D)J recombination or SHM occur centromeric to J_H and telomeric to Sμ. The

region is indicated by red arrowheads. Recent data indicates that these breakpoints may be mediated by combination enzymatic activity of AID/RAG. Breakpoints mediated by CSR occur within or near switch regions, and are indicated by orange arrowheads. (B) The clonal V(D)J post-switch *IGH* locus at 14q32. Breakpoints mediated by post-switch or subsequent post-germinal CSR occur in hybrid switch regions, and are indicated by yellow arrowheads. (C) Summary of myeloma breakpoints, possible aberrant mechanisms, and involved translocations.

1.9.2 *IGH* breakpoints in t(11;14)

The translocation event t(11;14) involves 14q32 and 11q13, and displays a prevalence of ~20% among myeloma patients. In contrast to t(4;14), aberrant CSR is responsible for only 50% of t(11;14) in myeloma (reviewed by [57]). Some of these events show breakpoints involving recombined hybrid switch region sequences as DNA from chromosome band 11q13 has been shown to be joined to (Sμ/Sγ) (Figure 1-2B: yellow arrowhead) in MM patients[90]. This suggests that this translocation event is more complex than canonical CSR, providing evidence that a translocation event occurred post-switch, or due to successive rounds of CSR.

The remaining t(11;14) involve breakpoints in J_H5, J_H6, or the region upstream of Sμ (Figure 1-2A: red arrowheads) and may be the result of aberrant V(D)J recombination or SHM[90,91]. Several studies of IgM myelomas demonstrate that t(11;14) is overrepresented in this group. In a collection of 33 IgE, IgD, IgM and nonsecretory myeloma patients, 83% displayed t(11;14). Seven of the eight IgM myeloma patients characterized were identified as t(11;14). In contrast, the IgG and IgA control population of MM patients had an incidence of t(11;14) of 15% and 10%, respectively[92]. A similar, more recent study of ten patients with IgM myeloma showed that 5/8 cases assessed had t(11;14). Interestingly, the t(11;14) translocation has not been found in IgM malignancies classified as Waldenstrom's macroglobulinemia[93].

1.9.3 *IGH* breakpoints in t(14;16)

The translocation event involved in t(14;16) involves 14q32 and 16q23, and displays a prevalence of ~5% among myeloma patients[94]. Partly due to the low clinical frequency, much less information is available regarding the *IGH* breakpoints in this translocation type. In a study of 5 HMCL with t(14;16), two 5' *IGH* switch breakpoints on der(16) mapped to Sμ (Figure 1-2A: first orange arrowhead). Of the four 3' *IGH* switch breakpoints

identified on der(14), two mapped to Sμ, one to Sγ (Figure 1-2A: second orange arrowhead), and one Sμ/Sγ (Figure 1-2B: yellow arrowhead). The fifth cell line displayed a der(14) breakpoint located near J5 (Figure 1-2A: first red arrowhead). (reviewed by [65,86])

The above processes provide an explanation for the aberrant recombination mechanisms involved in creating DNA DSBs in the *IGH* locus. For translocations to occur, however, DSBs must be generated on the potential partner chromosome as well. Potential mechanisms to achieve this are presented below.

1.10 "OFF-TARGET" ACTIVITIES OF AID AND RAG

It has been known for some time that in diffuse large cell lymphoma, aberrant SHM results in frequent mutation of the genes *PAX, MYC*, *RHOH*, and *PIM-1*. Interestingly, each of these four oncogenes is also involved in chromosomal translocations with breakpoints situated within the mutated regions, indicating the involvement of "off-target" AID activity in the generation of translocations[95]. Recently, Liu *et al.* demonstrated

that in addition to the above-listed genes, AID has the potential to trigger mutations in numerous other tumor-related genes, including *H2AX*, *OCAB* and *EBF1* in normal B-cells, indicating that the mutations may result from the breakdown of high-fidelity repair during B-cell transformation[96]. It was recently demonstrated that AID is essential for the DSBs that form in *MYC/IGH* translocations seen in activated B-cells, and that this activity is dependent upon a functional *MYC* and *IGH* promoter[97]. The rate-limiting step in the formation of translocations is the generation of DSBs in *MYC* (which is lower than in *IGH*), and appears to be the result of errors in the otherwise relatively error-free repair of AID lesions in *MYC*. This suggests that a faulty repair mechanism may also be responsible for the breakage at *MYC*.

Further studies demonstrate that both RAG and AID, either alone or in concert, are also capable of "off-target" activities involving oncogenes. In an effort to understand the mechanisms involving DSBs in *BCL-2*, *CCND1* (*BCL-1*), and the B lineage transcription factor *E2A*, Tsai *et al.* analyzed 1700 breakpoints known to occur in human lymphomas, and determined that a large proportion of the breakpoints are enriched in CpG dinucleotides[98]. They show that T:G mismatches can generate a DNA

structure that is recognized as a substrate by the RAG endonuclease complex. Since the cytosine of the CpG dinucleotide is a target for methylation, resulting in the conversion of cytosine to thymine, they theorize that AID may deaminate methylated CpG dinucleotides resulting in a T:G mismatches which are acted upon by RAG. This theory relies on the premise that B-cells can express both RAG and AID simultaneously, which has recently been shown[99]. Of interest, error-prone BER and MMR that occurs during SHM can result in T:G mismatches (reviewed by [77]).

1.10.1 Breakpoints mapped to 4p16

The 4p16 breakpoints seen in t(4;14) are located at several sites near or within *MMSET*, approximately 80-150 kb centromeric to the 5' end of *FGFR3* (reviewed by [62,86-88]). Several breakpoints appear to cluster in region surrounding exon 1, and introns 3, and 4 of *MMSET*, however the significance of these breakpoint clusters is not known (reviewed by [57,100]). The apparently exclusive identification of CSR *IGH* breakpoints in t(4;14) suggests that off-target CSR is responsible for the generation of DSBs at 4p16.

1.10.2 Breakpoints mapped to 11q13

The 11q13 breakpoints seen in t(11;14) are dispersed over a 360 kb region between *CCND1* and *MYEOV,* centromeric to *CCND1*[91]. There is no apparent clustering in the 150 kb Major Translocation Cluster (MTC) as is seen in mantle cell lymphoma (reviewed by [86]). As mentioned, the breakpoints do not cluster, but neither are they excluded from the smaller region. Tsai *et* al. mapped ten *CCND1* breakpoints outside of the MTC that were located an average 8.8 base pairs from CpG dinucleotides[98]. Based on the recent work of Wang *et al.*[99] it is feasible that the breaks seen in 11p13 could be attributed not only to aberrant V(D)J recombination or SHM, but also to the action of AID on methylated CpGs and late B-cell RAG activity.

1.10.3 Breakpoints mapped to 16q23

Fragile sites are observed as breaks, gaps, or decondensations in metaphase chromosomes when cells are grown under conditions of replicative stress. Recent evidence supports a relationship between fragile sites and regions of DNA instability in cancers, including FRA16 in MM. Of the five t(14;16) HMCL characterized, four breakpoints were identified in 16q23. The sequence data collected for these breakpoints

indicate that all four translocations map within the FRA16D fragile site[101]. Of great interest, it has recently been shown that AID induces DSBs in a murine model at two locations within the fragile site containing *WWOX*[102] (the human homolog of *WWOX* is located within FRA16). Breakpoints identified on der(14) mapped to Sμ, to a hybrid switch region, and to the J_H region; indicating that off-target CSR, V(D)J recombination, and/or SHM may be responsible for the DSBs in 16q23.

In light of the evidence presented above, it is highly probable that the DSBs generated in putative oncogene partners that are necessary for the translocations evident in myeloma result from "off-target" activities of AID, RAG, or SHM. However, as well as generating the breaks, it is necessary to repair them, and in the case of translocations, aberrant repair mechanisms may be contributing to the translocation frequency, as DSBs on homologous chromosomes fail to repair with one another.

1.11 THE ROLE OF NON-HOMOLOGOUS END-JOINING (NHEJ) IN THE GENESIS OF TRANSLOCATIONS IN MYELOMA

Two major repair pathways are responsible for the repair of DSBs in DNA; homologous recombination (HR), and NHEJ. HR is most active in the late S/G2 phase of the cell cycle, and is dependent upon sequence homology of the DSBs. NHEJ, however, can function throughout the cell cycle, and requires little or no sequence homology (reviewed by [83]). Similar to most DNA repair pathways, NHEJ involves the following steps: (i) detection of the DSB and stabilization of the DNA ends; (ii) resection of damaged DNA; and (iii) DNA ligation to repair the phosphodiester backbone. NHEJ is initiated at the sites of DSBs by the heterodimer Ku70/Ku86. The toroidal Ku complex slips onto and binds DNA on either side of the DSB in a sequence-independent manner[103]. It appears to "anchor" the ends of the DSBs[7], and prevents the use of homologies during recombination (reviewed by [104]). The Ku complex recruits the DNA-dependent protein kinase catalytic subunit (DNA-PKcs), and it has been shown that Ku86 is necessary for the recruitment[105]. Ku86 possesses a flexible C-terminal "arm", which allows for interactions with DNA-PKcs on both sides of the DSB, promoting trans-autophosphorylation of the kinase. The auto-

phosphorylation of DNA-PKcs modulates its dynamics and stability at DSBs[106], and the Ku:DNA-PKcs complex is believed to "tether" the ends of the DSB. DNA-PKcs recruits the nuclease Artemis, which can act as an exonuclease or an endonuclease (reviewed by [107]). Ku recruits the ligase, XLF: XRCC4:DNA ligase IV to ligate the DNA ends post-processing. Ku can recruit these factors in any order to work on either end of the DSB. Additionally, the nuclease and ligase activities can work on the "top" strand of the break independently of the "bottom" strand[108]. When the classical NHEJ pathway is impaired, an alternative end-joining pathway is operative that appears to utilize microhomology (reviewed by [83]).

NHEJ is required for the resolution of DSBs generated by CSR and V(D)J recombination. Several factors of the NHEJ pathway are essential for V(D)J recombination, including the Ku heterodimer, DNA-PKcs, and XRCC4, as mice lacking any of these proteins fail to develop B-cells (reviewed by [104]). All three proteins are involved in the repair of DSBs in CSR; however, only Ku is essential for CSR to occur (reviewed by [104,109]). This suggests the use of an alternative repair mechanism to resolve the DSBs caused by CSR.

1.11.1 Ku86v

Of interest, a study of 14 myeloma patients demonstrated that 100% expressed a 69 kDa variant of Ku86 (Ku86v) with a truncated C terminus[110]. Two of the patients expressed full-length Ku86 in addition to the variant. All cells retained the ability to bind to DNA ends, although this binding appeared decreased as compared to cells from normal bone marrow samples. The cells expressing Ku86 and Ku86v exhibited normal Ku-DNA-PKcs complex formation but decreased DNA-PKcs kinase activity. Intriguingly, both activities were absent from the cells expressing only Ku86v. This is consistent with the findings that the DNA binding motifs of Ku86 are located in the N-terminus[111], and the DNA-PKcs binding domain in the C-terminus[112]. The cells expressing only Ku86v displayed increased sensitivity to irradiation and chemotherapeutic agents[110]. These results were later challenged by Kato *et al.* who failed to identify Ku86v in 16 MM cell lines or cells isolated from 6 patients[113]. They theorized that the Ku86v in the former study was the result of protein degradation during sample preparation; however, no evaluation of Ku86 function was provided[113]. Supporting the results of Tai *et al.*[110], a recent study identified two HMCL that consistently express full-length Ku86 as well as Ku86v, and suggests that the generation of the variant Ku in MM

cells is an innate process. The study implicates serine proteases as important for the generation of Ku86v in intact myeloma cells[114].

Studies in cells isolated from patients with chronic lymphocytic leukemia (CLL) mimic the results of the original myeloma study. A Ku86 doublet, consisting of 69 and 71 kDa proteins was detected in B-cell extracts from 4/9 CLL patients. Three of the four patients had low DNA-PKcs activity and sensitivity to a chemotherapeutic agent[115]. In a separate study of cells isolated from 96 CLL patients, 33% displayed translocations when B-cells were stimulated with CD40L. The cells were able to generate many different translocations, but with several recurring breakpoints in chromosome regions known to harbor oncogenes, including 6p21, 14q32, and 18q21[116]. The promiscuity of recurrent partners in the translocations of CLL patients is similar to that seen in MM. This suggests that expression of a variant Ku86 protein may be a critical factor in the development of chromosomal instability and translocations in MM.

The mechanisms discussed above provide possible explanations for the generation and aberrant repair of DNA DSBs in *IGH* and potential partner loci in MM. What is not currently known is whether genome organization

in the cells of patients contributes to the generation of chromosomal translocations in MM, or to the selection of a specific partner with *IGH*. MM provides an ideal model to investigate the hypothesis that the spatial organization of translocation-prone gene loci (TPGL) contributes to the formation of chromosomal translocations involving specific loci, as the three most recurrent translocations observed in MM occur with different clinical frequencies: t(11;14) - 20%; t(4;14)- 15-20%; and t(14;16) - 5%. Genome positioning of *FGFR3*, *CCND1*, and *c-MAF* in the nucleus may place these oncogenes in distinct and differential proximities to *IGH*, resulting in "favoured" loci pairing that predisposes patients to specific translocations.

1.12 WORKING HYPOTHESIS

I propose that genome organization of translocation-prone gene loci in the interphase nucleus of non-malignant cells from patients with MM influences their potential for translocation with *IGH*. As a corollary, I predict that the genome organization in uninvolved cells from MM patients will differ from that of their counterparts in healthy donors.

1.13 REFERENCES

1. Balmain A. Cancer genetics: from Boveri and Mendel to microarrays. Nat Rev Cancer. 2001;1:77-82.
2. Nambiar M, Kari V, Raghavan SC. Chromosomal translocations in cancer. Biochim Biophys Acta. 2008;1786:139-152.
3. Martin LD, Belch AR, Pilarski LM. Promiscuity of translocation partners in multiple myeloma. J Cell Biochem;109:1085-1094.
4. Nussenzweig A, Nussenzweig MC. Origin of chromosomal translocations in lymphoid cancer. Cell;141:27-38.
5. Nikiforova MN, Stringer JR, Blough R, Medvedovic M, Fagin JA, Nikiforov YE. Proximity of chromosomal loci that participate in radiation-induced rearrangements in human cells. Science. 2000;290:138-141.
6. Aten JA, Stap J, Krawczyk PM, et al. Dynamics of DNA double-strand breaks revealed by clustering of damaged chromosome domains. Science. 2004;303:92-95.
7. Soutoglou E, Dorn JF, Sengupta K, et al. Positional stability of single double-strand breaks in mammalian cells. Nat Cell Biol. 2007;9:675-682.
8. Cremer T, Cremer C. Rise, fall and resurrection of chromosome territories: a historical perspective. Part II. Fall and resurrection of chromosome territories during the 1950s to 1980s. Part III. Chromosome territories and the functional nuclear architecture: experiments and models from the 1990s to the present. Eur J Histochem. 2006;50:223-272.
9. Schardin M, Cremer T, Hager HD, Lang M. Specific staining of human chromosomes in Chinese hamster x man hybrid cell lines demonstrates interphase chromosome territories. Hum Genet. 1985;71:281-287.

10. Cremer T, Cremer C. Chromosome territories, nuclear architecture and gene regulation in mammalian cells. Nat Rev Genet. 2001;2:292-301.

11. Parada L, Misteli T. Chromosome positioning in the interphase nucleus. Trends Cell Biol. 2002;12:425-432.

12. Parada LA, Roix JJ, Misteli T. An uncertainty principle in chromosome positioning. Trends Cell Biol. 2003;13:393-396.

13. Taslerova R, Kozubek S, Bartova E, Gajduskova P, Kodet R, Kozubek M. Localization of genetic elements of intact and derivative chromosome 11 and 22 territories in nuclei of Ewing sarcoma cells. J Struct Biol. 2006;155:493-504.

14. Lanctot C, Cheutin T, Cremer M, Cavalli G, Cremer T. Dynamic genome architecture in the nuclear space: regulation of gene expression in three dimensions. Nat Rev Genet. 2007;8:104-115.

15. Mayer R, Brero A, von Hase J, Schroeder T, Cremer T, Dietzel S. Common themes and cell type specific variations of higher order chromatin arrangements in the mouse. BMC Cell Biol. 2005;6:44.

16. Murmann AE, Gao J, Encinosa M, et al. Local gene density predicts the spatial position of genetic loci in the interphase nucleus. Exp Cell Res. 2005;311:14-26.

17. Croft JA, Bridger JM, Boyle S, Perry P, Teague P, Bickmore WA. Differences in the localization and morphology of chromosomes in the human nucleus. J Cell Biol. 1999;145:1119-1131.

18. Cremer M, Kupper K, Wagler B, et al. Inheritance of gene density-related higher order chromatin arrangements in normal and tumor cell nuclei. J Cell Biol. 2003;162:809-820.

19. Tanabe H, Muller S, Neusser M, et al. Evolutionary conservation of chromosome territory arrangements in cell nuclei from higher primates. Proc Natl Acad Sci U S A. 2002;99:4424-4429.

20. Tanabe H, Kupper K, Ishida T, Neusser M, Mizusawa H. Inter- and intra-specific gene-density-correlated radial chromosome territory arrangements are conserved in Old World monkeys. Cytogenet Genome Res. 2005;108:255-261.

21. Habermann FA, Cremer M, Walter J, et al. Arrangements of macro- and microchromosomes in chicken cells. Chromosome Res. 2001;9:569-584.

22. Mehta IS, Figgitt M, Clements CS, Kill IR, Bridger JM. Alterations to nuclear architecture and genome behavior in senescent cells. Ann N Y Acad Sci. 2007;1100:250-263.

23. Meaburn KJ, Cabuy E, Bonne G, et al. Primary laminopathy fibroblasts display altered genome organization and apoptosis. Aging Cell. 2007;6:139-153.

24. Kim SH, McQueen PG, Lichtman MK, Shevach EM, Parada LA, Misteli T. Spatial genome organization during T-cell differentiation. Cytogenet Genome Res. 2004;105:292-301.

25. Stadler S, Schnapp V, Mayer R, et al. The architecture of chicken chromosome territories changes during differentiation. BMC Cell Biol. 2004;5:44.

26. Parada LA, McQueen PG, Misteli T. Tissue-specific spatial organization of genomes. Genome Biol. 2004;5:R44.

27. Meaburn KJ, Misteli T, Soutoglou E. Spatial genome organization in the formation of chromosomal translocations. Semin Cancer Biol. 2007;17:80-90.

28. Guasconi V, Souidi M, Ait-Si-Ali S. Nuclear positioning, gene activity and cancer. Cancer Biol Ther. 2005;4:134-138.

29. Roix JJ, McQueen PG, Munson PJ, Parada LA, Misteli T. Spatial proximity of translocation-prone gene loci in human lymphomas. Nat Genet. 2003;34:287-291.

30. Misteli T. Concepts in nuclear architecture. Bioessays. 2005;27:477-487.

31. Williams RR, Azuara V, Perry P, et al. Neural induction promotes large-scale chromatin reorganisation of the Mash1 locus. J Cell Sci. 2006;119:132-140.

32. Kosak ST, Skok JA, Medina KL, et al. Subnuclear compartmentalization of immunoglobulin loci during lymphocyte development. Science. 2002;296:158-162.

33. Skok JA, Brown KE, Azuara V, et al. Nonequivalent nuclear location of immunoglobulin alleles in B lymphocytes. Nat Immunol. 2001;2:848-854.

34. Roldan E, Fuxa M, Chong W, et al. Locus 'decontraction' and centromeric recruitment contribute to allelic exclusion of the immunoglobulin heavy-chain gene. Nat Immunol. 2005;6:31-41.

35. Williams RR, Broad S, Sheer D, Ragoussis J. Subchromosomal positioning of the epidermal differentiation complex (EDC) in keratinocyte and lymphoblast interphase nuclei. Exp Cell Res. 2002;272:163-175.

36. Mahy NL, Perry PE, Bickmore WA. Gene density and transcription influence the localization of chromatin outside of chromosome territories detectable by FISH. J Cell Biol. 2002;159:753-763.

37. Meaburn KJ, Misteli T. Cell biology: chromosome territories. Nature. 2007;445:379-781.

38. Liyanage M, Weaver Z, Barlow C, et al. Abnormal rearrangement within the alpha/delta T-cell receptor locus in lymphomas from Atm-deficient mice. Blood. 2000;96:1940-1946.

39. Parada LA, McQueen PG, Munson PJ, Misteli T. Conservation of relative chromosome positioning in normal and cancer cells. Curr Biol. 2002;12:1692-1697.

40. Neves H, Ramos C, da Silva MG, Parreira A, Parreira L. The nuclear topography of ABL, BCR, PML, and RARalpha genes: evidence for gene proximity in specific phases of the cell cycle and stages of hematopoietic differentiation. Blood. 1999;93:1197-1207.

41. Sirohi B, Powles R. Multiple myeloma. Lancet. 2004;363:875-887.

42. Kuehl WM, Bergsagel PL. Multiple myeloma: evolving genetic events and host interactions. Nat Rev Cancer. 2002;2:175-187.

43. Society CC. Canadian Cancer Society's Steering Committee: Candian Cancer Statistics 2010. Vol. Canadian Cancer Society, 2010. Toronto; 2010.

44. Sagar L, MD and Asst. Professor DoTR, B-cell Malignancy Program, Medicine EUSo. Multiple Myeloma Research Foundation - Intro to Myeloma; 2005

45. Szczepek AJ, Seeberger K, Wizniak J, Mant MJ, Belch AR, Pilarski LM. A high frequency of circulating B cells share clonotypic Ig heavy-chain VDJ rearrangements with autologous bone marrow plasma cells in multiple myeloma, as measured by single-cell and in situ reverse transcriptase-polymerase chain reaction. Blood. 1998;92:2844-2855.

46. Billadeau D, Ahmann G, Greipp P, Van Ness B. The bone marrow of multiple myeloma patients contains B cell populations at different stages of differentiation that are clonally related to the malignant plasma cell. J Exp Med. 1993;178:1023-1031.

47. Bergsagel PL, Smith AM, Szczepek A, Mant MJ, Belch AR, Pilarski LM. In multiple myeloma, clonotypic B lymphocytes are detectable among CD19+ peripheral blood cells expressing CD38, CD56, and monotypic Ig light chain. Blood. 1995;85:436-447.

48. Pilarski LM, Belch AR. Clonotypic myeloma cells able to xenograft myeloma to nonobese diabetic severe combined immunodeficient mice

copurify with CD34 (+) hematopoietic progenitors. Clin Cancer Res. 2002;8:3198-3204.

49. Reiman T, Seeberger K, Taylor BJ, et al. Persistent preswitch clonotypic myeloma cells correlate with decreased survival: evidence for isotype switching within the myeloma clone. Blood. 2001;98:2791-2799.

50. Adamia S, Reiman T, Crainie M, Mant MJ, Belch AR, Pilarski LM. Intronic splicing of hyaluronan synthase 1 (HAS1): a biologically relevant indicator of poor outcome in multiple myeloma. Blood. 2005;105:4836-4844.

51. Kirshner J, Thulien KJ, Martin LD, et al. A unique three-dimensional model for evaluating the impact of therapy on multiple myeloma. Blood. 2008;112:2935-2945.

52. Pilarski LM, E. B, M.J. M, et al. Multiple myeloma includes CD20+ B and plasma cells that persist in patients treated with rituximab. Clinical Medicine: Oncology. 2008;2:275-281.

53. Rasmussen T, Lodahl M, Hancke S, Johnsen HE. In multiple myeloma clonotypic CD38- /CD19+ / CD27+ memory B cells recirculate through bone marrow, peripheral blood and lymph nodes. Leuk Lymphoma. 2004;45:1413-1417.

54. Matsui W, Huff CA, Wang Q, et al. Characterization of clonogenic multiple myeloma cells. Blood. 2004;103:2332-2336.

55. Smadja NV, Fruchart C, Isnard F, et al. Chromosomal analysis in multiple myeloma: cytogenetic evidence of two different diseases. Leukemia. 1998;12:960-969.

56. Raab MS, Podar K, Breitkreutz I, Richardson PG, Anderson KC. Multiple myeloma. Lancet. 2009;374:324-339.

57. Gabrea A, Leif Bergsagel P, Michael Kuehl W. Distinguishing primary and secondary translocations in multiple myeloma. DNA Repair (Amst). 2006;5:1225-1233.

58. Fabris S, Agnelli L, Mattioli M, et al. Characterization of oncogene dysregulation in multiple myeloma by combined FISH and DNA microarray analyses. Genes Chromosomes Cancer. 2005;42:117-127.

59. Liebisch P, Dohner H. Cytogenetics and molecular cytogenetics in multiple myeloma. Eur J Cancer. 2006;42:1520-1529.

60. Kuppers R. Mechanisms of B-cell lymphoma pathogenesis. Nat Rev Cancer. 2005;5:251-262.

61. Martinez-Garcia E, Popovic R, Min DJ, et al. The MMSET histone methyl transferase switches global histone methylation and alters gene expression in t(4;14) multiple myeloma cells. Blood;117:211-220.

62. Keats JJ, Reiman T, Maxwell CA, et al. In multiple myeloma, t(4;14)(p16;q32) is an adverse prognostic factor irrespective of FGFR3 expression. Blood. 2003;101:1520-1529.

63. Fonseca R, Blood EA, Oken MM, et al. Myeloma and the t(11;14)(q13;q32); evidence for a biologically defined unique subset of patients. Blood. 2002;99:3735-3741.

64. Moreau P, Facon T, Leleu X, et al. Recurrent 14q32 translocations determine the prognosis of multiple myeloma, especially in patients receiving intensive chemotherapy. Blood. 2002;100:1579-1583.

65. Chesi M, Bergsagel PL, Shonukan OO, et al. Frequent dysregulation of the c-maf proto-oncogene at 16q23 by translocation to an Ig locus in multiple myeloma. Blood. 1998;91:4457-4463.

66. Hurt EM, Wiestner A, Rosenwald A, et al. Overexpression of c-maf is a frequent oncogenic event in multiple myeloma that promotes proliferation and pathological interactions with bone marrow stroma. Cancer Cell. 2004;5:191-199.

67. Avet-Loiseau H, Facon T, Grosbois B, et al. Oncogenesis of multiple myeloma: 14q32 and 13q chromosomal abnormalities are not

randomly distributed, but correlate with natural history, immunological features, and clinical presentation. Blood. 2002;99:2185-2191.

68. Avet-Loiseau H, Malard F, Campion L, et al. Translocation t(14;16) and multiple myeloma: is it really an independent prognostic factor? Blood;117:2009-2011.

69. Matsuda F, Ishii K, Bourvagnet P, et al. The complete nucleotide sequence of the human immunoglobulin heavy chain variable region locus. J Exp Med. 1998;188:2151-2162.

70. Fugmann SD, Lee AI, Shockett PE, Villey IJ, Schatz DG. The RAG proteins and V(D)J recombination: complexes, ends, and transposition. Annu Rev Immunol. 2000;18:495-527.

71. Kelsoe G. The germinal center: a crucible for lymphocyte selection. Semin Immunol. 1996;8:179-184.

72. Papavasiliou FN, Schatz DG. Cell-cycle-regulated DNA double-stranded breaks in somatic hypermutation of immunoglobulin genes. Nature. 2000;408:216-221.

73. Bross L, Fukita Y, McBlane F, Demolliere C, Rajewsky K, Jacobs H. DNA double-strand breaks in immunoglobulin genes undergoing somatic hypermutation. Immunity. 2000;13:589-597.

74. Peters A, Storb U. Somatic hypermutation of immunoglobulin genes is linked to transcription initiation. Immunity. 1996;4:57-65.

75. Fukita Y, Jacobs H, Rajewsky K. Somatic hypermutation in the heavy chain locus correlates with transcription. Immunity. 1998;9:105-114.

76. Di Noia JM, Neuberger MS. Molecular mechanisms of antibody somatic hypermutation. Annu Rev Biochem. 2007;76:1-22.

77. Peled JU, Kuang FL, Iglesias-Ussel MD, et al. The biochemistry of somatic hypermutation. Annu Rev Immunol. 2008;26:481-511.

78. Gonzalez D, van der Burg M, Garcia-Sanz R, et al. Immunoglobulin gene rearrangements and the pathogenesis of multiple myeloma. Blood. 2007;110:3112-3121.

79. Chaudhuri J, Basu U, Zarrin A, et al. Evolution of the immunoglobulin heavy chain class switch recombination mechanism. Adv Immunol. 2007;94:157-214.

80. Honjo T, Nakai S, Nishida Y, et al. Rearrangements of immunoglobulin genes during differentiation and evolution. Immunol Rev. 1981;59:33-67.

81. Schrader CE, Guikema JE, Linehan EK, Selsing E, Stavnezer J. Activation-induced cytidine deaminase-dependent DNA breaks in class switch recombination occur during G1 phase of the cell cycle and depend upon mismatch repair. J Immunol. 2007;179:6064-6071.

82. Rada C, Di Noia JM, Neuberger MS. Mismatch recognition and uracil excision provide complementary paths to both Ig switching and the A/T-focused phase of somatic mutation. Mol Cell. 2004;16:163-171.

83. Kotnis A, Du L, Liu C, Popov SW, Pan-Hammarstrom Q. Non-homologous end joining in class switch recombination: the beginning of the end. Philos Trans R Soc Lond B Biol Sci. 2009;364:653-665.

84. Taylor BJ, Kriangkum J, Pittman JA, et al. Analysis of clonotypic switch junctions reveals multiple myeloma originates from a single class switch event with ongoing mutation in the isotype-switched progeny. Blood. 2008;112:1894-1903.

85. Keats JJ, Reiman T, Belch AR, Pilarski LM. Ten years and counting: so what do we know about t(4;14)(p16;q32) multiple myeloma. Leuk Lymphoma. 2006;47:2289-2300.

86. Bergsagel PL, Kuehl WM. Chromosome translocations in multiple myeloma. Oncogene. 2001;20:5611-5622.

87. Chesi M, Nardini E, Lim RS, Smith KD, Kuehl WM, Bergsagel PL. The t(4;14) translocation in myeloma dysregulates both FGFR3 and a novel gene, MMSET, resulting in IgH/MMSET hybrid transcripts. Blood. 1998;92:3025-3034.

88. Fenton JA, Pratt G, Rawstron AC, et al. Genomic characterization of the chromosomal breakpoints of t(4;14) of multiple myeloma suggests more than one possible aetiological mechanism. Oncogene. 2003;22:1103-1113.

89. Ackroyd S, O'Connor SJ, Rawstron AC, Owen RG. IgM myeloma with t(4;14)(p16;q32). Cancer Genet Cytogenet. 2005;162:183-184.

90. Fenton JA, Pratt G, Rothwell DG, Rawstron AC, Morgan GJ. Translocation t(11;14) in multiple myeloma: Analysis of translocation breakpoints on der(11) and der(14) chromosomes suggests complex molecular mechanisms of recombination. Genes Chromosomes Cancer. 2004;39:151-155.

91. Janssen JW, Vaandrager JW, Heuser T, et al. Concurrent activation of a novel putative transforming gene, myeov, and cyclin D1 in a subset of multiple myeloma cell lines with t(11;14)(q13;q32). Blood. 2000;95:2691-2698.

92. Avet-Loiseau H, Garand R, Lode L, Harousseau JL, Bataille R. Translocation t(11;14)(q13;q32) is the hallmark of IgM, IgE, and nonsecretory multiple myeloma variants. Blood. 2003;101:1570-1571.

93. Avet-Loiseau H, Garand R, Lode L, Robillard N, Bataille R. 14q32 Translocations discriminate IgM multiple myeloma from Waldenstrom's macroglobulinemia. Semin Oncol. 2003;30:153-155.

94. Bergsagel PL, Kuehl WM. Molecular pathogenesis and a consequent classification of multiple myeloma. J Clin Oncol. 2005;23:6333-6338.

95. Pasqualucci L, Neumeister P, Goossens T, et al. Hypermutation of multiple proto-oncogenes in B-cell diffuse large-cell lymphomas. Nature. 2001;412:341-346.

96. Liu M, Duke JL, Richter DJ, et al. Two levels of protection for the B cell genome during somatic hypermutation. Nature. 2008;451:841-845.

97. Robbiani DF, Bothmer A, Callen E, et al. AID is required for the chromosomal breaks in c-myc that lead to c-myc/IgH translocations. Cell. 2008;135:1028-1038.

98. Tsai AG, Lu H, Raghavan SC, Muschen M, Hsieh CL, Lieber MR. Human chromosomal translocations at CpG sites and a theoretical basis for their lineage and stage specificity. Cell. 2008;135:1130-1142.

99. Wang JH, Gostissa M, Yan CT, et al. Mechanisms promoting translocations in editing and switching peripheral B cells. Nature. 2009;460:231-236.

100. Keats JJ, Maxwell CA, Taylor BJ, et al. Overexpression of transcripts originating from the MMSET locus characterizes all t(4;14)(p16;q32)-positive multiple myeloma patients. Blood. 2005;105:4060-4069.

101. Krummel KA, Roberts LR, Kawakami M, Glover TW, Smith DI. The characterization of the common fragile site FRA16D and its involvement in multiple myeloma translocations. Genomics. 2000;69:37-46.

102. Staszewski O, Baker RE, Ucher AJ, Martier R, Stavnezer J, Guikema JE. Activation-induced cytidine deaminase induces reproducible DNA breaks at many non-Ig Loci in activated B cells. Mol Cell;41:232-242.

103. Walker JR, Corpina RA, Goldberg J. Structure of the Ku heterodimer bound to DNA and its implications for double-strand break repair. Nature. 2001;412:607-614.

104. Stavnezer J, Guikema JE, Schrader CE. Mechanism and regulation of class switch recombination. Annu Rev Immunol. 2008;26:261-292.

105. Uematsu N, Weterings E, Yano K, et al. Autophosphorylation of DNA-PKCS regulates its dynamics at DNA double-strand breaks. J Cell Biol. 2007;177:219-229.

106. Hammel M, Yu Y, Mahaney BL, et al. Ku and DNA-dependent protein kinase dynamic conformations and assembly regulate DNA binding and the initial non-homologous end joining complex. J Biol Chem;285:1414-1423.

107. Mahaney BL, Meek K, Lees-Miller SP. Repair of ionizing radiation-induced DNA double-strand breaks by non-homologous end-joining. Biochem J. 2009;417:639-650.

108. Lieber MR, Lu H, Gu J, Schwarz K. Flexibility in the order of action and in the enzymology of the nuclease, polymerases, and ligase of vertebrate non-homologous DNA end joining: relevance to cancer, aging, and the immune system. Cell Res. 2008;18:125-133.

109. Casellas R, Nussenzweig A, Wuerffel R, et al. Ku80 is required for immunoglobulin isotype switching. EMBO J. 1998;17:2404-2411.

110. Tai YT, Teoh G, Lin B, et al. Ku86 variant expression and function in multiple myeloma cells is associated with increased sensitivity to DNA damage. J Immunol. 2000;165:6347-6355.

111. Osipovich O, Duhe RJ, Hasty P, Durum SK, Muegge K. Defining functional domains of Ku80: DNA end binding and survival after radiation. Biochem Biophys Res Commun. 1999;261:802-807.

112. Singleton BK, Torres-Arzayus MI, Rottinghaus ST, Taccioli GE, Jeggo PA. The C terminus of Ku80 activates the DNA-dependent protein kinase catalytic subunit. Mol Cell Biol. 1999;19:3267-3277.

113. Kato M, Iida S, Komatsu H, Ueda R. Lack of Ku80 alteration in multiple myeloma. Jpn J Cancer Res. 2002;93:359-362.

114. Gullo CA, Ge F, Cow G, Teoh G. Ku86 exists as both a full-length and a protease-sensitive natural variant in multiple myeloma cells. Cancer Cell Int. 2008;8:4.

115. Muller C, Salles B. Regulation of DNA-dependent protein kinase activity in leukemic cells. Oncogene. 1997;15:2343-2348.

116. Mayr C, Speicher MR, Kofler DM, et al. Chromosomal translocations are associated with poor prognosis in chronic lymphocytic leukemia. Blood. 2006;107:742-751.

Chapter Two: Patient-specific nuclear positioning and spatial proximity of translocation-prone gene loci in B-cells from patients with multiple myeloma

Parts of this chapter were presented in an oral session at the American Society of Hematology annual meeting (Orlando, December 2010). Lorri D. Martin, Jana Harizanova, George Zhu, Andrew Belch, Sabine Mai, and Linda M. Pilarski. Cancer-Specific Nuclear Positioning of Translocation Prone Gene Loci In Non-Malignant B-Cells From Patients with Multiple Myeloma. Blood (ASH Annual Meeting Abstracts). Nov 2010; 116:783. Lorri D Martin was presented with an ASH travel award for this work, and was awarded the Canadian Hematology Society Research Award: PhD and Post-Doctoral Category.

L.D. Martin designed the research, conducted experiments, performed data analysis and data presentation, organized statistical analysis, and wrote the Chapter. 3-D analysis software design and statistical analysis were contributed by others.

A version of this chapter has been submitted for publication. Lorri D. Martin[1], Jana Harizanova[2,3], George Zhu[1], Christiaan H. Righolt[2,4], Andrew R. Belch[1], Sabine Mai[2], and Linda M. Pilarski[1]. Patient-specific nuclear positioning and spatial proximity of translocation-prone gene loci in B-cells from patients with multiple myeloma.

2.1 INTRODUCTION

Accumulating evidence suggests that the non-random nature of spatial genome organization contributes to the formation of chromosomal translocations; specifically, that spatial proximity of potential translocation partners influences translocation potential. Spatial proximity of translocation partners varies in different tissues, and in different stages of differentiation. In murine models, chromosomes 12 and 15, which participate in translocations characteristic of lymphoma, are frequently found in close proximity in normal lymphocytes, but not in hepatocytes where they do not translocate[1]. Chromosomes 5 and 6, which frequently translocate in murine hepatomas and are spatially proximal in hepatocytes, are not proximal in lymphocytes[2]. The genes PML and RARα which participate in t(15;17) of acute promyelocytic leukemia, and the genes ABL and BCR, which participate in t(9;22) of chronic myelogenous leukemia, demonstrate spatial proximity in a heterogenous population of hematopoietic precursors more frequently than in differentiated lymphocytes[3]. The clinical frequency with which *MYC* is

involved in translocations with three potential partners correlates with spatial proximity to *MYC* in a lymphoblastic cell line[4].

There are possible limitations to these studies[5]. Thus far, the genomic regions analyzed have been in: (i) normal cells from healthy donors (the assumption being that genome positioning in normal cells from healthy donors does not differ from normal, non-translocated cells from affected patients); (ii) heterogenous cell populations from patients (when the original cell of translocation origin may be unclear); (iii) murine models; and (iv) cell lines, which are transformed and may not reflect positioning *in vivo*. Purified subpopulations of normal cells from affected patients have not been studied, or been compared to purified subsets from healthy donors. We speculated that the genome organization differs in normal cells from cancer patients as compared to normal cells from healthy donors (HD). Patient-specific arrangement of gene loci in normal cell subsets from patients may influence the potential of specific genes to undergo translocations, through positioning that differs from that in healthy individuals. Our working assumption is that proximity of particular loci in patient-derived normal cells may closely reflect loci positioning present at the time when a cancer-specific translocation initially formed, perhaps

favouring translocations between proximal loci in a patient-specific manner.

Multiple myeloma (MM) is a fatal tumour of B-lineage hematopoietic cells, resulting in an accumulation of malignant plasma cells (PCs) in the bone marrow (BM). MM is characterized by karyotypic instability, including recurrent chromosomal translocations involving the *IGH* locus. MM provides an ideal model to study the proposal that spatial proximity of potential translocation partners influences translocation outcome in a patient-specific manner, as the *IGH* locus participates in translocations with the *FGFR3* and *CCND1* with similar clinical frequencies. Mapping of the position of these three translocation-prone gene loci (TPGL), and a control locus known not to participate in translocations with *IGH*, *TGFBR2*, will allow us to evaluate the effect of radial positioning and spatial proximity on translocation potential. The observation of a similar radial positioning pattern *and* spatial proximity of *IGH* and *FGFR3*, and of *IGH* and *CCND1* that differs from *IGH* and *TGFBR2* may indicate that in addition to spatial proximity, radial position within the nucleus influences translocation potential.

Utilizing 3-D FISH and 3-D analysis techniques, we studied genome organization in normal, non-translocated cell populations isolated from healthy donors (HD) and MM patients at two stages of differentiation: CD34+ hematopoietic progenitor cells (HPC), and CD19+ B-cells. The analysis of genome positioning in purified HPC characterizes genome organization in the earliest stage of hematopoietic cell lineage; subsequent analysis of the genome organization of purified B-cells provides information regarding the cell lineage that gives rise to MM, and allows for the comparison of positioning patterns of hematopoietic cells at sequential stages of differentiation. The comparison of the positioning patterns in normal cells from MM patients with those from healthy donors enables us to evaluate the hypothesis that genome organization differs in patient-derived normal cells, and influences translocation potential of specific gene loci with *IGH*. By extrapolation, we speculate that the favoured loci positioning observed in patients already diagnosed with MM may have been an important contributor to *IGH* translocation in the original parent B-cell that gave rise to MM. Using this system, we found specific radial and relative positioning of *FGFR3*, *CCND1*, and *IGH* in B-cells from MM patients, suggesting that radial positioning and spatial proximity of

TPGL are patient-specific and are likely to influence translocation potential.

2.2 MATERIALS AND METHODS

2.2.1 Materials

Approval for acquisition of patient material used in this study was provided by the institutional review boards of the University of Alberta, and Alberta Health Services. According to the Declaration of Helsinki, written informed consent was obtained from patients (n=55) presenting at the Cross Cancer Institute. Bone marrow (BM), peripheral blood (PB), and G-CSF mobilized blood (MB) were collected from patients during clinical visits. Healthy donor hematopoietic progenitor cells (pooled cord blood CD34+ cells from 10 donors) were purchased from Stem Cell Technologies (Vancouver, BC). Human lymphocytes were isolated from age matched healthy donors (HD) (n=9). Ficoll-Pacque™ was from Pfizer (New York, NY). CD138, CD34, and CD45 antibodies were from BD Biosciences (San Jose, CA). CD19 antibody was FMC63[6]. EasySep® immunomagnetic sorting reagents and magnets were obtained from Stem

Cell Technologies (Vancouver, BC). Fluorescent in situ hybridization probes were from Vysis® (Abbott Laboratories, Abbott Park, IL), and BAC probes were purchased from Empire Genomics (Buffalo, NY).

2.2.2 Cell isolation

Mononuclear cells were isolated from all samples using Ficoll-Paque™ gradient separation as per the manufacturer's instructions. For 3-D FISH, cell populations were isolated according to manufacturer's instructions using immunomagnetic selection kits as follows: HPC were isolated from MB samples using a human CD34 positive selection kit; B-cells were isolated from PB and MB samples using a human CD19 positive selection kit. A representative sample from each purified population was stained with CD34-PE and CD45-FITC, and CD19-FITC respectively, and analyzed by FACSort® (BD Biosciences) to confirm purity. Purity in patient subsets ranged from 80-99% (mean=91%) for HPC, and 90-99% (mean=96%) for CD19+ B lymphocytes. Purity for subsets from HD ranged from 83-99% (mean=93%) for CD19+ B lymphocytes. Following purification, cells were suspended in 50% FBS/RPMI solution for adhesion to poly-L-lysine coated slides. Spherical cells adhered to glass slides with

poly-l-lysine maintain a width/height ratio between 1 and 1.5, considered to be a good preservation of nuclear shape[7].

2.2.3 Two-dimensional (2-D) FISH

2-D FISH was used as a first step to identify patients with PC positive for t(4;14) or t(11,14) for subsequent study. BM patient samples were enriched for mononuclear cells, and immobilized onto a glass slide by centrifugation. May-Grunwald/Giemsa stained PC were identified by morphology using the Duet® microscope scanning system (Bioview Ltd., Rehovot, Israel), and positions on the slide were measured and recorded. Accurate identification of each PC was confirmed visually. The slide was destained in methanol:acetic acid (3:1) in preparation for 2-D FISH. Four commercial Vysis® probe sets were used for each BM sample: LSI IGH dual colour break apart probe for the detection of chromosome breakage at the 14q32 locus; and three LSI dual colour, dual fusion probes: IGH/FGFR3 for the detection of t(4;14)(p16;q32); IGH/CCND1 XT for the detection of t(11;14)(q13;q32), and LSI IGH/c-MAF for the detection of t(14;16)(q32;q23). Probe maps are available at *FISH Chromosome Search 2011*[8]. For simplicity, the latter three probe sets will be referred to as *IGH:FGFR3*, *IGH:CCND1*, and *IGH:c-MAF* respectively, and loci

identified as *FGFR3, CCND1, c-MAF,* and *IGH* for the remainder of the paper. Denaturation and hybridization were performed according to manufacturer's instructions. The slide was counterstained using DAPI-containing VECTASHIELD®. FISH analysis and recording was done according to recommendations for FISH in MM[9,10].

2.2.4 Three-dimensional (3-D) FISH

The 3-D FISH method maintains chromatin structure to the level of 1Mb chromatin domains, making it suitable for studies of the relative positions of CTs and individual genes[11]. Three commercial probe sets (*IGH:FGFR3, IGH:CCND1,* and *IGH:c-MAF*) and one commercial BAC probe (Empire Genomics Cy5-labelled RP11-1080C17) for *TGFBR2* (negative control locus) were employed for 3-D FISH. The *TGFBR2* BAC probe was used in conjunction with the *IGH:CCND1* probe for *IGH:TGFBR2* analyses.

Cell adhesion, fixation, and permeabilization were performed as previously described for cells in suspension[12], with minor modifications. A 20x20 mm area on the slide was identified using a diamond pencil, and incubated with 150 μl poly-L-lysine hydrobromide (1mg/ml) for 1 hour (h) at RT. The slide was rinsed with ddH_2O and air-dried. 40 μl of purified cell

suspension containing ~1x10^5 cells was placed on the poly-L-lysine coated area and incubated at 37°C, 5% CO_2 for 1-2 h in a moist chamber. The cells were fixed in 4% PFA/PBS for 10' at RT, and washed in 1x PBS at RT for 3x 5'. This fixation method is considered to be the "gold standard" for 3-D FISH[7]. The slide was incubated in 0.01 M HCl for 20' and transferred to 20% glycerol/PBS for overnight (O/N) incubation at 4°C. Each slide underwent 4-5 freeze-thaw cycles using liquid nitrogen. Slides were washed in 0.05% Triton X100/PBS for 3x 5', and incubated in 0.1 M HCl for 5'. They were then washed in 2x PBS for 2x 5', and incubated in pepsin (0.005% in 0.1 M HCl) at 37°C for 3-5'. Slides were incubated in 1x PBS/50mM $MgCl_2$ at RT for 5' to inactivate the pepsin, and washed in 1x PBS for 2x 5'. They were post-fixed in 1% PFA/PBS at RT for 10', and washed at RT in 1x PBS for 5'. The slides were loaded with 200μl RNAse A (200 μg/ml) and incubated at 37°C for 30', and then washed twice in 2x SSC for 5'. They were transferred to 50% formamide/2x SSC and incubated at 4°C for a minimum of 24h before hybridization. Slides were removed from 50% formamide/2x SSC and excess fluid drained.

10 μl of desired probe(s) was added to the target area, cover-slipped, and sealed with rubber cement. Nuclei on the slide were co-denatured with

probe at 75°C for 5', and hybridized in a moist chamber for 18-48 h at 37°C. Post-hybridization, slides were washed in 2x SSC at 37°C with shaking for 3x 5', and then in 0.1x SSC at 60°C with shaking for 3x 5'. Slides were rinsed briefly in 2x SSC at RT, and coverslip-mounted using DAPI-containing VECTASHIELD® mounting medium (Vector Laboratories, Burlingame, CA).

2.2.5 Image acquisition

Images of 2-D May-Grunwald/Giemsa stained slides were acquired using a 40x (NA 0.75) dry objective lens on a Zeiss Axioplan 2 upright microscope as part of the Duet® imaging system (Bioview Ltd., Rehovot, Israel). 2-D FISH images were acquired using the 63x (NA 0.95) dry objective lens. For 3-D FISH, 3-D z-stacks (a series of optical sections along the z-axis of the cell) were acquired using 63x (NA 1.4) oil objective lens on a Zeiss LSM 710 confocal microscope with Zen 2009 acquisition software set at scan zoom x3, pixel size 0.9 μm x 0.9 μm, with an optical step size of 0.2 μm. Z stacks of ~1000 nuclei from MM samples and 300 nuclei from controls were analyzed in this study (see Table 2-1). To enhance the signal-to-noise ratio of the images and to decrease background noise, images were subsequently deconvolved using

Huygens Essential deconvolution software (Scientific Volume Imaging, Netherlands). The program utilizes classic maximum likelihood estimation with a theoretical point spread function[13,14].

2.2.6 Quantitative analysis of FISH signal distributions

The quantitative data analyses were performed using *ChromoView* software[15], based on MATLAB (The MathWorks, USA) and DIPimage toolbox (Quantitative Imaging Group, TU-Delft, The Netherlands). The multidimensional image data sets were linearly resampled in the axial direction to obtain isotropic voxel size. The loci and cell nucleus were segmented with an isodata threshold[16].

The following parameters were calculated: (i) center of mass (CM) of each locus; (ii) CM and diameter of the nucleus; (iii) Euclidian distance between CM of each loci pair as a fraction of the equivalent nuclear radius; (iv) radial position of segmented object with respect to the nucleus center; and (v) presence of overlap in segmented loci. The equivalent radius was defined as the geometric mean of the radii of 2 equivalent spheres, with respectively the same surface area and the same volume as the nucleus.

To assess radial position of the object within the nucleus, a radial arm D_N was projected from the nuclear CM toward the nuclear boundary passing through the CM of the locus[17]. The distance D_i of the region with respect to the nucleus center was estimated as a fraction of the radial arm D_N, as $D_i = D_0/D_N$, where D_O is Euclidian distance between CM of each locus and the CM of the nucleus.

2.3 RESULTS

2.3.1 Radial positioning of translocation-prone gene loci (TPGL) *IGH*, *FGFR3*, and *CCND1* in the interphase nucleus of HPC and B-cells

2.3.1.1 TPGL maintain a central position in the interphase nucleus in HPC

(i) Radial Position: The spatial genome organization of TPGL and the negative control locus in HPC isolated from MM patients and HD was characterized using 3-D FISH. Loci were visualized in 450 cells from 8 patients and 90 cells from a pool of 10 donors (Table 2-1) to produce z-stacks using a confocal laser scanning microscope (Figure 2-1). None of the HPC harboured translocations.

We characterized the relative radial distribution (RRD) of each locus in the nuclear volume by measuring the distance of each fluorescent signal from the nuclear center (Figure 2-2ABC).

Table 2-1: Origin (cell type) of samples and number of nuclei analyzed per probe by 3-D FISH.

	HPC (# of nuclei)		B-cells (# of nuclei)	
IGH:FGFR3	180 (*n*=6)	30	180 (*n*=6)	90 (*n*=3)
Total	**450**	**90**	**450**	**210**

MM - multiple myeloma; pts - patients; HD - healthy donors; dnrs - donors

n= number of patients or donors tested per probe type (30 cells per patient or donor)

* pooled cord blood (10 donors)

The radial distribution was normalized to the size of each nucleus, and only nuclei with two signals per gene were analyzed. *IGH, FGFR3,* and *CCND1* are on average localized in a radial shell at ~60% of the radius (0.6 RRD) (Figure 2-3A). The negative control locus, *TGFBR2*, displayed a more peripheral positioning, in a radial shell at ~73% of the nuclear radius (0.73 RRD) (Figure 2-3A).

(ii) Specificity of Radial Position: To determine specificity of the radial position for each locus, we used the cumulative frequencies of each locus RRD (Figure 2-4AB), and applied pairwise statistics (two-sided Kolmogorov-Smirnov test) to each locus combination (Table 2-2). HPC from MM patients and from HD were analyzed separately. We determined that in HPC from MM patients, *IGH, FGFR3,* and *CCND1* were in significantly different shells within the nuclear space than *TGFBR2* ($p<0.001$).

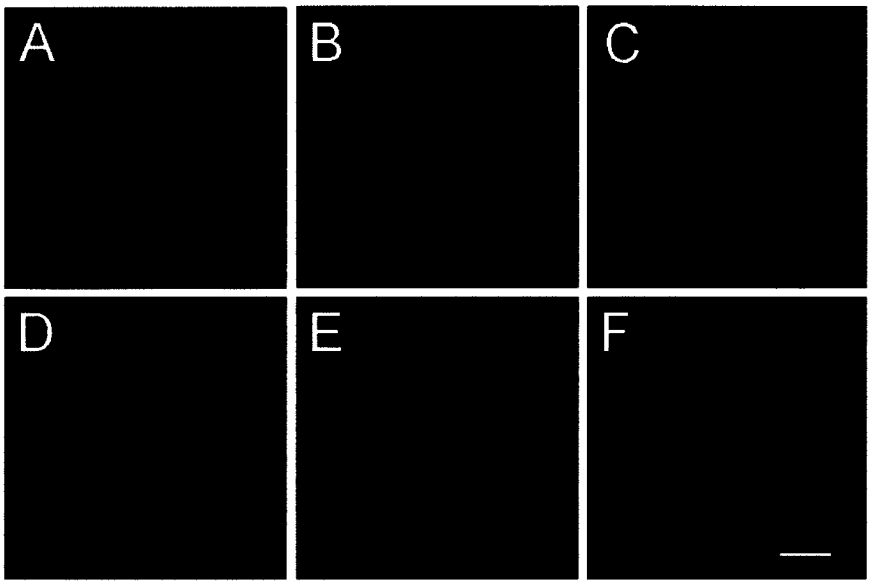

Figure 2-1: Visualization of translocation-prone gene loci in B-cells and HPC using 3-D FISH and confocal microscopy. 3-D FISH was performed on B-cells and HPC from MM patients. 3-D z-stacks were acquired using a 63x (NA 1.4) oil objective lens on a Zeiss LSM 710 confocal microscope, with Zen 2009 acquisition software set at scan zoom x3, pixel size 0.9 μm x 0.9 μm, with an optical step size of 0.2 μm. Panels (A-C) B-cells; panels (D-F) HPC (A) *IGH* (green) and *FGFR3* (red). (B) *IGH* (green) and *CCND1* (red). (C) *IGH* (green) and control locus, *TGFBR2* (red). The second *TGFBR2* locus is hidden inside the nucleus. (D) *IGH* (green) and *FGFR3* (red). (E) *IGH* (green) and *CCND1* (red). (F) *IGH* (green) and *TGFBR2* (red). On average, *IGH*, *FGFR3*, and *CCND1* maintain a more central radial position in the interphase nucleus (ABE); whereas *TGFBR2* maintains a more peripheral location (CF). The radial position is an average of all radial positions observed, however, as can be seen for *FGFR3* (red) in (D), where one of the *FGFR3* alleles is positioned at the nuclear periphery. Scale bar = 3 μm.

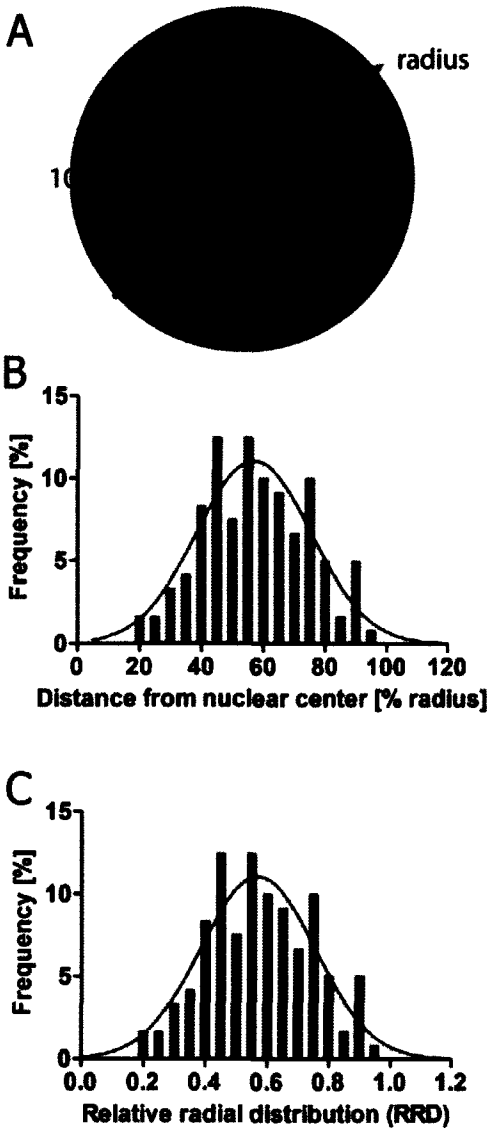

Figure 2-2: Distribution of gene loci in the interphase nucleus. (A) Model of radial positioning of multiple gene loci with clustering in a radial shell at ~55% of the cell radius. (B) Distribution of the radial positioning of the same gene loci expressed as the distance of the loci from the center of the nucleus [% of radius]. (C) The distribution of gene loci in the nucleus can also be expressed as relative radial distribution (RRD).

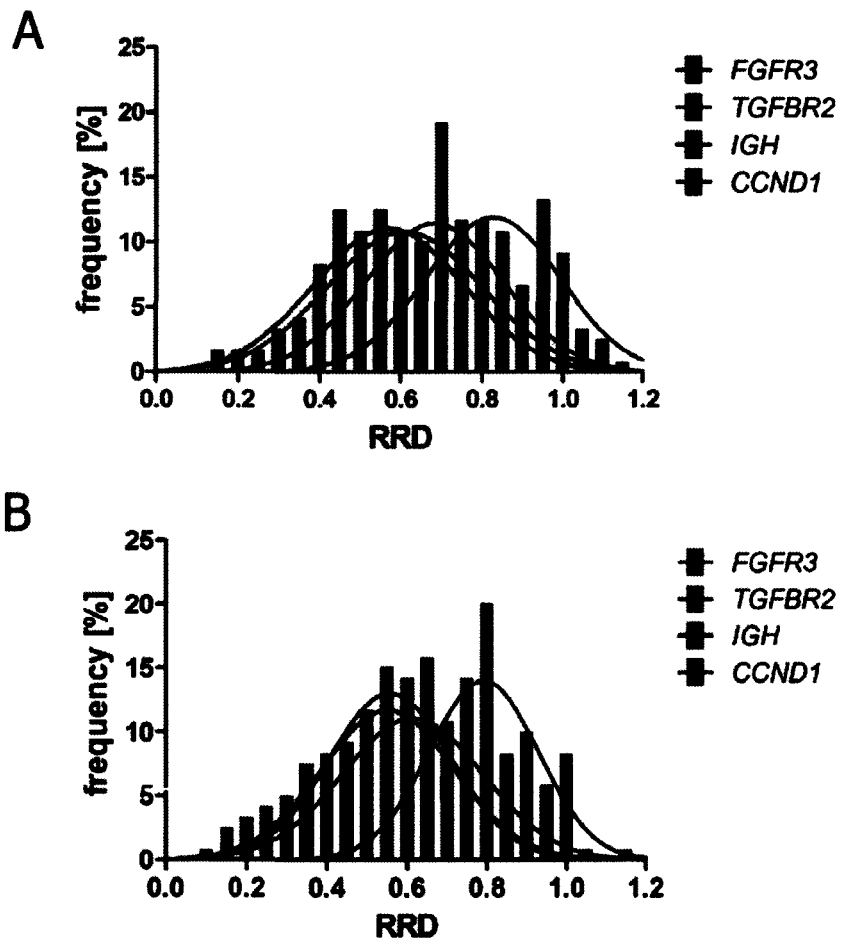

Figure 2-3: Non-random radial positioning of gene loci in HPC and B-cells. Gene loci were detected in PFA-fixed cells using commercial dual-fusion or commercial BAC probes. (A) TPGL (*IGH, FGRF3, CCND1*) in HPC isolated from MM patients have a similar radial distribution [% of radius] in the cell nucleus. *TGFBR2* has a more peripheral radial distribution. (B) TPGL loci in B-cells isolated from MM patients have a similar radial distribution [% of radius], which is more internal than in HPC. *TGFBR2* maintains the same peripheral distribution in B-cells as in HPC, providing an internal control.

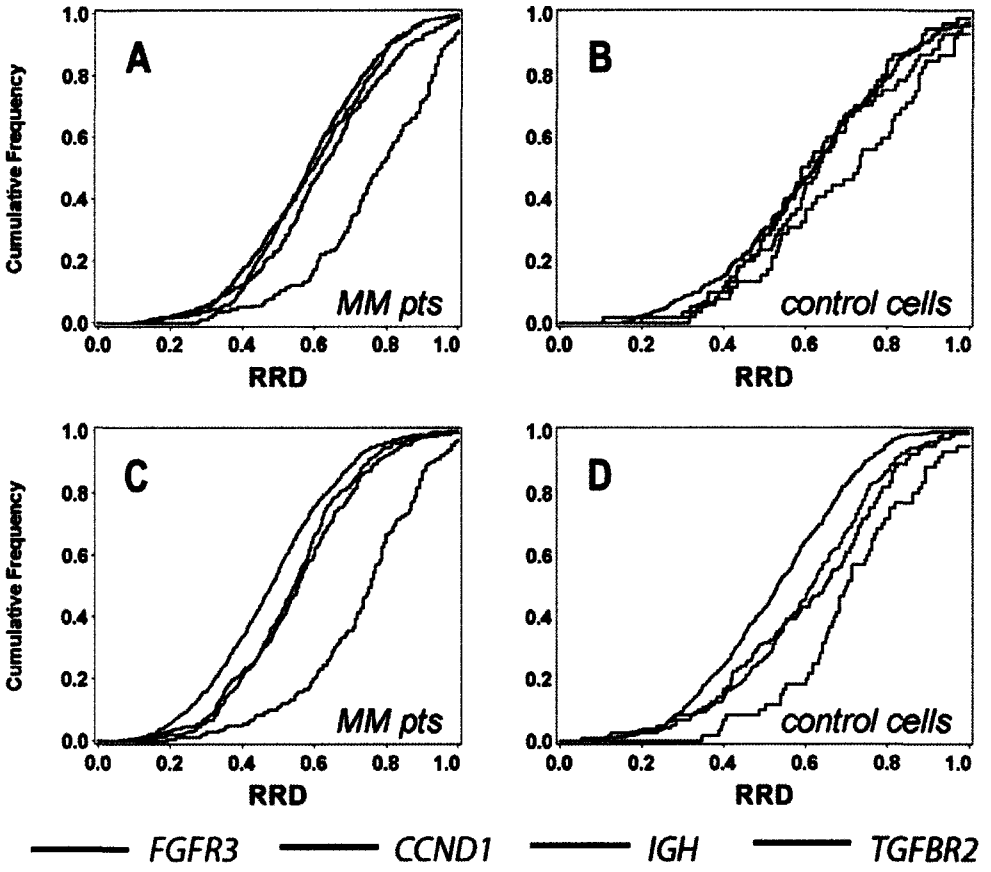

Figure 2-4: Cumulative distribution of relative radial positioning of gene loci in HPC and B-cells. Gene loci were detected in PFA-fixed cells using commercial dual-fusion or commercial BAC probes. (**A**) Radial positioning [% of radius] of TPGL compared to negative control locus *TGFBR2* in HPC from MM patients. All TLPG are more centrally located in the cell nucleus than *TGFBR2.* (**B**) Only *IGH* is more centrally located than *TGFBR2* in HPC isolated from pooled donors. All other loci have similar distributions. (**C**) B-cells isolated from myeloma patients; and (**D**) B-cells isolated from HD. All gene loci have different radial distributions except for *FGFR3* and *CCND1* which are positioned similarly for both cell types. *n= 90-180* per gene for cells from myeloma patients, and *n=30-90* per gene for control cells.

Table 2-2: Pairwise comparison of the relative radial distribution (RRD) of different gene loci in the interphase nucleus of HPC and B-cells.

Gene pair RRD comparison		HPC *p*-values		B-cells *p*-values	
		MM pts	HD	MM pts	HD
IGH	*FGFR3*	0.011	0.878	<0.001	<0.001
IGH	*CCND1*	0.475	0.860	<0.001	<0.001
IGH	*TGFBR2*	<0.001	0.033	<0.001	<0.001
CCND1	*FGFR3*	0.143	0.809	0.341	0.656
TGFBR2	*CCND1*	<0.001	0.182	<0.001	0.001
TGFBR2	*FGFR3*	<0.001	0.055	<0.001	0.013

MM pts - multiple myeloma patients; HD - healthy donors

p-values obtained from two-sided Kolmogorov-Smirnov tests

There was no significant difference in the shells occupied by *CCND1* and *IGH (p=0.475)*, and *CCND1* and *FGFR3 (p=0.143)*. In HPC from HD, only *IGH* and *TGFBR2* occupied significantly different shells (Figure 2-4B)*(p=0.033)*.

(iii) Radial Position Based on Translocation Type: To investigate the radial position of the loci in non-translocated HPC from seven MM patients, based on the translocation type identified in autologous PCs, we categorized the HPC as originating from t(4;14) patients (n=4) or t(11;14)

patients (n=3) and utilized RRD cumulative frequencies to determine pairwise statistics for each gene locus. We compared HPC from each type of MM patient (characterized by translocation type) vs. HPC from pooled HD (Figure 2-5A-H), and HPC from t(4;14) patients vs. HPC from t(11;14) patients (Figure 2-5I-L). Each locus was positioned similarly in HPC from patients and controls, and no difference in position was observed between HPC from MM with t(4;14) PCs compared to HPC from MM with t(11;14) PCs. Cumulatively, this study of radial positioning provides evidence that in HPC, individual locus positioning among MM patients (regardless of translocation type) and HD is not significantly different.

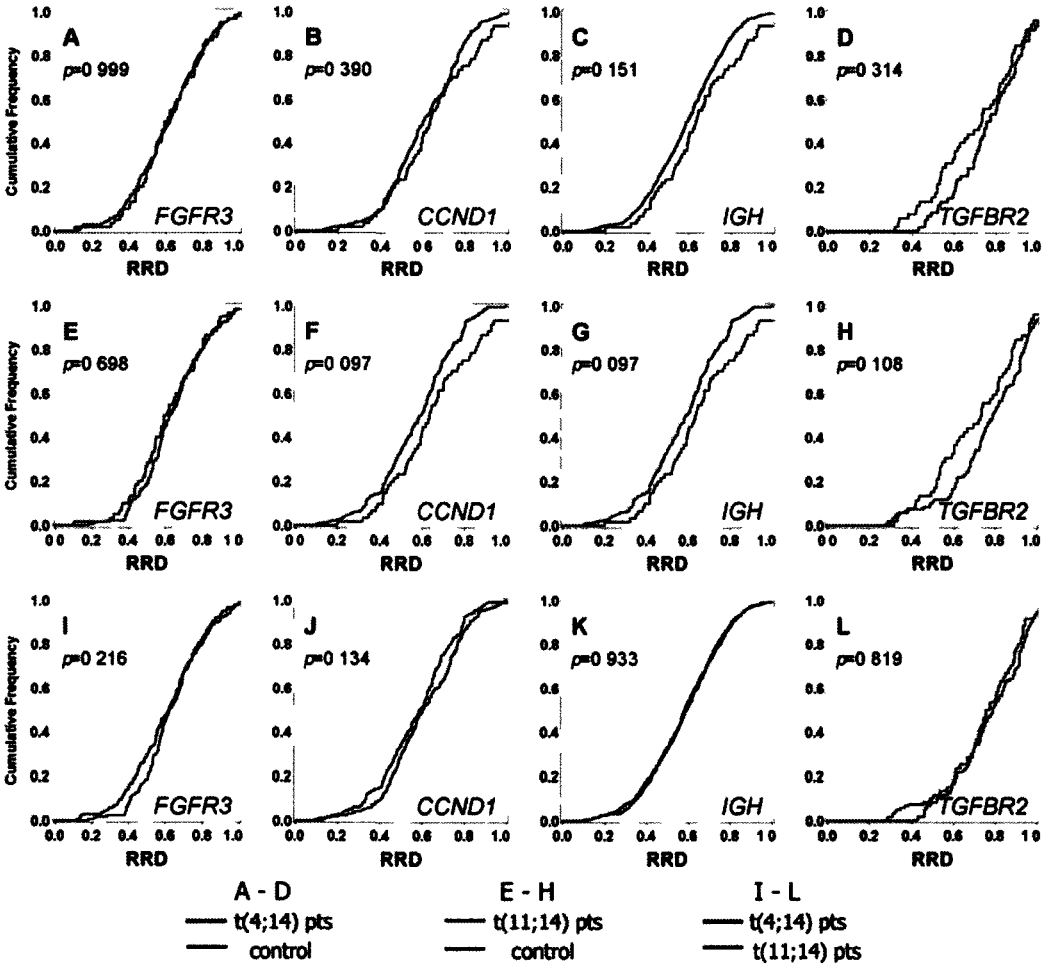

Figure 2-5: Radial distribution [% of radius] of translocation-prone and control genes in HPC. (A-H) 3-D FISH was performed on HPC from MM patients. Patients were categorized according to the translocation type of their plasma cells. The relative radial distributions (RRD) for each gene are shown with comparison to HPC from pooled cord bloods (HD control). (A-D) t(4;14) patients. (E-H) (11;14) patients. (I-L) Radial distributions for each gene shown with comparison between HPC from patients with t(4;14) vs. patients with t(11;14). Pairwise comparisons of cumulative radial distributions were performed using a two-sided Kolmogorov-Smirnov test. n= 90-180 per gene for cells from myeloma patients, and n= 30 per gene for pooled control cells.

2.3.1.2 Patient-specific positioning of FGFR3, CCND1, and IGH in non-translocated B-cells from MM patients

(i) Relative Radial Distribution (RRD): To assess the spatial organization of TLPG and the negative control locus in patient-derived B-cells and HD B-cells, we utilized the same methods and statistical analysis as for HPC. We visualized the loci in 450 cells from patients (n=7) and 210 cells from HD (n=5) (Table 2-1) to produce 3-D z-stacks using a confocal laser scanning microscope, and characterized the RRD of each locus in the nuclear volume by measuring the distance of each fluorescent signal from the nuclear center (Figure 2-2ABC). *IGH* localized most internally in a shell at ~48% of the radius (0.48 RRD), while *FGFR3* and *CCND1* localized in close proximity in a shell at ~54% of the radius (0.54 RRD) (Figure 2-3B). The negative control locus, *TGFBR2*, displayed a more peripheral location, at ~74% of the radius (0.74 RRD) (Figure 2-3B). *FGFR3* and *CCND1* occupied a radial position more proximal to *IGH* than to *TGFBR2* (Figure 2-3B).

(ii) Specificity of Radial Position: To determine whether the radial position was specific for each of the respective loci in B-cells, we again used cumulative frequencies of each gene locus RRD (Figure 2-4CD), and

applied pairwise statistics between each locus combination (Table 2-2). Patient-derived B-cells were analyzed independently of HD B-cells. We established that all gene loci demonstrated significantly different positioning relative to one another in B-cells from MM and in HD controls (p<0.02), with the exception of *FGFR3* and *CCND1* (Table 2-2). This provides evidence indicating the similar radial positions of these two loci in B-cells.

(iii) Radial Position Based on Translocation Type: To investigate the radial position of these three loci in B-cells from seven MM patients, we characterized them as originating from t(4;14) (n=4) or t(11;14) (n=3) patients, and utilized RRD cumulative frequencies to determine pairwise statistics for each gene locus. Two comparisons were made: (a) cells from MM patients with each translocation type vs. cells from HD (Figure 2-6A-H); and (b) cells from t(4;14) patients vs. cells from t(11;14) patients (Figure 2-6I-L]. The radial position of *TGFBR2* did not change significantly among all cell types. It, therefore, acts as an internal control. In contrast, the TPGL loci were positioned differently in B-cells from MM patients (regardless of translocation type) as compared to cells from HD (p<0.05). Comparing t(4;14) with t(11;14) MM, we observed no significant differences in loci position between translocation types for each gene

(Figure 2-6I-L). This suggests that loci positioning in normal B-cells is not different for individuals who have developed MM, but different from those who have not developed MM (age-matched healthy donors).

(iv) Radial position of loci in HPC vs. B-cells: To determine whether locus positioning was significantly different in HPC as compared to B-cells, we used cumulative frequencies of the gene RRD for each locus and performed pairwise statistical analysis between cell types. Cells from HD were analyzed independently of patient-derived cells. We first compared the radial position of each locus in HPC to B-cells from HD (Figure 2-4BD). There were no significant differences in the radial positions of gene loci between these control populations of HPC and B-cells, with the exception of the *IGH* locus, which occupies a more internal position in HD B-cells (Table 2-3).

We then compared the radial position of TPGL in patient-derived HPC and B-cells (Figure 2-4AC), and determined that TPGL are located more towards the periphery of the nucleus in patient HPC than in patient B-cells (Table 2-3). The position of the negative control locus, *TGFBR2* does not change significantly (p=0.216) in either cell type, acting as an internal control.

To summarize the overall analysis of radial positioning in HPC and B-cells, we provide evidence that:

(i) radial positioning of TPGL in patient-derived HPC is not significantly different from radial positioning in HD HPC;

(ii) radial positioning of *FGFR3* and *CCND1* in HD HPC is not significantly different from radial positioning in HD B-cells;

(iii) *IGH*, *FGFR3*, and *CCND1* are positioned significantly more internally in the nucleus of patient-derived B-cells than in HD B-cells; and

(iv) *IGH*, *FGFR3*, and *CCND1* are positioned significantly more internally in the nucleus of patient-derived B-cells than of patient-derived HPC. Collectively, these data demonstrate patient-specific radial positioning of TPGL in normal B-cells from MM patients with t(4;14) and t(11;14).

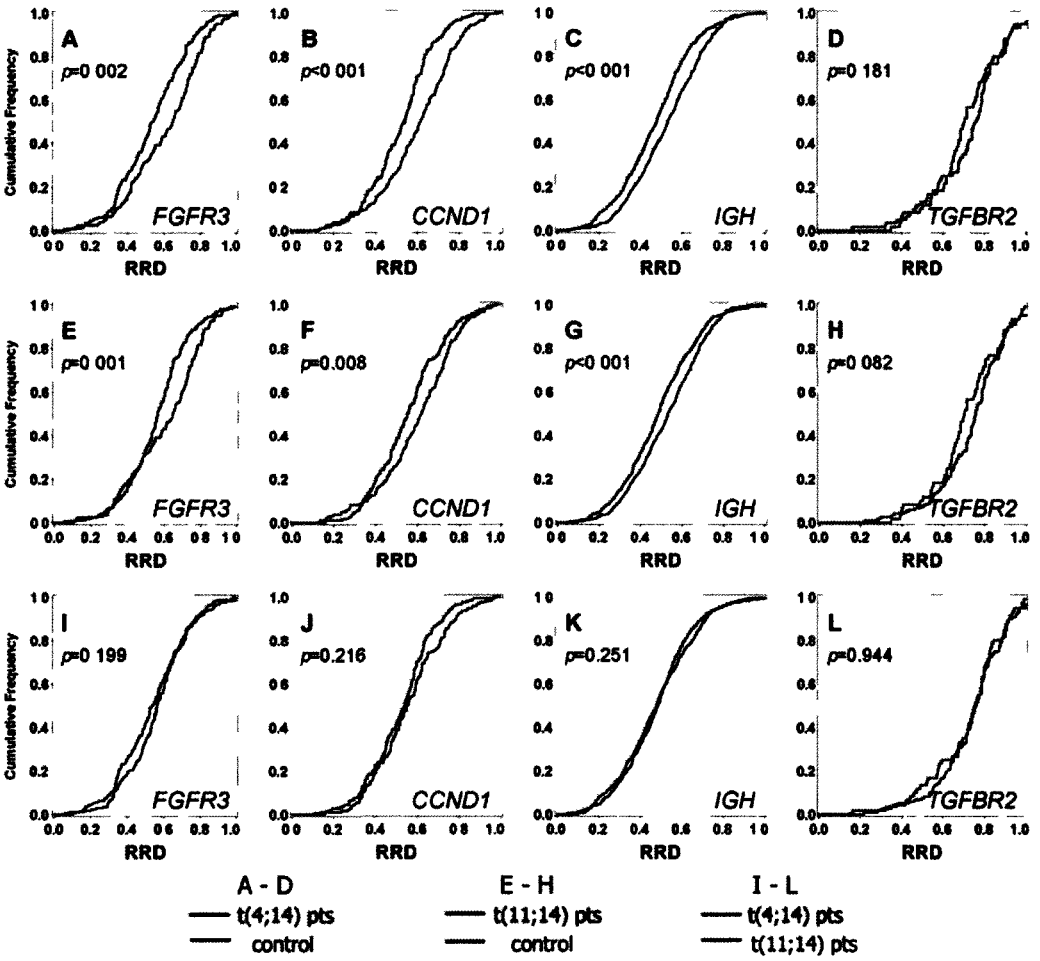

Figure 2-6: Radial distribution [% of radius] of translocation-prone and control genes in B-cells. (A-H) 3-D FISH was performed on B-cells from MM patients. Patients were categorized according to the translocation type found in their plasma cells. The radial distributions (RRD) for each gene are shown with comparison to B cells from HD controls (n=9 individuals). (A-D) t(4;14) patients. (E-H) (11;14) patients. (I-L) Radial distributions for each gene shown with comparison between B-cells from MM patients with t(4;14) vs. MM patients with t(11;14). Pairwise comparisons of cumulative radial distributions were performed using a two-sided Kolmogorov-Smirnov test. n= 90-180 per gene for cells from MM patients, and n= 30-90 per gene for control cells.

Table 2-3: Pairwise comparison of the relative radial distribution (RRD) of the same gene locus in the interphase nucleus of HPC and B-cells.

	MM pts	HD
FGFR3	0.002	0.000
CCND1	<0.001	0.309
IGH	<0.001	<0.001
TGFBR2	0.216	0.431

MM pts - multiple myeloma patients; HD - healthy donors

p-values obtained from two-sided Kolmogorov-Smirnov tests

2.3.2 Relative positioning of translocation-prone gene loci (TPGL) *IGH*, *FGFR3*, and *CCND1* in the interphase nucleus of HPC and B-cells

2.3.2.1 TPGL are closer in MM-derived B-cells than in HPC from patients or subsets from HD

To provide a definitive measurement of proximity, we determined the average intergene distance for each potential translocation pair, by measuring distance between the centers of mass (Figure 2-7) for three pairs: *IGH:FGFR3, IGH:CCND1,* and *IGH:TGFBR2;* in HPC from patients or HD (Figure 2-8A), and in B-cells from patients or HD (Figure 2-8B).

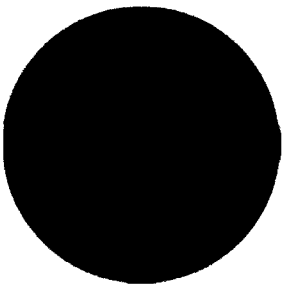

Figure 2-7: Determination of average intergene distances. The average intergene distance was determined by measuring the 4 possible distances between the centers of mass of each of the two different loci (red and green) and calculating the average of the 4 distances.

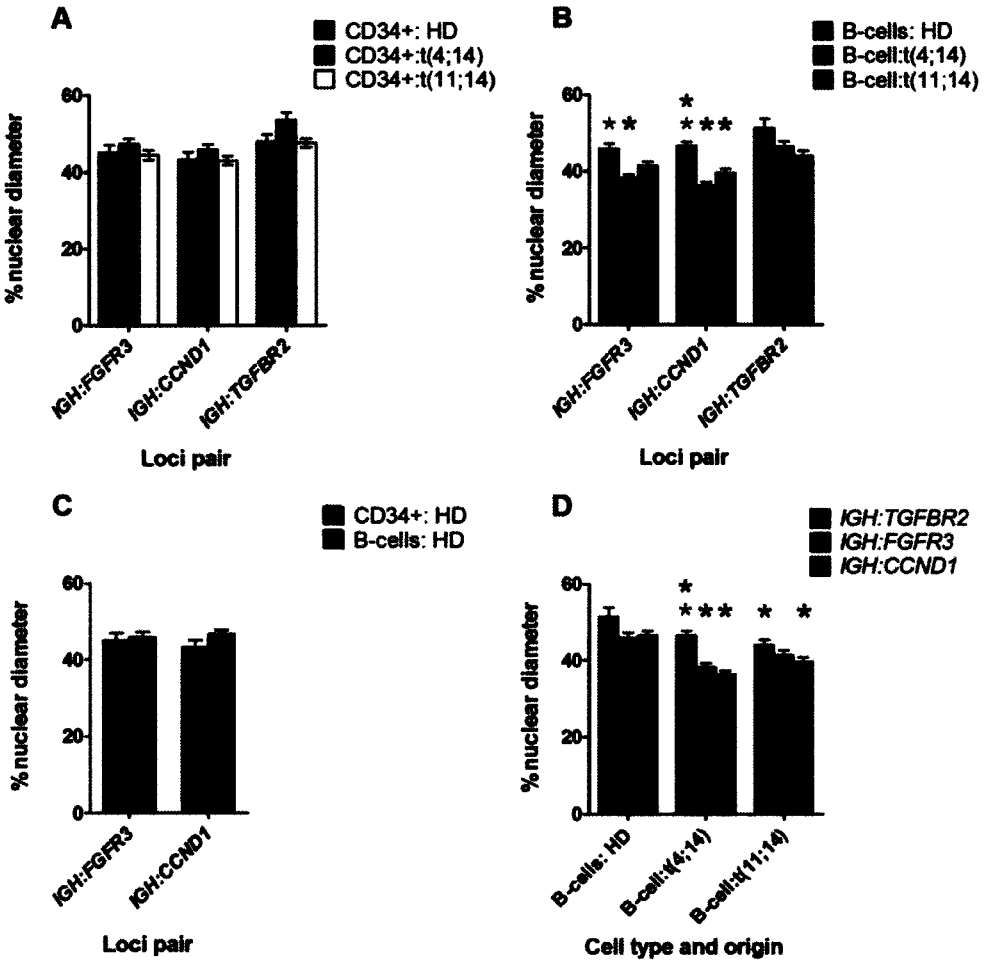

Figure 2-8: Average intergene distances (AGD) between loci in HPC and B-cells. [nuclear diameter] (A) Comparison of AGD for each loci pair in HPC from MM patients and HD. (B) Comparison of AGD for each loci pair in B-cells from MM patients and HD. (C) Comparison of AGD for each loci pair in HPC and B-cells from HD. (D) AGD of TPGL, *IGH:FGFR3* and *IGH:CCND1*, as compared to *IGH* and control locus *TGFBR2*, in B-cell subsets. (B) and (D) present different comparisons of the same data. Pairwise comparisons of the AGD obtained using two-sided Kolmogorov-Smirnov tests. Coloured asterisks correspond to bars of the same colour. A coloured asterisk above a bar indicates a significant difference in the

frequency depicted by the bar as compared to the frequency depicted by the bar corresponding to the colour of the asterisk.

We applied pairwise statistics (two-sided Kolmogorov-Smirnov test) to compare each average intergene distance for each patient type and each average intergene distance for HD. No significant differences in average intergene distances was observed between patient HPC (regardless of translocation type) and HD HPC (Figure 2-8A) (Table 2-4).

Table 2-4: Average intergene distances as fraction of the equivalent nuclear diameter [%] and pairwise comparison of the intergene distances in HPC and B-cells from HD and MM patients.

	HD	MM pts t(4;14)	*p*-value	HD	MM pts t(11;14)	*p*-value
IGH:CCND1	43.2	45.8	0.544	43.2	43.0	0.701
B-cells - average distance (% nuclear diameter)						
IGH:FGFR3	45.9	38.2	<0.001	45.9	41.4	0.053
IGH:TGFBR2	51.4	46.5	0.055	51.4	44.0	0.026

MM pts - multiple myeloma patients; HD - healthy donors

p-values obtained from two-sided Kolmogorov-Smirnov tests

In contrast, in patient B-cells, *IGH:FGFR3* and *IGH:CCND1* in t(4;14) patients and *IGH:CCND1* in t(11;14) patients were significantly closer than the same genes in HD B-cells (Figure 2-8B) (Table 2-4). There was no significant difference in average intergene distances between HD HPC and HD B-cells (Figure 2-8C) (Table 2-5).

Table 2-5: Average intergene distances as fraction of the equivalent nuclear diameter [%] and pairwise comparison of the intergene distances in HPC and B-cells from HD.

Locus pair	HD HPC	HD B-cells	*p*-value
IGH:FGFR3	45.0	45.0	0.861
IGH:CCND1	43.2	46.6	0.247
IGH:FGFR3	48.0	51.4	0.150

HD - healthy donors

p-values obtained from two-sided Kolmogorov-Smirnov tests

These data demonstrate that average intergene distances are not significantly different among HPC from patients and HD, or HD B-cells. *IGH:FGFR3* and *IGH:CCND1* are significantly more proximal in patient B-cells than in patient HPC, HD HPC or HD B-cells.

2.3.2.2 IGH:FGFR3 and IGH:CCND1 have smaller intergene distances than the IGH:TGFBR2 control in patient B-cells but not in HD B-cells

We applied pairwise statistics to compare the following average intergene distances to one another: *IGH:FGFR3* vs. *IGH:TGFBR2; IGH:CCND1* vs. *IGH:TGFBR2;* and *IGH:FGFR3* vs. *IGH:CCND1* (Figure 2-8D) (Table 2-6).

Table 2-6: Pairwise comparison of loci pair average intergene distances in B-cells from HD and MM patients.

(intergene distances compared)		HD	MM pts t(4;14)	MM pts t(11;14)
IGH:FGFR3	*IGH:TGFBR2*	0.067	<0.001	0.266
IGH:FGFR3	*IGH:CCND1*	0.437	0.610	0.068

MM pts - multiple myeloma patients; HD - healthy donors

p-values obtained from two-sided Kolmogorov-Smirnov tests

In t(4;14) patients, *IGH:FGFR3* and *IGH:CCND1* intergene distances were smaller than the *IGH:TGFBR2* intergene distance. In t(11;14) patients, *IGH* and *CCND1* were closer together than *IGH* and *TGFBR2*. The three comparisons were made in B-cells from HD and no differences were observed. Collectively, this analysis of TPGL average intergene distances

suggests that the distance between *IGH* and the two translocation-prone gene loci may influence translocation potential in patient-derived B-cells.

2.4 DISCUSSION

We characterized the radial and relative positioning of TPGL and a negative control locus to better understand the role of nuclear location and spatial proximity in the genesis of translocations. Specifically, we wanted to investigate the influence of genome positioning on translocation potential, using ex-vivo cells from multiple myeloma patients as our "model". Our working hypothesis was that spatial positioning in the nucleus might differ in patient-derived cells as compared to the same subsets from HD. Our working assumption was that TPGL positioning in presumptively normal cells from cancer patients reflects "favoured" pairing that in the past may have facilitated *IGH* translocations and ultimately cancer. 3-D FISH imaging and quantitative analysis of gene radial positioning in normal HPC and B-cells from patients with MM shows that TPGL appear to have an intrinsically interior position within the nucleus, and that the control locus, *TGFBR2* is more peripherally located. We

demonstrate that the radial positioning of TPGL among HD HPC, HD B-cells and patient HPC is significantly different from that in patient B-cells, even though the spatial position of the negative control locus *TGFBR2* is static among all cell types. We provide evidence that the translocation-prone loci, *FGFR3, CCND1,* and *IGH* in patient-derived B-cells are positioned significantly more internally in the interphase nucleus as compared to HPC from HD or MM patients and B-cells from HD, indicating patient-specific positioning of TPGL in B-cells. By extrapolation, patient-specific positioning of TPGL in patient B-cells may in the past have predisposed cells to the *IGH* translocations that are characteristic of the malignant clone in these MM patients.

A specific translocation requires that three events occur: (1) formation of DNA double strand breaks (DSBs) in specific potential partner loci, (2) proximity of broken ends of the same specific loci, and (3) illegitimate joining of the heterologous ends[18,19]. The mechanisms by which the broken ends of chromosomes at specific loci come into contact in the nucleus of the cell are not yet known. Currently, two hypotheses exist: the 'contact-first' model suggests that the interaction necessary to produce translocations between DSBs at specific loci on different chromosomes

can only take place when the loci co-localize in the nucleus[1]. Conversely, the 'breakage-first' model proposes that DSBs at specific loci on different chromosomes form at distant sites and that the broken DNA ends can roam the nuclear space to "find" potential partners for translocations[20]. In support of the 'contact-first' model, it has recently been demonstrated that the DNA ends at double strand breaks remain positionally immobile[21], supporting the idea that translocation-prone loci pairs must be in close proximity to undergo translocations.

The data presented here support the 'contact-first' model in which spatial proximity of TPGL contributes to the formation of translocations. In B-cells from patients with t(4;14) myeloma, *IGH* and *FGFR3*, and *IGH* and *CCND1* are significantly closer to one another than in the other cell subsets, and significantly closer than *IGH* and the control locus, *TGFBR2*. In B-cells from patients with t(11;14) myeloma, *IGH* and *CCND1* are significantly closer to each other than in the remaining cell subsets, and significantly closer than *IGH* and *TGFBR2*. We do not, however, observe a difference in the average intergene distances between HPC from HD and MM patients; or between HD HPC and HD B-cells. Collectively, these data suggest that spatial proximity may influence translocation potential in

B-cells from MM patients, and a bias towards translocations involving *IGH*, *FGFR3*, and *CCND1*, that is not observed in B-cells from HD or in HPC from patients or HD. It is probable that the spatial organization of TPGL in patient-derived B-cells was similar in the original B-cell which gave rise to the malignant clone in MM, and thus influenced the selection of the *IGH* translocation partner within that cell.

Although spatially proximal, translocations have not been reported involving *FGFR3* and *CCND1*, suggesting that an additional mechanism, most likely involving *IGH*, is necessary for translocations to occur. Recent reports indicate that ongoing transcription is necessary for functional activity of *IGH* diversification enzymes[22-24], and that these same enzymes have off-target effects on proximal genes[25-28]. This report of patient-specific positioning of TPGL in B-cells from t(4;14) and t(11;14) MM patients supports the likelihood that translocations occur only in specific sites within the nucleus. *IGH* and one of its translocation partners, *FGFR3* or *CCND1* may come together briefly to a 'transcription factory'[29-31], be acted upon by the diversification enzymes to create simultaneous DSBs, and be aberrantly repaired by non-homologous or alternative end-joining to create specific translocations. We speculate that patient-specific

positioning of active TPGL in B-cells from MM patients may promote the formation of clinically important *IGH* translocations, perhaps through co-localization of TPGL to nuclear transcription factories. Additional experimentation will further elucidate this idea.

2.5 REFERENCES

1. Nikiforova MN, Stringer JR, Blough R, Medvedovic M, Fagin JA, Nikiforov YE. Proximity of chromosomal loci that participate in radiation-induced rearrangements in human cells. Science. 2000;290:138-141.
2. Parada LA, McQueen PG, Misteli T. Tissue-specific spatial organization of genomes. Genome Biol. 2004;5:R44.
3. Neves H, Ramos C, da Silva MG, Parreira A, Parreira L. The nuclear topography of ABL, BCR, PML, and RARalpha genes: evidence for gene proximity in specific phases of the cell cycle and stages of hematopoietic differentiation. Blood. 1999;93:1197-1207.
4. Roix JJ, McQueen PG, Munson PJ, Parada LA, Misteli T. Spatial proximity of translocation-prone gene loci in human lymphomas. Nat Genet. 2003;34:287-291.
5. Soutoglou E, Misteli T. On the contribution of spatial genome organization to cancerous chromosome translocations. J Natl Cancer Inst Monogr. 2008:16-19.
6. Szczepek AJ, Seeberger K, Wizniak J, Mant MJ, Belch AR, Pilarski LM. A high frequency of circulating B cells share clonotypic Ig heavy-chain VDJ rearrangements with autologous bone marrow plasma cells in multiple myeloma, as measured by single-cell and in situ reverse transcriptase-polymerase chain reaction. Blood. 1998;92:2844-2855.
7. Hepperger C, Otten S, von Hase J, Dietzel S. Preservation of large-scale chromatin structure in FISH experiments. Chromosoma. 2007;116:117-133.
8. FISH Chromosome Search. Abbott Park: Abbott Molecular; 2010.
9. Recommendations for FISH in multiple myeloma: http://www.cytogenetics.org.uk/prof_standards/myeloma.htm; Mar 11, 2005.

10. Fonseca R, Barlogie B, Bataille R, et al. Genetics and cytogenetics of multiple myeloma: a workshop report. Cancer Res. 2004;64:1546-1558.

11. Solovei I, Cavallo A, Schermelleh L, et al. Spatial preservation of nuclear chromatin architecture during three-dimensional fluorescence in situ hybridization (3D-FISH). Exp Cell Res. 2002;276:10-23.

12. Cremer M, Grasser F, Lanctot C, et al. Multicolor 3D Fluorescence In Situ Hybridization for Imaging Interphase Chromosomes. Methods Mol Biol. 2008;463:205-239.

13. Holmes TJ, Bhattacharyya, S., Cooper, J.A., Hanzel, D., Krishnamurthi, V., Lin, W., Roysam, B., Szarowski, D.H., Turner, J.T. Light Microscopic Images Reconstructed by Maximum Likelihood Deconvolution. In: Pawley J, ed. The Handbook of Biological Confocal Microscopy (ed 2nd Edition). New York: Plenum Press; 1995.

14. Biggs DCS. Clearing Up Deconvolution
Biophotonics International
2004:32-37.

15. Harizanova J, Taylor-Kashton C, Mai S. Summary of the quantitative analyses of the three-dimensional distribution of chromosomes in mouse cells. AACR; 2008.

16. Ridler TW CS. Picture thresholding using an iterative selection method. IEEE Trans on Systems, Man and Cybernetics 1978;SMC-8:630-632.

17. Sarkar R GA, Vermolen BJ, Garini Y, Mai S. . Alterations of Centromere Positions in Nuclei of Immortalized and Malignant Mouse Lymphocytes. Cytometry Part A 2007;71A:386-392.

18. Martin LD, Belch AR, Pilarski LM. Promiscuity of translocation partners in multiple myeloma. J Cell Biochem;109:1085-1094.

19. Nussenzweig A, Nussenzweig MC. Origin of chromosomal translocations in lymphoid cancer. Cell;141:27-38.

20. Aten JA, Stap J, Krawczyk PM, et al. Dynamics of DNA double-strand breaks revealed by clustering of damaged chromosome domains. Science. 2004;303:92-95.

21. Soutoglou E, Dorn JF, Sengupta K, et al. Positional stability of single double-strand breaks in mammalian cells. Nat Cell Biol. 2007;9:675-682.

22. Peters A, Storb U. Somatic hypermutation of immunoglobulin genes is linked to transcription initiation. Immunity. 1996;4:57-65.

23. Fukita Y, Jacobs H, Rajewsky K. Somatic hypermutation in the heavy chain locus correlates with transcription. Immunity. 1998;9:105-114.

24. Schrader CE, Guikema JE, Linehan EK, Selsing E, Stavnezer J. Activation-induced cytidine deaminase-dependent DNA breaks in class switch recombination occur during G1 phase of the cell cycle and depend upon mismatch repair. J Immunol. 2007;179:6064-6071.

25. Pasqualucci L, Neumeister P, Goossens T, et al. Hypermutation of multiple proto-oncogenes in B-cell diffuse large-cell lymphomas. Nature. 2001;412:341-346.

26. Robbiani DF, Bothmer A, Callen E, et al. AID is required for the chromosomal breaks in c-myc that lead to c-myc/IgH translocations. Cell. 2008;135:1028-1038.

27. Liu M, Duke JL, Richter DJ, et al. Two levels of protection for the B cell genome during somatic hypermutation. Nature. 2008;451:841-845.

28. Tsai AG, Lu H, Raghavan SC, Muschen M, Hsieh CL, Lieber MR. Human chromosomal translocations at CpG sites and a theoretical basis for their lineage and stage specificity. Cell. 2008;135:1130-1142.

29. Branco MR, Pombo A. Intermingling of chromosome territories in interphase suggests role in translocations and transcription-dependent associations. PLoS Biol. 2006;4:e138.

30. Osborne CS, Chakalova L, Brown KE, et al. Active genes dynamically colocalize to shared sites of ongoing transcription. Nat Genet. 2004;36:1065-1071.

31. Lever E, Sheer D. The role of nuclear organization in cancer. J Pathol;220:114-125.

Chapter Three: Locus positioning in the interphase nucleus suggests more random events generate t(14;16) as compared to t(4;14) or t(11;14) translocations in multiple myeloma

Parts of this chapter were presented in an oral session at the American Society of Hematology annual meeting (Orlando, December 2010). Lorri D. Martin, Jana Harizanova, George Zhu, Andrew Belch, Sabine Mai, and Linda M. Pilarski. Cancer-Specific Nuclear Positioning of Translocation Prone Gene Loci In Non-Malignant B-Cells From Patients with Multiple Myeloma. Blood (ASH Annual Meeting Abstracts). Nov 2010; 116:783. Lorri D Martin was presented with an ASH travel award for this work, and was awarded the Canadian Hematology Society Research Award: PhD and Post-Doctoral Category.

L.D. Martin designed the research, conducted experiments, performed data analysis and data presentation, organized statistical analysis, and wrote the Chapter. 3-D analysis software design and statistical analysis were contributed by others.

3.1 INTRODUCTION

Multiple myeloma (MM) is a fatal malignant tumour of terminally differentiated B-cells that results in the accumulation of malignant plasma cells (PCs) in the bone marrow (BM). Karyotypic instability, including chromosomal translocations, is a hallmark of MM. The translocations most frequently involve the *IGH* locus at 14q32, as with many B-cell malignancies[1,2], and are believed to be mediated by errors in *IGH* rearrangements and DNA repair processes[3,4]. Although most other B-cell malignancies harbour a single, specific *IGH* translocation partner, MM displays a promiscuity of recurrent partners with *IGH*. These include *CCND1* (t11;14)(q13;q32), *FGFR3* t(4;14)(p16;q32), and *c-MAF* t(14;16)(p16;q32). These recurrent translocations are considered primary events in transformation[5], and occur with different clinical frequencies: t(11;14) - 20%; t(4;14)- 15%; and t(14;16) - 5%.

The mechanisms of locus selection for participation in chromosome translocations is poorly understood; it is known, however, that genes proximal to one another are more likely to participate in a translocation

event than those which are distal. Loci positioning in relation to chromosome translocations has only recently been addressed in the context of MM where we determined that the gene loci most frequently involved in translocations in MM, *IGH*, *FGFR3*, and *CCND1* [termed translocation-prone gene loci (TPGL)] display patient-specific positioning, and are closer together in the nucleus than a negative control locus, *TGFBR2*, in normal, non-translocated B-cells from t(4;14) and t(11;14) patients as compared to B-cells from healthy donors (HD) (Chapter 2). This correlation between spatial proximity and translocation potential is supported by earlier work with murine models[6,7] and heterogenous cell subsets[8,9]. Furthermore, in an EBV-transformed B lymphoblastoid cell line, spatial proximity of genetic loci in the interphase nucleus correlated with translocation frequency in patients with lymphoma[10].

The nuclear and relative positioning of *IGH*, *FGFR3*, *CCND1*, *c-MAF*, and the control locus, *TGFBR2* have not been characterized in B-cells from t(14;16) MM; nor has the positioning of *c-MAF* been characterized in B-cells from t(4;14) and t(11;14) patients. It is not known whether the spatial positioning of *c-MAF* in relation to *IGH* influences translocation potential of these two loci in B-cells from MM patients. Based on our previous work,

we considered the possibility that *IGH* and *c-MAF* would be closer together than *IGH* and *FGFR3*, or *IGH* and *CCND1* in the nucleus of B-cells from t(14;16) patients. Alternatively, *IGH* and *c-MAF* could be closer together in B-cells from t(14;16) patients than in B-cells from t(4;14) and t(11;14) patients. In either scenario, the spatial proximity of *c-MAF* with *IGH* could influence the translocation potential of that locus in cells from t(14;16) patients. A third possibility was that *FGFR3*, *CCND1*, and *c-MAF* would be equally close to, or equally distant from *IGH* in the nucleus of B-cells from all MM translocation types tested, which would suggest that selection of a specific translocation partner based on spatial proximity was a random event, and that additional factors influenced partner selection.

To determine the consistency of *IGH* and TPGL positioning among translocation subtypes of MM patients, we utilized 3-D FISH and 3-D analysis techniques. We investigated loci positioning in normal, non-translocated B-cells from MM patients and HD to determine whether genome organization influences translocation potential. The comparison of radial and relative positioning patterns in normal cells from MM patients and HD enables us to further evaluate the hypothesis that genome organization, particularly the existence or not of "favoured" translocation

partners, differs in patient-derived normal cells as compared to HD, and influences translocation potential of specific gene loci with *IGH* in a patient-specific manner.

In contrast to the other patient subtypes t(4;14) and t(11;14), we observed that the relative and radial positions of TPGL and the control locus are not significantly different in B-cells from t(14;16) patients as compared to HD. We determined that *c-MAF* maintains a consistent peripheral average radial position in B-cells from MM patients that is not different from its positioning in HD. Unlike positioning in the nucleus of cells from t(4;14) and t(11;14) patients, *IGH* is equivalently distal to all recurrent potential translocation partners in B-cells from t(14;16) patients. *IGH* and *c-MAF* are significantly further apart in B-cells from all translocation types than is the case for *IGH* and *FGFR3* in cells from t(4;14) patients, or *IGH* and *CCND1* in t(11;14) patients. These findings suggest: (i) a bias against the formation of a translocation involving *IGH* and *c-MAF* existed in the B-cells of patients who ultimately developed *IGH/FGFR3* or *IGH/CCND1* translocations; and (ii) in the original B-cell that acquired a t(14;16) translocation, selection of a translocation partner may have been a

relatively random event, reflected in the lower clinical frequency of t(14;16) myeloma, as compared to t(11;14) or t(4;14) myelomas.

3.2 MATERIALS/METHODS

3.2.1 Materials

The institutional review boards of the University of Alberta, and Alberta Health Services approved this study. Written informed consent was obtained from 55 patients presenting at the Cross Cancer Institute, according to the Declaration of Helsinki. Peripheral blood (PB), and G-CSF mobilized blood (MB) samples were collected from patients during clinical visits. Human lymphocytes were isolated from 5 healthy donors (HD). Ficoll-Pacque™ was from Pfizer (New York, NY). CD19 antibody was FMC63[11]. EasySep® immunomagnetic purification reagents and magnets were purchased from Stem Cell Technologies (Vancouver, BC). BAC probes were purchased from Empire Genomics (Buffalo, NY), and fluorescent in situ hybridization probes were from Vysis® (Abbott Laboratories, Abbott Park, IL).

3.2.2 Cell isolation

Mononuclear cells were isolated from all samples using Ficoll-Paque™ gradient separation as per the manufacturer's instructions. For 3-D FISH, B-cells were isolated from PB and MB samples using a human CD19 immunomagnetic selection kit from Stem Cell Technologies (Vancouver, BC) according to manufacturer's instructions. A representative sample from each purified population was stained with CD19-FITC and analyzed by FACSort® (BD Biosciences, Franklin Lakes, NJ) to confirm purity. Purity in patient B-cells ranged from 90-99% (mean=96%), and from 83-99% (mean=93%) in HD B-cells. Following purification, cells were suspended in 50% FBS/RPMI solution for adhesion to poly-L-lysine coated slides.

3.2.3 Two-dimensional (2-D) FISH

2-D FISH was used as a first step to identify patients with PCs positive for t(4;14), t(11,14), and t(14;16) for subsequent study. The method has been described previously (Chapter 2). Four commercial Vysis® probe sets (Abbott Laboratories, Abbott Park, IL) were used for each BM sample: LSI IGH dual colour break apart probe for the detection of chromosome breakage at the 14q32 locus; and three LSI dual colour, dual fusion

probes: IGH/FGFR3 for the detection of t(4;14)(p16;q32); IGH/CCND1 XT for the detection of t(11;14)(q13;q32), and IGH/c-MAF for the detection of t(14;16)(q32;q23). For simplicity, the latter three probe sets will be referred to as *IGH:FGFR3*, *IGH:CCND1*, and *IGH:c-MAF* respectively, and loci identified as *FGFR3, CCND1*, *c-MAF,* and *IGH* for the remainder of the paper. Denaturation and hybridization was performed according to manufacturer's instructions. The slide was counterstained using DAPI-containing VECTASHIELD® (Abbott Laboratories, Abbott Park, IL). FISH analysis and recording was done according to recommendations for FISH in MM[12,13].

3.2.4 Three-dimensional (3-D) FISH

Three commercial probe sets (*IGH:FGFR3*, *IGH:CCND1,* and *IGH:c-MAF*) and one commercial BAC probe (Empire Genomics Cy5-labelled RP11-1080C17) for *TGFBR2* (negative control locus) were employed for 3-D FISH. The *TGFBR2* BAC probe was used in conjunction with the *IGH:CCND1* probe for *IGH:TGFBR2* analyses.

Cell adhesion, fixation, and permeabilization were performed as previously described for cells in suspension[14], with minor modifications (for a

complete methodology, see Chapter 2). 10 μl of desired probe(s) was added to the target area, cover-slipped, and sealed with rubber cement. Nuclei on the slide were co-denatured with probe at 75°C for 5', and hybridized in a moist chamber for 18-48 h at 37°C. Post-hybridization, slides were washed in 2x SSC at 37°C with shaking for 3x 5', and then in 0.1x SSC at 60°C with shaking for 3x 5'. Slides were rinsed briefly in 2x SSC at RT, and then mounted with coverslips using DAPI-containing VECTASHIELD® mounting medium (Abbott Laboratories, Abbott Park, IL).

3.2.5 Image acquisition

Images of 2-D May-Grunwald/Giemsa stained slides were acquired using a 40x (NA 0.75) dry objective lens on a Zeiss Axioplan 2 upright microscope as part of the Duet® imaging system (Bioview Ltd., Rehovot, Israel). 2-D FISH images were acquired using the 63x (NA 0.95) dry objective lens. For 3-D FISH, 3-D z-stacks were acquired using 63x (NA 1.4) oil objective lens on a Zeiss LSM 710 confocal microscope with Zen 2009 acquisition software set at scan zoom x3, pixel size 0.9 μm x 0.9 μm, with an optical step size of 0.2 μm. Z stacks of 810 nuclei from 8 MM patients, and 210 nuclei from 5 HD were analyzed in this study (see Table

1). To enhance the signal-to-noise ratio of the images and to decrease background noise, images were subsequently deconvolved using Huygens Essential deconvolution software (Scientific Volume Imaging, Netherlands). The program utilizes classic maximum likelihood estimation with a theoretical point spread function[15,16].

3.2.6 Quantitative analysis of FISH signal distributions

The quantitative data analyses were performed using ChromoView software[17], based on MATLAB (The MathWorks, USA) and DIPimage toolbox (Quantitative Imaging Group, TU-Delft, The Netherlands). The multidimensional image data sets were linearly resampled in the axial direction to obtain isotropic voxel size. The loci and cell nucleus were segmented with an isodata threshold[18].

The following parameters were calculated: (i) center of mass (CM) of each locus; (ii) CM and diameter of the nucleus; (iii) Euclidian distance between CM of each loci pair as a fraction of the equivalent nuclear radius; (iv) radial position of segmented object with respect to the nucleus center; and (v) presence of overlap in segmented loci. The equivalent radius was

defined as the geometric mean of the radii of 2 equivalent spheres, with respectively the same surface area and the same volume as the nucleus.

To assess radial position of the object within the nucleus, a radial arm D_N was projected from the nuclear CM toward the nuclear boundary passing through the CM of the locus[19]. The distance D_i of the region in respect of the nucleus center was estimated as a fraction of the radial arm D_N, as $D_i = D_0 / D_N$, where D_O is Euclidian distance between CM of each locus and the CM of the nucleus. The distance D_i denotes the radial shell where the locus is located.

3.3 RESULTS

3.3.1 The radial positioning of TPGL in B-cells from t(14;16) patients does not differ from that in B-cells from HD

We first investigated the average radial position of TPGL, *FGFR3*, *CCND1*, *c-MAF*, and the negative control locus, *TGFBR2*, in B-cells isolated from t(14;16) MM patients and HD using 3-D FISH. Loci were visualized in 420 individual cells (Table 3-1) to produce 3-D z-stacks using a confocal laser scanning microscope; none of these cells harboured

translocations. We characterized the average radial position of each locus in the nuclear volume by measuring the distance of each fluorescent signal from the nuclear center (Figure 2-2). The radial position of each locus was normalized to the size of each nucleus, and only nuclei with two signals per gene were analyzed. The average radial position of each locus in the interphase nucleus in B-cells from t(14;16) MM and from HD is presented in Table 3-2.

Table 3-1: B-cell origin of samples and number of nuclei analyzed per probe by 3-D FISH.

	t(4;14) (pts=3)	t(11;14) (pts=3)	t(14;16) (pts=2)	HD (dnrs=3)
CT11:*CCND1*	90 (*n*=3)	90 (*n*=3)	60 (*n*=2)	60 (*n*=2)
CT3:*TGFBR2*	30 (*n*=1)	30 (*n*=1)	30 (*n*=1)	30 (*n*=1)

MM - multiple myeloma; pts - patients; HD - healthy donors; dnrs - donors
n= number of patients or donors tested per probe type (30 cells per patient or donor)
All B-cells purified from peripheral blood, except for B-cells from t(14;16) patients which were purified from mobilized blood

---

On average, *CCND1* and *IGH* localized most internally in a shell at ~57% of the radius. The average radial position of *FGFR3* was in a shell at ~65% of the radius and *c-MAF* at ~67% of the radius. The negative control locus, *TGFBR2*, displayed the most peripheral radial position at

---

Table 3-2: Average radial position [% of the radius] of TPGL and the control locus *TGFBR2* in the interphase nucleus of B-cells from t(14;16) patients or HD, and pairwise comparison of the relative radial distribution (RRD) of *IGH* and TPGL or *TGFBR2* and TPGL.

		t(14;16) pts			HD		
IGH	*FGFR3*	56.7	65.3	<0.001	52.8	59.7	<0.001
IGH	*c-MAF*	56.7	68.4	<0.001	52.8	65.7	<0.001
TGFBR2	*FGFR3*	70.0	65.3	0.089	71.4	59.7	0.013
TGFBR2	*c-MAF*	70.0	68.4	0.945	71.4	65.7	0.172

pts - patients; HD - healthy donors

p-values obtained from two-sided Kolmogorov-Smirnov tests

~70% of the radius. In B-cells from HD, the average position of *IGH* was a shell at ~53% of the radius. *FGFR3*, and *CCND1* occupied similar radial

shells at ~60% of the average radius. On average, *c-MAF* localized to a radial shell at ~66% of the radius and *TGFBR2* at ~71% of the radius. Figure 3-1 depicts the relative radial distributions (RRD) (Figure 2-2) of each gene locus in B-cells from t(14;16) patients (Figure 3-1A) and B-cells from HD (Figure 3-1B).

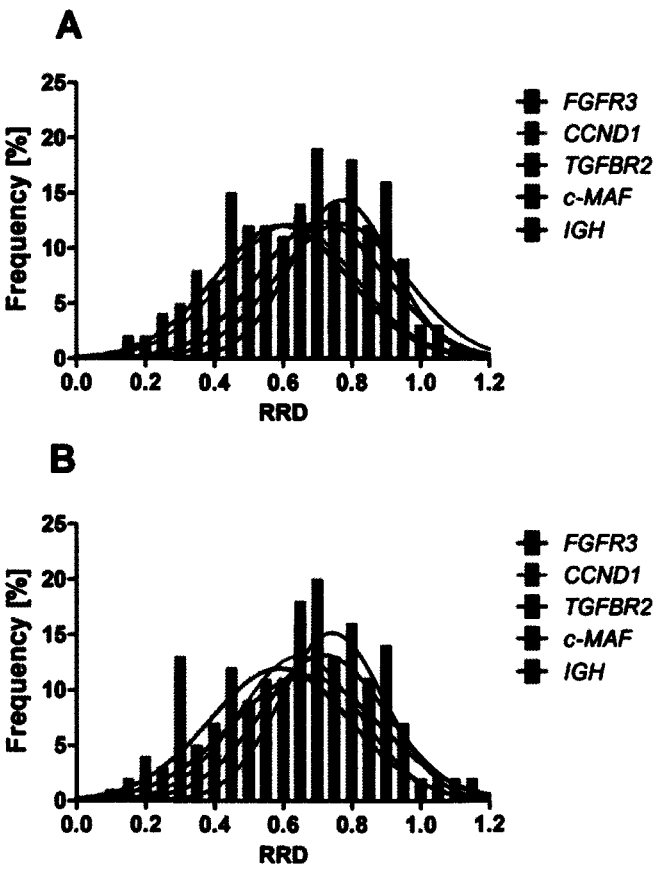

Figure 3-1: Non-random radial positioning of gene loci in the nucleus of B-cells from t(14;16) MM patients or HD. Gene loci were detected in PFA-

fixed cells using commercial dual-fusion or commercial BAC probes. (**A**) Relative radial distribution of the translocation-prone gene loci (TPGL), *IGH, FGRF3, CCND1, c-MAF* and the control locus, *TGFBR2* in B-cells from t(14;16) patients. (**B**) Relative radial distribution of the TPGL and the control locus, *TGFBR2* in B-cells from HD. The average radial position of *IGH, FGRF3, CCND1, c-MAF,* and the control locus, *TGFBR2* is not different between the cell subsets. *c-MAF* and *TGFBR2* maintain a peripheral distribution in B-cells from t(14;16) patients and HD.

We wanted to analyze the radial position of the translocation partners *FGFR3*, *CCND1*, and *c-MAF* relative to *IGH*, and relative to the control locus *TGFBR2* in B-cells from t(14;16) patients and in HD. We used the cumulative frequencies of each locus RRD (Figure 3-2AB), and applied pairwise statistics (two-sided Kolmogorov-Smirnov test) to each locus combination (Table 3-2). B-cells from t(14;16) MM patients (Figure 3-2A) were analyzed independently of HD B-cells (Figure 3-2A). In B-cells from patients with t(14;16), each gene locus demonstrated positioning significantly different from *IGH* within the nuclear space ($p<0.001$), except for *CCND1*.

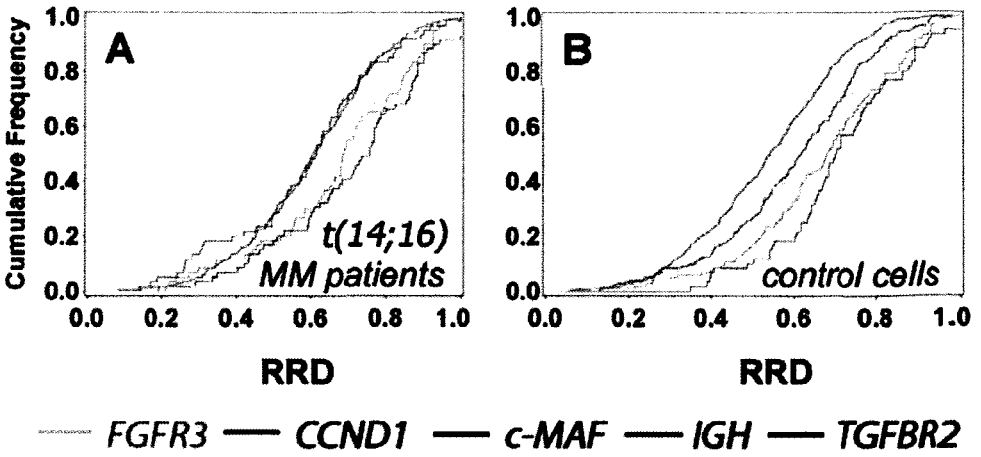

Figure 3-2: Cumulative distribution of relative radial positioning of gene loci in B-cells from t(14;16) patients and HD. Gene loci were detected in PFA-fixed cells using commercial dual-fusion or commercial BAC probes. (A) Cumulative distribution in B-cells from t(14;16) patients. *IGH* and *CCND1* occupy radial shells that are not significantly different from each other and are located more centrally in the nucleus. *FGFR3*, *c-MAF*, and *TGFBR2* are positioned in radial shells that are not significantly different from each other and are peripherally located in the nucleus. (B) Cumulative distribution in B-cells from HD. *FGFR3* and *CCND1* occupy radial shells that are significantly different than the radial shells occupied by *IGH* and *TGFBR2*. *c-MAF* and *TGFBR2* occupy shells that are not significantly different from each other and maintain peripheral positioning. Pairwise comparisons were calculated from Kolmogorov-Smirnov tests and *p*-values are listed in Table 3-3. n=60 for each TPGL for cells from t(14;16) patients and HD control cells, and n=30 for *TGFBR2* in both cell subsets.

In contrast to its proximity with *IGH*, *CCND1* occupied a radial shell significantly different from that of *TGFBR2* (p<0.001). The positions of

FGFR3 and *c-MAF* were not significantly different from that of *TGFBR2*. In B-cells from HD, all loci had positioning significantly different from *IGH* ($p<0.001$). *FGFR3*, *CCND1*, and *IGH* had radial positioning significantly different from *TGFBR2* ($p<0.02$). However, *c-MAF* and *TGFBR2* occupied radial shells that were not significantly different. These data provide evidence that *IGH* occupies a radial shell that is significantly different from those occupied by *FGFR3*, *c-MAF* and *TGFBR2* in the nucleus of B-cells from t(14;16) patients and HD. By comparison to *FGFR3*, *c-MAF*, like *TGFBR2*, is localized closer to the nuclear periphery in either B-cell subset.

We compared the RRD of *FGFR3*, *CCND1*, *c-MAF*, *IGH*, and *TGFBR2* in B-cells from t(14;16) MM patients to the RRD of the same locus in B-cells from HD (Figure 3-3ADGJM). We found no significant difference in the radial positioning of each individual locus between patient and HD B-cell subsets. This suggests that the radial positioning of each individual locus does not vary between B-cells from t(14;16) patients and B-cells from HD.

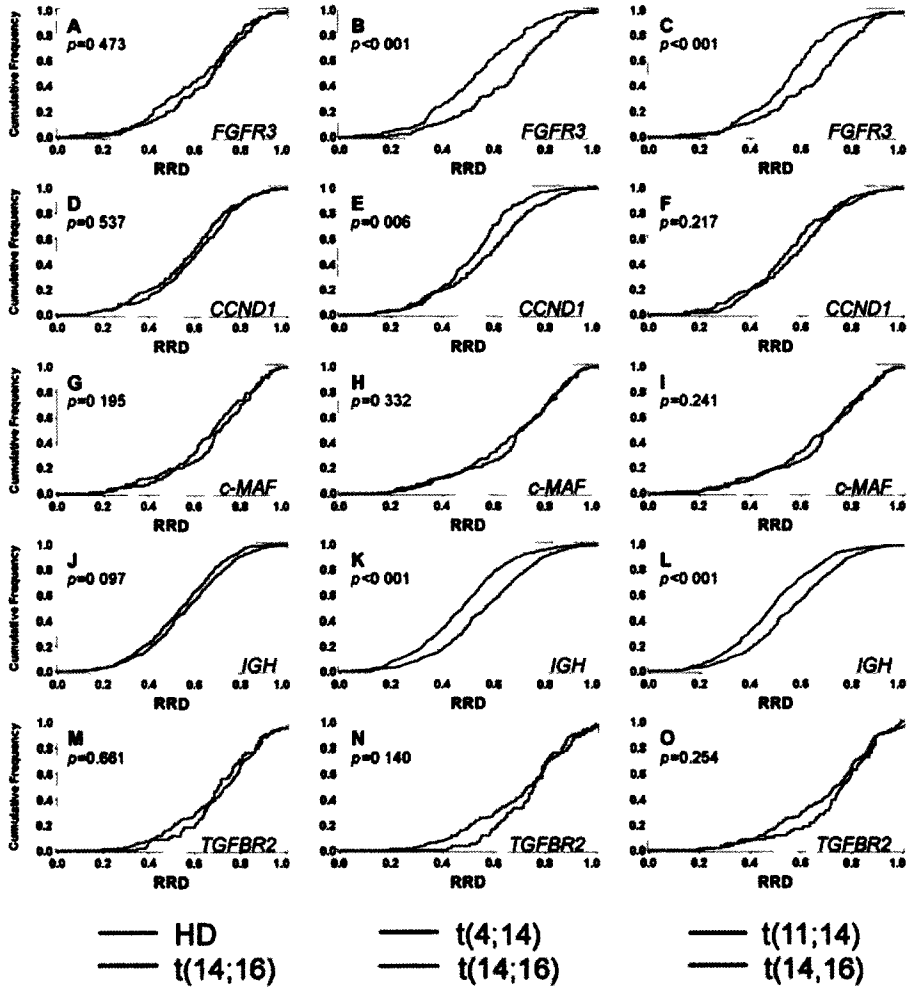

Figure 3-3: Radial distribution of translocation-prone and control genes in B-cells. 3-D FISH was performed on B-cells from MM patients and HD. Patients were categorized according to the translocation type of their plasma cells. Cumulative frequency graphs to quantify the relative radial distributions (RRD) for each gene are shown with comparison to B-cells from t(14;16) patients. (ADGJM) B-cells from HD. (BEHKN) B-cells from (4;14) patients. (CFILO) B-cells from (11;14) patients. Pairwise comparisons of cumulative radial distributions were performed using a two-sided Kolmogorov-Smirnov test. n= 60 for each TPGL for cells from

t(14;16) patients and HD, n= 90 for each TPGL for cells from t(4;14) and t(11;14) patients, and n=30 for *TGFBR2* for all cell types.

3.3.2 Like *TGFBR2*, *c-MAF* maintains a position in the nuclear periphery of B-cells from all patient translocation types

We compared the radial positioning of *FGFR3*, *CCND1*, *c-MAF*, *IGH*, and *TGFBR2* in B-cells from patients with t(14;16) to B-cells from patients with t(4;14), or t(11;14) (Figure 3-3). We utilized RRD cumulative frequencies to determine pairwise statistics for each gene locus. Two comparisons were made: (i) B-cells from t(14;16) patients and B-cells from t(4;14) patients (Figure 3-3BEHKN); and (ii) B-cells from t(14;16) patients vs. B-cells from t(11;14) (Figure 3-3CFILO). As compared to t(14;16) patients, *FGFR3* was positioned significantly more centrally in the nucleus in t(4;14) and t(11;14) patients (p<0.001 for both comparisons). *CCND1* localized more centrally in t(4;14) patients (p=0.006), and showed no difference in positioning in cells from t(11;14) patients as compared to cells from t(14;16) patients.

IGH was positioned significantly more centrally in B-cells from t(4;14) and t(11;14) patients as compared to positioning in B-cells from t(14;16)

patients (p<0.001). However, the radial positions of *TGFBR2* and *c-MAF* were not significantly different among translocation types. This provides evidence that the radial positioning of *IGH* and *FGFR3* in B-cells from t(14;16) patients is significantly different when compared to B-cells from patients with t(4;14) and t(11;14) MM, but is not significantly different when compared to HD B-cells. Furthermore, *c-MAF* maintains a peripheral position in the nucleus comparable to that of the control locus, *TGFBR2,* in all cell types tested here.

3.3.3 Spatial proximity of *IGH* and TPGL, or *IGH* and *TGFBR2* is not significantly different in B-cells from t(14;16) MM patients and HD

To quantify spatial proximity, we determined the average intergene distance for each loci pair. The average intergene distance was determined by measuring the 4 possible distances between the centers of mass of each different locus (Figure 3-4A), and calculating the average of the 4 distances for each of the three TPGL pairs, *IGH:FGFR3, IGH:CCND1,* and *IGH:c-MAF* in B-cells from t(14;16) patients and HD (Figure 3-4B). We utilized pairwise statistics (two-sided Kolmogorov-Smirnov test) to perform three comparisons for this study: (i) average

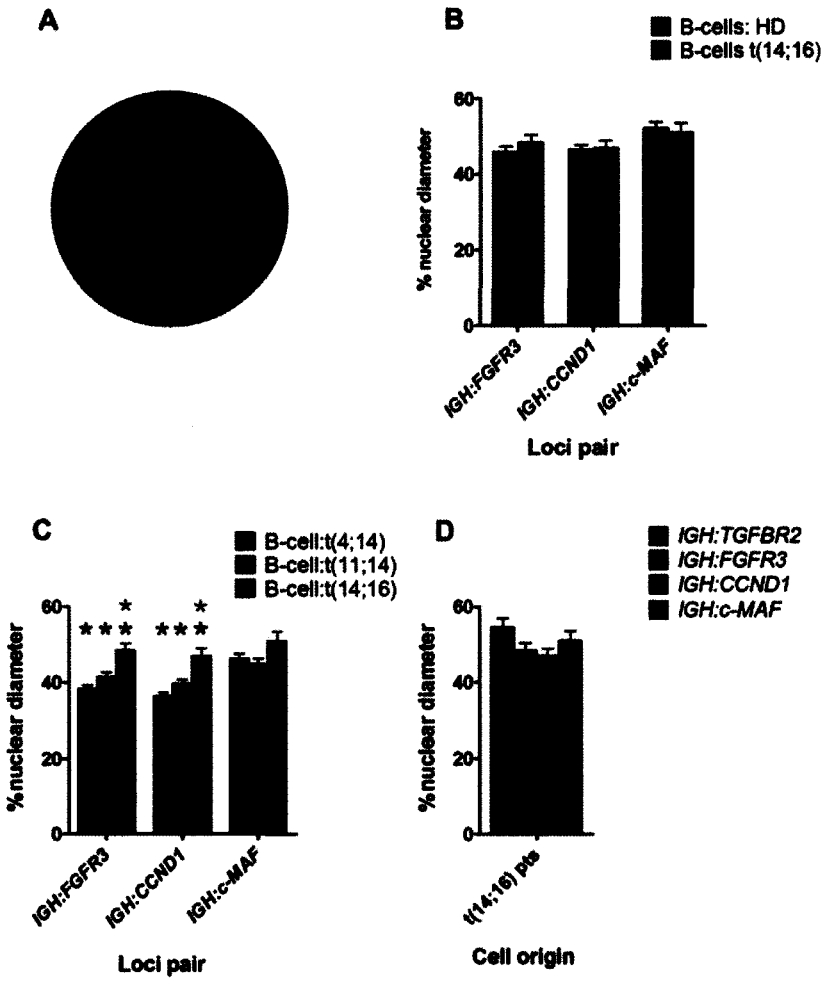

Figure 3-4: Average intergene distances (AGD) between loci as a fraction of the equivalent nuclear diameter [%] in B-cells from MM patients and healthy donors (HD). 3-D FISH was performed on B-cells from MM patients and HD. Patients were categorized according to the translocation type of their plasma cells. (A) The AGD was determined by measuring the 4 possible distances between the centers of mass of each of the two different loci and calculating the average of the 4 distances. (B) Comparison of AGD for the loci pairs shown between B-cells from t(14;16)

patients and B-cells from HD. (C) Comparison of AGD for the loci pairs shown in B-cells from each translocation type. (D) Comparison of AGD of each loci pair shown to one another in B-cells from t(14;16) patients. Pairwise comparisons of the frequencies of extra-territorial locus positioning were obtained using two-sided Kolmogorov-Smirnov tests. Coloured asterisks correspond to bars of the same colour. A coloured asterisk above a bar indicates a significant difference in the frequency depicted by the bar as compared to the frequency depicted by the bar corresponding to the colour of the asterisk. n= 3 patients for t(4;14) and t(11;14); n= 2 patients for t(14;16) and n= 3 donors for HD.

---

intergene distances for each loci pair in cells from t(14;16) patients and from HD; (ii) average intergene distances for each loci pair in cells from t(14;16) patients and from t(4;14) patients; and (iii) average intergene distances for each loci pair in cells from t(14;16) patients and from t(11;14) patients.

No significant differences were observed in the average intergene distances of each loci pair in B-cells from t(14;16) patients as compared to HD (Figure 3-4B) (Table 3-3). This differs from our analysis of t(4;14) and t(11;14) patients (Chapter 2), where we observed that the average

intergene distances between *IGH* and *FGFR3* or *IGH* and *CCND1* were significantly less than those in HD B-cells.

Table 3-3: Average intergene distances as fraction of the equivalent nuclear diameter [%] and pairwise comparison of the intergene distances in B-cells from HD and t(14;16) MM patients.

Loci pair	Average intergene distance (% of nuclear diameter)		
	B-cells		
	t(14;16) pts	HD	*p*-value
IGH:FGFR3	48.4	45.9	0.148
IGH:CCND1	45.9	46.6	0.486
IGH:c-MAF	51.0	52.3	0.840
IGH:MAFB	54.1	53.4	0.055

pts - patients; HD - healthy donors

p-values obtained from two-sided Kolmogorov-Smirnov tests

We next compared the average intergene distances of the three TPGL pairs in B-cells from patients with t(14;16) to B-cells from patients with t(4;14) or t(11;14) (Figure 3-4C) (Table 3-4). We determined that the average intergene distances between *IGH* and *FGFR3 or IGH* and *CCND1* were significantly less in B-cells from t(4;14) and t(11;14) patients than those from t(14;16) MM patients. There was no difference in the average intergene distances between *IGH* and *c-MAF* among the three

translocation types. Although *IGH* and *FGFR3* or *IGH* and *CCND1*, are further apart in B-cells from t(14;16) patients than they are in t(4;14) and t(11;14) patients, average intergene distances in cells from t(14;16) patients do not significantly differ from HD cells.

Table 3-4: Average intergene distances as fraction of the equivalent nuclear diameter [%] and pairwise comparison of the intergene distances in B-cells from MM patients.

	Average distance [% nuclear diameter]			Pairwise comparison	
	t(14;16) pts	t(4;14) pts	t(11;14) pts	*p*-value	*p*-value
IGH:CCND1	46.9	36.3	39.6	<0.001	0.014
IGH:TGFBR2	54.5	46.5	44.0	0.002	<0.001

pts - patients

p-values obtained from two-sided Kolmogorov-Smirnov tests

This accords with Chapter 2 showing that *FGFR3* and *CCND1* are closer to *IGH* in B-cells from t(4;14) and t(11;14) patients compared to HD, while disproving an interpretation that *IGH* and *FGFR3* or *IGH* and *CCND1* are "uniquely farther apart" in B-cells from t(14;16) patients.

3.3.4 *IGH* is equivalently distant from *FGFR3*, *CCND1*, *c-MAF*, or *TGFBR2* in B-cells from t(14;16) patients

Lastly, to determine whether *IGH* is closer to or further apart from *c-MAF* than to *FGFR3*, *CCND1*, or to the control locus TGFBR2 in the nucleus of B-cells from t(14;16) patients, we utilized pairwise statistics (two-sided Kolmogorov-Smirnov test) to compare three intergene distances: *IGH:FGFR3, IGH:CCND1,* and *IGH:TGFBR2*, against the average intergene distance for *IGH:c-MAF* (Figure 3-4D) (Table 3-5). We report that there are no significant differences in the average intergene distances between *IGH* and *c-MAF,* or *IGH* and *FGFR3*, *CCND1*, or *TGFBR2*, in B-cells from t(14;16) patients. The average intergene distance between *IGH* and *c-MAF,* however, was significantly greater than the average intergene distance between *IGH* and *FGFR3* in t(4;14) patients, or *IGH* and *CCND1* in t(11;14) patients (Table 3-5). This suggests that there may be a bias *against* translocations involving *IGH* and *c-MAF* in B-cells from patients with t(4;14) and t(11;14).

Table 3-5: Average intergene distances as fraction of the equivalent nuclear diameter [%] and pairwise comparisons of loci pair average intergene distances in B-cells from each translocation type subset.

Loci pair 1st	Loci pair 2nd	Average intergene distance [fraction of nuclear diameter]		
		t(14;16) patients		*p*-values
IGH:TGFBR2	*IGH:c-MAF*	54.5	51.0	0.964
IGH:FGFR3	*IGH:c-MAF*	48.4	51.0	0.964
IGH:CCND1	*IGH:c-MAF*	46.5	51.0	0.964
		t(4;14) patients		*p*-values
IGH:TGFBR2	*IGH:c-MAF*	46.5	46.2	0.736
IGH:FGFR3	*IGH:c-MAF*	38.2	46.2	<0.001
IGH:CCND1	*IGH:c-MAF*	39.5	46.2	<0.001
		t(11;14) patients		*p*-values
IGH:TGFBR2	*IGH:c-MAF*	43.5	44.9	0.964
IGH:FGFR3	*IGH:c-MAF*	41.4	44.9	0.108
IGH:CCND1	*IGH:c-MAF*	30.6	44.9	<0.001

p-values obtained from two-sided Kolmogorov-Smirnov tests

The complete analysis of average intergene distances provides evidence that, unlike its proximity to *FGFR3* and *CCND1* in t(4;14) and t(11;14) patients, *IGH* is equivalently distal to *FGFR3*, *CCND1*, *c-MAF*, and *TGFBR2* in B-cells from t(14;16) patients. These data suggest that, based on spatial proximity, there is no "favoured" translocation partner for *IGH* in t(14;16) cells.

3.4 DISCUSSION

Only 5% of MM patients with *IGH* translocations harbour PCs with t(14;16). It is not known why *c-MAF* participates in translocations with *IGH* at a substantially lower clinical frequency than do *FGFR3* or *CCND1*. Here we show, using 3-D FISH imaging and quantitative analysis of gene positioning, that *c-MAF* maintains a consistent peripheral radial positioning in the nucleus that is significantly different from the position of *IGH* in B-cells from HD and MM patients, regardless of translocation type. The radial position of *c-MAF* is not different from the radial position of the control locus, *TGFBR2*. The biological significance of the more peripheral location of *c-MAF* in the nucleus is not clear, but it may relate to gene function, as inactive genes have been shown to localize in the nuclear periphery[20,21].

We demonstrate that, unlike B-cells from patients with t(4;14) and t(11;14), where *IGH*, *FGFR3*, and *CCND1* occupy a significantly more central position in the nucleus than in HD, there is no difference in the radial positioning of *IGH*, *FGFR3*, and *CCND1* among B-cells from t(14;16)

patients and HD. This analysis provides evidence that the patient-specific central positioning of *IGH, FGFR3,* and *CCND1* seen in B-cells from patients with t(4;14) and t(11;14) is not maintained in B-cells from patients with t(14;16).

As in B-cells from HD (Chapter 2), we found that *IGH* and *FGFR3*, or *IGH* and *CCND1*, are farther apart in B-cells from t(14;16) patients than they are in B-cells from t(4;14) and t(11;14) patients. In B-cells from t(14;16) patients, we found no significant difference in the average intergene distance between *IGH:c-MAF* as compared to average intergene distances between *IGH:FGFR3*, *IGH:CCND1*, and *IGH* and the control locus, *TGFBR2*. Conversely, in B-cells from t(4;14), we observed that the average intergene distance between *IGH* and *FGFR3* was significantly less than the average intergene distance between *IGH* and *c-MAF*. Similarly, the average intergene distance between *IGH* and *CCND1* was significantly less in B-cells from t(11;14) patients than the average intergene distance between *IGH* and *c-MAF*. These data suggest that there may be a bias against the formation of translocations involving *IGH* and *c-MAF* in patients with t(4;14) and t(11;14) that is not seen in B-cells from patients with t(14;16). We conclude that individuals with t(14;16)

have a pattern of TPGL localization indistinguishable from that of HD, unlike individuals with the other recurrent *IGH* translocations, whose TPGL localization is significantly different from that in HD.

Based on the results presented here showing that no significant differences were found in the average intergene distances between *IGH* and *FGFR3*, *CCND1*, *c-MAF*, or the control locus, *TGFBR2* in B-cells from t(14;16) patients, there appears to be no physical rationale to support the hypothesis that spatial proximity influences the selection of an *IGH* translocation partner in cells from individuals who ultimately develop t(14;16) translocations. This is supported by the observation that the average radial positioning of each individual locus is the same as that in HD, where translocations rarely occur. The relative positioning of TPGL and the control locus suggests that spatial proximity, although necessary for the formation of translocations, is not the limiting factor in the selection of an *IGH* translocation partner in non-malignant B-cells from patients with t(14;16): it may be a more random choice than appears to be the case in B-cells from t(4;14) or t(11;14) patients. Furthermore, based on spatial proximity, *c-MAF* does not appear to be a favoured translocation partner in

B-cells from any of the patient types. This may provide a partial explanation for the low clinical frequency of t(14;16) (5%).

Despite these findings, *c-MAF* participates in recurrent *IGH* translocations while *TGFBR2* does not, suggesting the existence of other factors that promote t(14;16). *c-MAF* is located at 16q23, the site of FRA16D, one of the common fragile sites in the genome most sensitive to DNA breakage[22]. In human myeloma cell lines (HMCL) displaying t(14;16), four 16q23 breakpoints were positioned within FRA16D, in an area 550kb centromeric to *c-MAF*[23]. Based on experimental evidence, it has recently been hypothesized that the *IGH* V(D)J recombination enzymes, *RAG1* and *RAG2* may recognize and cleave DNA at non-B DNA structures[24], a feature shared by all fragile sites including FRA16D[25]. Furthermore, it has recently been demonstrated in a murine model that AID can induce DSBs in the fragile site containing *WWOX*)[26](the human homolog of *WWOX* is located within FRA16). *IGH* breakpoints identified on der(14) in HMCLs mapped to a switch region and to a location J_H5 in the *IGH* locus[23,27]. "Off-target" effects on either of these recombination enzymes could create simultaneous double strand breaks on the two loci, followed by aberrant repair involving non-homologous or alternative end-joining to create

t(14;16) derivative chromosomes. In B-cells from t(14;16) patients, *IGH* is no less spatially proximal to *c-MAF* than it is to *FGFR3*, *CCND1*, or the control locus, *TGFBR2*. This makes selection of *c-MAF* as a translocation partner based on spatial proximity alone, a random and infrequent event, that may be compensated by involvement of the fragile site to yield the low but readily detectable clinical frequency of t(14;16). The notion should be considered that events promoting recurrent t(14;16) translocations may be significantly different from those promoting t(4;14) or t(11;14) translocations. Translocations between *IGH* and *c-MAF* may arise only in the absence of close proximity to more frequent partners, as appears to be the case in non-malignant cells from individuals who ultimately develop t(14;16) MM.

3.5 REFERENCES

1. Fabris S, Agnelli L, Mattioli M, et al. Characterization of oncogene dysregulation in multiple myeloma by combined FISH and DNA microarray analyses. Genes Chromosomes Cancer. 2005;42:117-127.
2. Liebisch P, Dohner H. Cytogenetics and molecular cytogenetics in multiple myeloma. Eur J Cancer. 2006;42:1520-1529.
3. Martin LD, Belch AR, Pilarski LM. Promiscuity of translocation partners in multiple myeloma. J Cell Biochem;109:1085-1094.
4. Nussenzweig A, Nussenzweig MC. Origin of chromosomal translocations in lymphoid cancer. Cell;141:27-38.
5. Gabrea A, Leif Bergsagel P, Michael Kuehl W. Distinguishing primary and secondary translocations in multiple myeloma. DNA Repair (Amst). 2006;5:1225-1233.
6. Nikiforova MN, Stringer JR, Blough R, Medvedovic M, Fagin JA, Nikiforov YE. Proximity of chromosomal loci that participate in radiation-induced rearrangements in human cells. Science. 2000;290:138-141.
7. Parada LA, McQueen PG, Munson PJ, Misteli T. Conservation of relative chromosome positioning in normal and cancer cells. Curr Biol. 2002;12:1692-1697.
8. Neves H, Ramos C, da Silva MG, Parreira A, Parreira L. The nuclear topography of ABL, BCR, PML, and RARalpha genes: evidence for gene proximity in specific phases of the cell cycle and stages of hematopoietic differentiation. Blood. 1999;93:1197-1207.
9. Gandhi MS, Stringer JR, Nikiforova MN, Medvedovic M, Nikiforov YE. Gene position within chromosome territories correlates with their involvement in distinct rearrangement types in thyroid cancer cells. Genes Chromosomes Cancer. 2009;48:222-228.

10. Roix JJ, McQueen PG, Munson PJ, Parada LA, Misteli T. Spatial proximity of translocation-prone gene loci in human lymphomas. Nat Genet. 2003;34:287-291.

11. Szczepek AJ, Seeberger K, Wizniak J, Mant MJ, Belch AR, Pilarski LM. A high frequency of circulating B cells share clonotypic Ig heavy-chain VDJ rearrangements with autologous bone marrow plasma cells in multiple myeloma, as measured by single-cell and in situ reverse transcriptase-polymerase chain reaction. Blood. 1998;92:2844-2855.

12. Recommendations for FISH in multiple myeloma: http://www.cytogenetics.org.uk/prof_standards/myeloma.htm; Mar 11, 2005.

13. Fonseca R, Barlogie B, Bataille R, et al. Genetics and cytogenetics of multiple myeloma: a workshop report. Cancer Res. 2004;64:1546-1558.

14. Cremer M, Grasser F, Lanctot C, et al. Multicolor 3D Fluorescence In Situ Hybridization for Imaging Interphase Chromosomes. Methods Mol Biol. 2008;463:205-239.

15. Holmes TJ, Bhattacharyya, S., Cooper, J.A., Hanzel, D., Krishnamurthi, V., Lin, W., Roysam, B., Szarowski, D.H., Turner, J.T. Light Microscopic Images Reconstructed by Maximum Likelihood Deconvolution. In: Pawley J, ed. The Handbook of Biological Confocal Microscopy (ed 2nd Edition). New York: Plenum Press; 1995.

16. Biggs DCS. Clearing Up Deconvolution. Biophotonics International 2004:32-37.

17. Harizanova J, Taylor-Kashton C, Mai S. Summary of the quantitative analyses of the three-dimensional distribution of chromosomes in mouse cells. AACR; 2008.

18. Ridler TW CS. Picture thresholding using an iterative selection method. IEEE Trans on Systems, Man and Cybernetics 1978;SMC-8:630-632.

19. Sarkar R GA, Vermolen BJ, Garini Y, Mai S. . Alterations of Centromere Positions in Nuclei of Immortalized and Malignant Mouse Lymphocytes. Cytometry Part A 2007;71A:386-392.

20. Ragoczy T, Bender MA, Telling A, Byron R, Groudine M. The locus control region is required for association of the murine beta-globin locus with engaged transcription factories during erythroid maturation. Genes Dev. 2006;20:1447-1457.

21. Williams RR, Azuara V, Perry P, et al. Neural induction promotes large-scale chromatin reorganisation of the Mash1 locus. J Cell Sci. 2006;119:132-140.

22. Durkin SG, Glover TW. Chromosome fragile sites. Annu Rev Genet. 2007;41:169-192.

23. Chesi M, Bergsagel PL, Shonukan OO, et al. Frequent dysregulation of the c-maf proto-oncogene at 16q23 by translocation to an Ig locus in multiple myeloma. Blood. 1998;91:4457-4463.

24. Lieber MR, Raghavan SC, Yu K. Mechanistic aspects of lymphoid chromosomal translocations. J Natl Cancer Inst Monogr. 2008:8-11.

25. Burrow AA, Williams LE, Pierce LC, Wang YH. Over half of breakpoints in gene pairs involved in cancer-specific recurrent translocations are mapped to human chromosomal fragile sites. BMC Genomics. 2009;10:59.

26. Staszewski O, Baker RE, Ucher AJ, Martier R, Stavnezer J, Guikema JE. Activation-induced cytidine deaminase induces reproducible DNA breaks at many non-Ig Loci in activated B cells. Mol Cell;41:232-242.

27. Bergsagel PL, Kuehl WM. Chromosome translocations in multiple myeloma. Oncogene. 2001;20:5611-5622.

Chapter Four: Extra-territorial positioning of translocation-prone gene loci may participate in the genesis of translocations

Parts of this chapter were presented in an oral session at the American Society of Hematology annual meeting (Orlando, December 2010). Lorri D. Martin, Jana Harizanova, George Zhu, Andrew Belch, Sabine Mai, and Linda M. Pilarski. Cancer-Specific Nuclear Positioning of Translocation Prone Gene Loci In Non-Malignant B-Cells From Patients with Multiple Myeloma. Blood (ASH Annual Meeting Abstracts). Nov 2010; 116:783. Lorri D Martin was presented with an ASH travel award for this work, and was awarded the Canadian Hematology Society Research Award: PhD and Post-Doctoral Category.

L.D. Martin designed the research, conducted experiments, performed data analysis and data presentation, organized statistical analysis, and wrote the Chapter. 3-D analysis software design and statistical analysis were contributed by others.

4.1 INTRODUCTION

During the formation of the interphase nucleus in higher organisms, each chromosome decondenses to form a distinct, limited space, known as a chromosome territory (CT)[1-4]. The spatial organization of chromosome territories in the nucleus is not random, as chromosome positioning is tissue- and cell-type specific[5,6], and has been shown to correlate with gene density as well as with chromosome size[5]. Non-random positioning patterns also extend to the positioning of gene loci[7] (Chapter 2), and gene positioning can vary according to transcriptional status[8,9].

Although chromosomes occupy distinct territories, chromatin at the edges of CTs can intermingle[10], and genomic regions can "loop out" of their respective CTs[11,12]. Several studies provide compelling evidence that extra-territorial positioning (ETP) of specific genes is a contributing factor to gene regulation, as genes that "loop out" of their respective CTs are actively transcribed[8,11-13], and co-localize in transcription factories[8]. Among chromosomes that participate in translocations, the degree of intermingling has been shown to parallel their observed translocation

frequencies, providing support for the idea that intermingling correlates with translocation potential[10]. Recently, genes involved in translocations in thyroid cancer were observed to position at the periphery of their respective CTs, suggesting that the location of specific loci relative to their CTs correlates with participation in translocations[14].

We sought to investigate the idea that ETP of translocation-prone gene loci (TPGL) may influence translocation potential. Spatial proximity of genetic loci in the interphase nucleus correlates with translocation frequency[7,14,15] (Chapter 2), as proximal genes are more likely to participate in a translocation event than those which are distal. Spatial proximity of translocation partners varies in different tissues, and at different stages of differentiation[6,15,16]. Gene looping outside of CTs may be a direct mechanism by which translocation-prone genes from different chromosomes are brought into spatial proximity with one another, with translocations as the indirect consequence. In addition, the chromatin in loops has been shown to be decondensed[13], and may be more susceptible to DSBs due to its extended nature.

We investigated the role of ETP of the TPGL (Figure 1-1), *FGFR3* (4p16), *CCND1* (11q13), and *c-MAF* (16q23) in the genesis of *IGH* (14q32) translocations in multiple myeloma (MM). MM is an incurable malignant tumour of terminally differentiated B-cells characterized by the clonal expansion of plasma cells in the bone marrow. These recurrent *IGH* translocations are considered primary events in transformation[17], and occur with different clinical frequencies: t(11;14) - 20%; t(4;14)- 15-20%; and t(14;16) - 5%; thereby providing an ideal model system to investigate the hypothesis that ETP of TPGL may influence translocation potential.

Most studies of genome organization with respect to translocation potential have utilized normal cells from healthy donors (HD); the assumption being that genome positioning in normal cells from healthy donors does not differ from positioning in normal, non-translocated cells from affected patients. We have previously provided evidence that *IGH* and *FGFR3*, and *IGH* and *CCND1* are closer together in the interphase nucleus of normal B-cells from MM patients than in normal B-cells from HD, suggesting an increased translocation potential in the patient-derived cells (Chapter 2). Therefore, in this study, we characterized ETP of TPGL in normal cell subsets from affected patients and from HD, to investigate

the hypothesis that ETP of translocation-prone genes may influence translocation potential in MM, and may be patient-specific. Patient-specific ETP in normal cells from MM patients may reflect the positioning that was present in the original cancer progenitor undergoing the initial translocation event, and may favour translocations between specific loci. We utilized 3-D FISH and 3-D analysis techniques to investigate ETP in normal, non-translocated cell populations of CD19+ B-cells isolated from MM patients and HD. We provide novel evidence that TPGL position outside of their respective CTs and co-localize with a potential translocation partner in the interphase nucleus. We found that the frequency of extra-territorial loci positioning of *FGFR3* and *CCND1* is greater than that for c-*MAF* or the control locus *TGFBR2*, but does not differ among B cells from MM or healthy donors. The frequency of extraterritorial TPGL mirrors the clinical frequency of translocations in MM patients. This novel work suggests that ETP of TPGL may influence the translocation potential of each locus.

4.2 MATERIALS/METHODS

4.2.1 Materials

The institutional review boards of the University of Alberta, and Alberta Health Services approved this study. Written informed consent was obtained from 55 patients presenting at the Cross Cancer Institute, according to the Declaration of Helsinki. Peripheral blood (PB) and G-CSF mobilized blood (MB) samples were collected from patients during clinical visits. Human lymphocytes were isolated from 9 healthy donors (HD). Ficoll-Pacque™ was from Pfizer (New York, NY). CD19 antibody was FMC63[18]. EasySep® immunomagnetic sorting reagents and magnets were obtained from BAC probes were purchased from Empire Genomics (Buffalo, NY), and fluorescent in situ hybridization probes were from Vysis® (Abbott Laboratories, Abbott Park, IL).

4.2.2 Cell isolation

Mononuclear cells were isolated from all samples using Ficoll-Paque™ gradient separation as per the manufacturer's instructions. For 3-D FISH, B-cells were isolated from PB and MB samples using a human CD19 positive selection kit (Stem Cell Technologies, Vancouver, BC). A

representative sample from each purified population was stained with CD19-FITC, and analyzed by FACSort® (BD Biosciences) to confirm purity. Purity of CD19+ B lymphocytes ranged from 90-99% (mean=96%) for patient B-cells and 83-99% (mean=93%) for HD B-cells. Following purification, cells were suspended in 50% FBS/RPMI solution for adhesion to poly-L-lysine coated slides.

4.2.3 Two-dimensional (2-D) FISH

2-D FISH was used as a first step to identify patients with PCs positive for t(4;14), t(11,14), and t(14;16) for subsequent study. The method has been described previously (Chapter 2). Four commercial Vysis® probe sets (Abbott Laboratories, Abbott Park, IL) were used for each BM sample: LSI IGH dual colour break apart probe for the detection of chromosome breakage at the 14q32 locus; and three LSI dual colour, dual fusion probes: IGH/FGFR3 for the detection of t(4;14)(p16;q32); IGH/CCND1 XT for the detection of t(11;14)(q13;q32), and IGH/c-MAF for the detection of t(14;16)(q32;q23). For simplicity, the latter three probe sets will be referred to as *IGH:FGFR3*, *IGH:CCND1*, and *IGH:c-MAF* respectively, and loci identified as *FGFR3, CCND1, c-MAF,* and *IGH* for the remainder of the paper. Denaturation and hybridization was performed according to

manufacturer's instructions. The slide was counterstained using DAPI-containing VECTASHIELD® (Abbott Laboratories, Abbott Park, IL). FISH analysis and recording was done according to recommendations for FISH in MM[19,20].

4.2.4 Three-dimensional (3-D) FISH

Three commercial probe sets (*IGH:FGFR3*, *IGH:CCND1,* and *IGH:c-MAF*) (Abbott Laboratories, Abbott Park, IL) and one commercial BAC probe (Empire Genomics Cy5-labelled RP11-1080C17) for *TGFBR2* (negative control locus) were employed for 3-D FISH. The *TGFBR2* BAC probe was used in conjunction with the *IGH:CCND1* probe for *IGH:TGFBR2* analyses. The following whole chromosome paints (WCP) were purchased from Applied Spectral Imaging (Reyhovot, Israel): WCP 4 (aqua), WCP11 (aqua), WCP16 (aqua), and WCP3 (aqua).

Cell adhesion, fixation, and permeabilization were performed as previously described for cells in suspension[21], with minor modifications (for a complete methodology, see Chapter 2). 10 μl of each desired probe(s) or WCP was added to the target area, which was then cover-slipped, and sealed with rubber cement. Nuclei on the slide were co-denatured with

probe at 75°C for 5', and hybridized in a moist chamber for 18-48 h at 37°C. Post-hybridization, slides were washed in 2x SSC at 37°C with shaking for 3x 5', and then in 0.1x SSC at 60°C with shaking for 3x 5'. Slides were rinsed briefly in 2x SSC at RT, and coverslip-mounted using DAPI-containing VECTASHIELD® mounting medium (Abbott Laboratories, Abbott Park, IL).

4.2.5 Image acquisition

Images of 2-D May-Grunwald/Giemsa stained slides were acquired using a 40x (NA 0.75) dry objective lens on a Zeiss Axioplan 2 upright microscope as part of the Duet® imaging system (Bioview Ltd., Rehovot, Israel). 2-D FISH images were acquired using the 63x (NA 0.95) dry objective lens. For 3-D FISH, 3-D z-stacks were acquired using 63x (NA 1.4) oil objective lens on a Zeiss LSM 710 confocal microscope with Zen 2009 acquisition software set at scan zoom x3, pixel size 0.9 μm x 0.9 μm, with an optical step size of 0.2 μm. Z stacks of 357 nuclei from MM samples, and 180 nuclei from controls were analyzed in this study (Table 4-1).

4.2.6 Quantitative analysis of FISH signal distributions

The quantitative data analyses were performed using *ChromoView* software[22], based on MATLAB (The MathWorks, USA) and DIPimage toolbox (Quantitative Imaging Group, TU-Delft, The Netherlands). The multi-dimensional image data sets were linearly resampled in the axial direction to obtain isotropic voxel size. The loci and cell nucleus were segmented with an isodata threshold[23].

The following parameters were calculated: (i) center of mass (CM) of each locus, and each CT; (ii) CM and diameter of the nucleus; (iii) radial position of the segmented object with respect to the nucleus center; and (iv) presence of overlap in segmented loci. The equivalent radius was defined as the geometric mean of the radii of 2 equivalent spheres, with respectively the same surface area and the same volume as the nucleus.

To assess radial position of the object within the nucleus, a radial arm D_N was projected from the nuclear CM toward the nuclear boundary passing through the CM of the locus[24]. The distance D_i of the region in respect of the nucleus center was estimated as a fraction of the radial arm D_N, as $D_i = D_0 / D_N$, where D_O is Euclidian distance between CM of each locus

and the CM of the nucleus. The distance D_i denotes the radial shell where the locus is located.

4.3 RESULTS

4.3.1 Average radial positioning of *FGFR3* and *CCND1* is significantly different than the average radial positioning of their respective CTs in B-cells from MM patients, but not in their counterparts from HD

We first determined the radial positioning of the translocation-prone gene loci (TPGL), *FGFR3*, *CCND1*, and *c-MAF*, and the control locus, *TGFBR2* in relation to their respective CTs: Ch4, Ch11, Ch16, and Ch3. The analysis of *IGH* in relation to CT14 was not investigated at this time due to the cross-reactivity of WCP 14 with the p arms of the other acrocentric chromosomes, Ch13, Ch15, Ch21, and Ch22. The radial position is a quantifiable indicator of the location of a genomic region in the interphase nucleus, and is defined as the position of the region along the radial axis between the center of the nucleus and the nuclear edge[25], essentially representing a shell within the nucleus at a given position. The radial position of each TPGL with respect to its CT provides a map of the sub-chromosomal positioning of each locus within the interphase nucleus.

Utilizing 3-D FISH, and a confocal laser scanning microscope, 354 CTs (Table 4-1) were visualized in 177 individual cells from 5 patients and 240 CTs were visualized in 120 individual cells from 3 HD to produce a 3-D z-stack of each cell.

Table 4-1: B-cell origin of samples and number of nuclei analyzed per probe by 3-D FISH.

	t(4;14) (*n*=2)	t(11;14) (*n*=2)	t(14;16) (*n*=1)	MM (pts =5)	HD (*n*=1)	MM (pts =5)	HD (*n*=1)
CT11:*CCND1*	60	60	-	120	60	60	30
CT3:*TGFBR2*	60	-	-	60	60	30	30

CT - chromosome territory; MM - multiple myeloma; pts - patients; HD - healthy donors
n= number of patients or donors tested (30 cells per patient or donor; except for t(14;16) patients: 27 cells per patient)
All B-cells purified from peripheral blood, except for B-cells from t(14;16) patients which were purified from mobilized blood

---

We characterized the average radial position of each CT in the nuclear volume by measuring the distance from the center of mass of each CT to

the center of mass of each nucleus. Only nuclei with two CTs were analyzed, and the radial position was normalized to the size of each nucleus. We then determined the average radial position of each of the TPGL, utilizing the same method as for the CTs. The average radial positions of *FGFR3*, *CCND1*, and *c-MAF* and their respective CTs in B-cells from MM patients or HD are presented in Table 4-2.

Table 4-2: Comparison of average radial position of chromosome territories and corresponding gene loci in the interphase nucleus of B-cells from MM patients and healthy donors (HD).

	MM patients			HD		
CT4: *FGFR3*	66.4	49.9	<0.001	68.3	58.9	0.065
CT16: *c-MAF*	56.3	63.0	0.118	55.6	63.0	0.047

CT -chromosome territory; MM - multiple myeloma; HD - healthy donors;
p-values obtained from Kolmogorov-Smirnov tests

FGFR3 and *CCND1* localized most centrally in B-cells from MM patients, in radial shells at ~50% of the radius (0.5 RRD). This is in accordance

with our previous data (Chapter 2). The relative radial distribution (RRD) was calculated (Figure 2-2) for each CT and gene locus and was used for subsequent analyses.

To assess the spatial organization of TPGL relative to their respective CTs in B-cells, we utilized the cumulative frequencies of each locus and each CT RRD, and applied pairwise statistics (two-sided Kolmogorov-Smirnov test) to each CT:locus combination for each cell type (Table 4-2). Specifically, we wanted to determine whether there was a significant difference in the average radial position of the locus center as compared to the average radial position of the CT center. A significant difference in positioning would indicate that the average locus is positioned away from the average center of its respective CT. We determined that, on average, *FGFR3* and *CCND1* were positioned in radial shells significantly different from the radial shells of the center of CT4 and CT11 respectively, in patient B-cells ($p<0.001$ for both comparisons). The difference in radial positioning observed between *FGFR3* and the center of CT4 was 16.5% of the nuclear radius. The difference in radial positioning of *CCND1* and the center of CT11 was 10.4% of the radius in B-cells from patients. Conversely, in HD B-cells there was no significant difference in the

average radial position of *FGFR3* and the CT4 center or between *CCND1* and the CT11 center. The average radial position of *c-MAF* was not significantly different than the average radial position of the CT16 center in B-cells from patients but is significantly different in B-cells from HD (p=0.05). The average radial position of the control locus, *TGFBR2* was significantly different than the CT3 center in MM patients and HD. In contrast to *FGFR3* and *CCND1* which inhabit a more interior shell, the radial shells holding *c-MAF* or *TGFBR2* are extending towards the periphery from their respective CTs (see below).

4.3.2 In B-cells, *FGFR3* and *CCND1* are positioned away from the center of their respective CTs towards the nuclear center

Interestingly, in B-cells from MM patients or from HD, *FGFR3* and *CCND1* were positioned in radial shells closer to the center of the nucleus than the position of the radial shells that contained the center of their respective CTs. In other words, on average, the loci positioned away from the center of their CTs towards the center of the nucleus. In contrast, *c-MAF* and *TGFBR2* were extended away from the center of their respective CTs towards the periphery of the nucleus. This directional positioning of TPGL in patients (Figure 4-1) may imply a functional role in gene regulation, or

lack thereof, as several genes have been observed to move from a peripheral position to the interior of the nucleus upon activation[26-28].

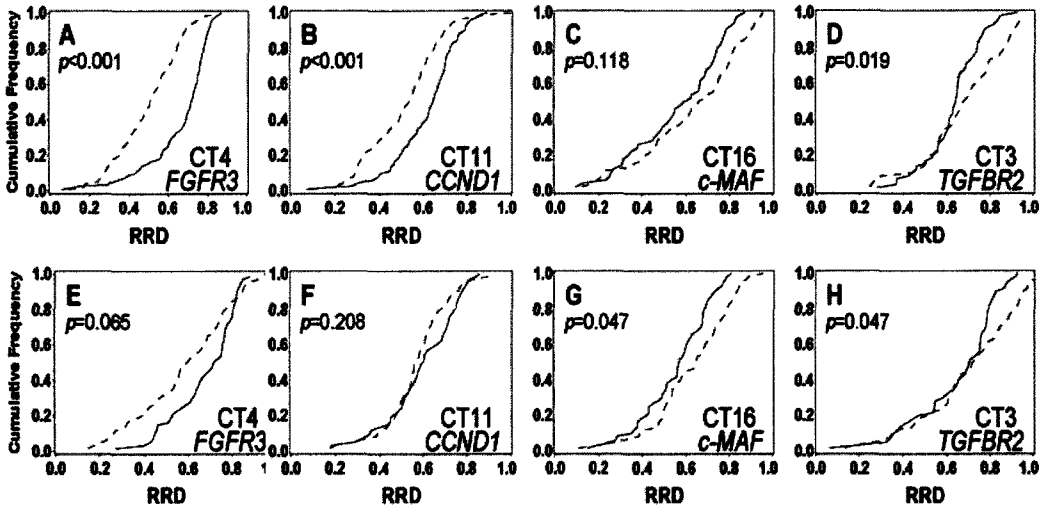

Figure 4-1: Directional positioning of translocation-prone gene loci (TPGL) and *TGFBR2* in MM patients and HD. 3-D FISH was performed on B-cells from MM patients. Cumulative frequency graphs to quantify the relative radial distributions (RRD) for each gene are shown with comparison to the RRD of their respective CTs. CT cumulative frequencies are denoted by solid lines; locus cumulative frequencies are denoted by dashed lines. **(A-D)** Comparison in patient B-cells. **(E-H)** Comparison in B-cells from HD. The average radial position of *FGFR3* and *CCND1* in patient B-cells is significantly more central in the nucleus than the center of their respective CTs. In contrast, the average radial position of *TGFBR2* in B-cells from patients and HD is significantly more peripheral in the nucleus than the center of CT3. *c-MAF* is more peripherally located

than the center of CT 16 in B-cells from HD. (Pairwise comparisons of cumulative radial distributions were performed using a two-sided Kolmogorov-Smirnov test. n= 120 chromosomes observed for *FGFR3* and *CCND1*, n= 54 chromosomes observed for *c-MAF*, and n=60 chromosomes for *TGFBR2*.

4.3.3 *FGFR3* and *CCND1* localize outside their respective CTs in a high frequency of B-cells from MM patients and HD

Utilizing the z-stack images recorded, we investigated the presence or absence of ETP of *FGFR3*, *CCND1*, *c-MAF*, and the control locus, *TGFBR2* in B-cells from patients and HD. A locus was considered external to its respective CT when the locus and the CT did not share a single voxel of registered signal in the 3-D space of the nucleus, as determined by our 3-D analysis software. We determined that in B-cells from MM patients and HD, the TPGL (*FGFR3*, *CCND1*, and *c-MAF)*, and the control locus, *TGFBR2* localized outside their respective CTs. (Figure 4-2); and that the proportion of TPGL signals positioning outside of their respective CTs varied among: (i) cell type and origin, and (ii) CT: locus type.

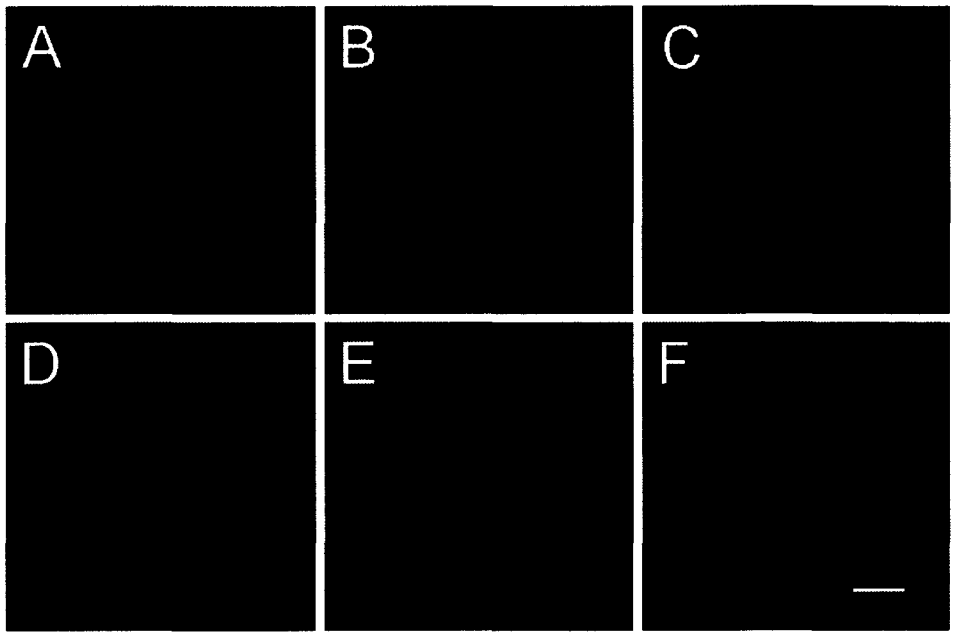

Figure 4-2: Extra-territorial positioning of gene loci in B-cells from MM patients and HD. 3-D FISH was performed on B-cells from MM patients and HD. 3-D z-stacks were acquired using a 63x (NA 1.4) oil objective lens on a Zeiss LSM 710 confocal microscope, with Zen 2009 acquisition software set at scan zoom x3, pixel size 0.9 μm x 0.9 μm, with an optical step size of 0.2 μm. Chromosome territories (CTs) (aqua) are hybridized with aqua whole chromosome paint. Gene loci (red) are hybridized with SpectrumOrange (Abbott Laboratories, Abbott Park, IL). The cell nucleus is stained with DAPI. (A-C) ETP of gene loci in patient B-cells. (A) One *FGFR3* locus is positioned outside of CT4. (B) Two *CCND1* loci are positioned outside of CT11. (C) One *c-MAF* locus is positioned outside of CT16. (D-F) ETP of gene loci in HD B-cells. (D) One *FGFR3* locus is positioned outside of CT4. (E) Two *CCND1* loci are positioned outside of CT11. (F) One *c-MAF* locus is positioned outside of CT16. On average, *FGFR3* and *CCND1* position away from the center of their respective CTs towards the nuclear center. In contrast, on average, *c-MAF* localizes

away from the center of CT16 towards the nuclear periphery. Scale bar = 3 μm.

For each of the TPGL: *FGFR3*, *CCND1*, and *c-MAF*, we investigated the frequency with which each locus positioned outside of their respective CTs for patient B-cells, and HD B-cells (Figure 4-3A) (Table 4-3). We utilized a logistic regression model with proportions of extra-territorial loci regressed on type of CT:locus pair, and compared the frequency of ETP of each locus between patient and HD B-cells (Table 4-3).

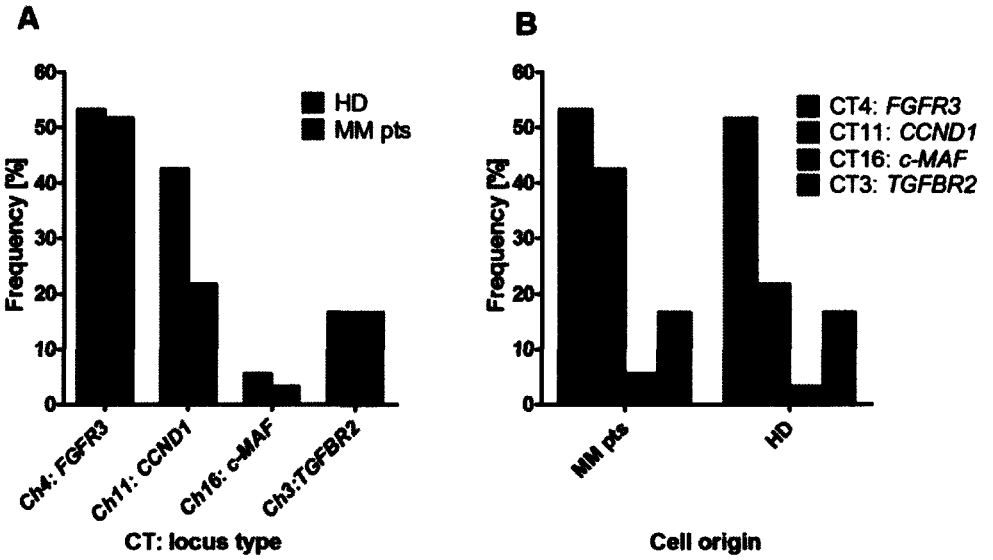

Figure 4-3: Frequency of ETP of the TPGL: *FGFR3*, *CCND1*, and *c-MAF* in B-cells between cell subsets. 3-D FISH was performed on B-cells from MM patients and from HD. (A) Frequencies of each locus signal external to their respective CTs in B-cells from MM patients as compared to B cells from HD. (B) Frequencies of locus signals external to their respective CTs relative to one another within only the population of B-cells from MM patients or within only in the B cells from HD. Pairwise comparisons of extra-territorial frequencies were performed using a logistic regression model and are listed in Tables 4-3, 4-4, and 4-5.

The frequency of ETP of *FGFR3* in patient B-cells and HD (53.3% and 51.7%) was not significantly different, nor was the frequency of ETP of *c-MAF* (5.6% and 3.3%) between the same cell subsets.

CCND1 was positioned outside of CT11 significantly more frequently in B-cells from patients as compared to HD (42.5% vs. 21.7%; p=0.007). The frequency of extra-territorial *TGFBR2* (16.7%) remained constant in patient and HD B-cells, providing an internal control.

Table 4-3: Comparison of the frequencies of signals external to their respective chromosome territories in cells from MM patients and HD.

	MM patients	HD	*p*-value
CT11:*CCND1*	42.5	21.7	0.007
CT3:*TGFBR2*	16.7	16.7	1.0

CT -chromosome territory; MM – multiple myeloma; HD - healthy donors
p-values obtained using a logistic regression model

We compared the frequencies of ETP in patient B-cells of the TPGL and the control locus, *TGFBR2* (Table 4-4). We found that *FGFR3* and *CCND1* positioned outside of their respective CTs significantly more frequently than the control locus, *TGFBR2*, positioned outside of CT3 (p<0.001 for both comparisons). There was no significant difference in the

ETP of *c-MAF* as compared to ETP of *TGFBR2* (p=0.075). These data suggest that in B-cells from MM patients, there may be an increased propensity for *FGFR3* and *CCND1* to position outside of their respective CTs as compared to the control locus. In contrast, *c-MAF* does not demonstrate an increased tendency to position outside CT16 as compared to the control locus.

Table 4-4: Pairwise comparison of the frequency of translocation-prone locus signals external to their respective CTs and the frequency of *TGFBR2* external to CT3 (control locus: CT) in patient B-cells.

	B-cells: MM patients		*p*-value
CT11:*CCND1* vs. CT3:*TGFBR2*	42.5	16.7	<0.001

CT -chromosome territory; MM – multiple myeloma

p-values obtained using a logistic regression model

4.3.4 In B cells, *FGFR3* and *CCND1* localize more frequently outside of their respective CTs than does *c- MAF*

We then compared the frequency of ETP of each TPGL locus to one another only within the MM subset or only within HD subset (Figure 4-3B) (Table 4-5, data rows 1-3). In B-cells from MM patients, there was a significantly higher frequency of ETP of *FGFR3* and *CCND1*, and a much reduced frequency of extra-territorial *c-MAF*. There was no significant difference in the ETP of *FGFR3* and *CCND1*.

Table 4-5: Pairwise comparisons of the frequencies of locus signals external to their respective chromosome territories in B-cells from MM patients and HD.

	B-cells - MM patients		*p*-value
CT4:*FGFR3* vs. CT16:*c-MAF*	53.3	5.6	<0.001
	B-cells - HD		
CT4:*FGFR3* vs. CT16:*c-MAF*	51.7	3.3	<0.001

CT -chromosome territory; MM – multiple myeloma; HD - healthy donors

p-values obtained using a logistic regression model

Essentially the same pattern was evident among B cells from HD (Table 4-5, data rows 4-6). This pattern of ETP of TPGL in patient and HD B-cells mirrors the clinical frequency of translocations in MM patients involving these loci, whereby *IGH*: *FGFR3* [t(4;14)] and *CCND1* [t(11;14)] participate in translocations more frequently than *c-MAF* [t(14;16)]. This work supports the idea that the frequency of ETP for *FGFR3*, *CCND1*, and *c-MAF* may influence translocation potential.

4.3.5 A proportion of TPGL that localize externally to their respective CTs co-localize with *IGH* in B-cells

For an *IGH* translocation to occur, the *IGH* locus must come into contact with its potential translocation partner. We therefore wanted to establish whether the TPGL positioned outside of their respective CTs also co-localized with *IGH* in the interphase nucleus. Long-range chromosomal interactions are highly transient,[29] and we were uncertain whether or not we would be able to visually capture the moment in time that an extra-territorial locus might co-localize with *IGH*. Utilizing the z-stacks previously recorded, and 3-D analysis software, we identified cells from each subset that contained an extra-territorial locus (defined as not

sharing a single voxel of registered signal with its respective CT in the 3-D space of the nucleus), and also had a locus that did share one or more voxels of registered signal with *IGH.* We then visually confirmed that the extra-territorial locus was the same locus that co-localized with *IGH.* We observed ETP of *FGFR3* and *CCND1* and co-localization with *IGH* in B-cells from patients (Figure 4-4AB) and HD. We did not, however, observe extra-territorial *c-MAF* co-localizing with *IGH.* These data support the idea that extra-territorial *FGFR3* and *CCND1* loci co-localize with their potential translocation partner *IGH* in the interphase nucleus (Figure 4-4).

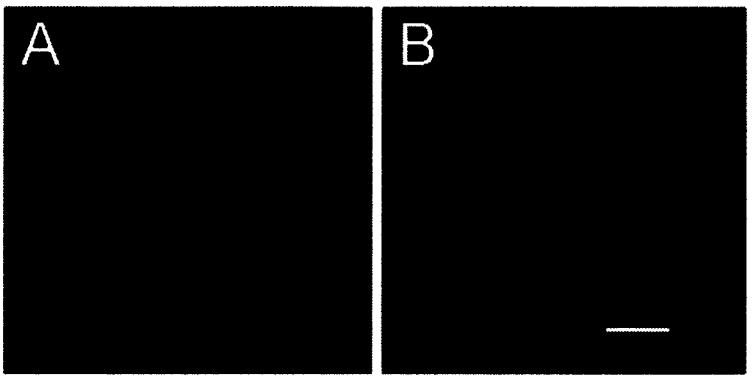

Figure 4-4: Extra-territorial *FGFR3* and *CCND1* partially co-localize with *IGH* in patient B-cells. 3-D FISH was performed on B-cells from MM patients. 3-D z-stacks were acquired using a 63x (NA 1.4) oil objective lens on a Zeiss LSM 710 confocal microscope, with Zen 2009 acquisition software set at scan zoom x3, pixel size 0.9 μm x 0.9 μm, with an optical step size of 0.2 μm. Chromosome territories (CT) (aqua) are hybridized with aqua whole chromosome paint. *FGFR3* and *CCND1* loci (red) are hybridized with SpectrumOrange (Abbott Laboratories, Abbott Park, IL). *IGH* (green) is hybridized with SpectrumGreen (Abbott Laboratories, Abbott Park, IL). The cell nucleus is stained with DAPI. (**A**) B-cells from patients with t(4;14). *FGFR3* extends outside of CT4 towards the nuclear center and partially co-localizes with *IGH*. (**B**) B-cells from patients with t(11;14). *CCND1* extends outside of CT 11 towards the nuclear center and partially co-localizes with *IGH*. Scale bar = 3μm.

4.4 DISCUSSION

The formation of chromosomal translocations requires three events. The chromosomes must be close together in the nucleus, undergo simultaneous DNA double strand breaks (DSBs), and be aberrantly repaired to generate fusion chromosomes. The order in which the first two events occur is controversial. Currently, two models for the formation of chromosomal translocations exist. The "breakage-first" model suggests that the chromosomes undergo DSBs at distant locations in the interphase nucleus and the broken ends roam freely to find a translocation partner. Conversely, the "contact-first" model suggests that the chromosomes are in close proximity prior to the formation of DSBs. The hypothesis that spatial proximity of translocation partners influences translocation outcome assumes the "contact-first" model, and evidence is accumulating in support of this model. It has been shown by us and others that spatial proximity of genetic loci in the interphase nucleus correlates with translocation frequency (Chapter 3), [7,14,15] and that broken chromosome ends in living cells are unable to move over large distances[30]. It seems likely, therefore, that the loci may make contact prior to breakage.

The mechanism by which genetic loci are brought into spatial proximity is unclear. Induced loci can travel distances of 1-5 μm through the interphase nucleus in an actin-dependent manner[31,32], and actively transcribed genes are known to "loop out" of their respective CTs to co-localize in transcription factories[8]. These studies point to an active mechanism for the movement of gene loci out of their respective CTs to transcription factories. ETP of translocation-prone genes, however, may also provide a direct mechanism through which translocation-prone genes from different chromosomes are brought into spatial proximity with one another, with translocations as the indirect consequence.

Our data provide novel evidence for ETP of the *IGH* translocation-prone gene loci: *FGFR3*, *CCND1*, and *c-MAF* in B-cells from patients and HD. In B-cells from patients, we show significant directional positioning of *FGFR3* and *CCND1* away from the center of their respective CTs towards the interior of the nucleus. This is in contrast to *c-MAF* and the control locus *TGFBR2*, which instead are positioned towards the periphery of the nucleus. The functional need for ETP may be gene regulation, as several genes have been observed to move from a peripheral position to the

interior of the nucleus upon activation[26-28]. In addition, we show that the two gene loci that participate in translocations most frequently with the *IGH* locus in patients with MM, *FGFR3* and *CCND1*, frequently extend outside of their respective CTs and occasionally co-localize with *IGH* in B-cells. To the best of our knowledge, this is the first report to demonstrate that ETP of genes provides a direct mechanism whereby translocation-prone genes from different chromosomes are brought into spatial proximity with one another. Although we did not observe extra-territorial *c-MAF* co-localizing with *IGH*, *c-MAF* must interact with *IGH* at some point to initiate a translocation event. Our failure to observe the interaction may be due to the highly transient nature of long-range chromosome interactions[29], and/or the fact that *c-MAF* participates in translocations with *IGH* at a lower frequency than *FGFR3* and *CCND1*. Conversely, *c-MAF* may not position outside of CT16 when it interacts with *IGH*.

For each of the TPGL, we compared the frequency of ETP between patient and HD B-cells. The frequency of extra-territorial *FGFR3* and *c-MAF*, being equally high or equally low, respectively, did not vary between B-cells from MM patients or HD, suggesting that the frequency of ETP of these loci is not different between the B-cell subsets. When we compared

the frequencies of ETP of each TPGL to one another *within* a given B-cell subset, we did observe differences. In B-cells from either patients or HD, *FGFR3* and *CCND1* localized outside of their respective CTs significantly more frequently than *c-MAF* localized outside of CT16. These data demonstrate that in B-cells, the ETP pattern of the *IGH* translocation-prone gene loci, *FGFR3*, *CCND1*, and *c-MAF* reflects the pattern of clinical frequencies of translocations involving these loci and *IGH* in MM patients; where *FGFR3* and *CCND1* participate in translocations more frequently than *c-MAF*. This suggests that the ETP of TPGL in B-cells influences their potential for participating in a translocation with *IGH*. It is probable that the extra-territorial loci positioning pattern of TPGL present in B-cells was also present in the original B-cell which gave rise to the malignant clone in MM, and thus influenced the selection of the *IGH* translocation partner within that cell. In summary, this work provides novel evidence that TPGL are frequently positioned outside of their respective CTs and co-localize with potential translocation partners in the interphase nucleus The study reported here suggests that the frequency of extra-territorial locus positioning is likely to exert a significant impact on translocation potential in B-cells.

4.5 REFERENCES

1. Cremer T, Cremer C. Chromosome territories, nuclear architecture and gene regulation in mammalian cells. Nat Rev Genet. 2001;2:292-301.
2. Parada L, Misteli T. Chromosome positioning in the interphase nucleus. Trends Cell Biol. 2002;12:425-432.
3. Schardin M, Cremer T, Hager HD, Lang M. Specific staining of human chromosomes in Chinese hamster x man hybrid cell lines demonstrates interphase chromosome territories. Hum Genet. 1985;71:281-287.
4. Pinkel D, Straume T, Gray JW. Cytogenetic analysis using quantitative, high-sensitivity, fluorescence hybridization. Proc Natl Acad Sci U S A. 1986;83:2934-2938.
5. Mayer R, Brero A, von Hase J, Schroeder T, Cremer T, Dietzel S. Common themes and cell type specific variations of higher order chromatin arrangements in the mouse. BMC Cell Biol. 2005;6:44.
6. Parada LA, McQueen PG, Misteli T. Tissue-specific spatial organization of genomes. Genome Biol. 2004;5:R44.
7. Roix JJ, McQueen PG, Munson PJ, Parada LA, Misteli T. Spatial proximity of translocation-prone gene loci in human lymphomas. Nat Genet. 2003;34:287-291.
8. Osborne CS, Chakalova L, Brown KE, et al. Active genes dynamically colocalize to shared sites of ongoing transcription. Nat Genet. 2004;36:1065-1071.
9. Osborne CS, Chakalova L, Mitchell JA, et al. Myc dynamically and preferentially relocates to a transcription factory occupied by Igh. PLoS Biol. 2007;5:e192.
10. Branco MR, Pombo A. Intermingling of chromosome territories in interphase suggests role in translocations and transcription-dependent associations. PLoS Biol. 2006;4:e138.

11. Volpi EV, Chevret E, Jones T, et al. Large-scale chromatin organization of the major histocompatibility complex and other regions of human chromosome 6 and its response to interferon in interphase nuclei. J Cell Sci. 2000;113 (Pt 9):1565-1576.

12. Williams RR, Broad S, Sheer D, Ragoussis J. Subchromosomal positioning of the epidermal differentiation complex (EDC) in keratinocyte and lymphoblast interphase nuclei. Exp Cell Res. 2002;272:163-175.

13. Chambeyron S, Bickmore WA. Chromatin decondensation and nuclear reorganization of the HoxB locus upon induction of transcription. Genes Dev. 2004;18:1119-1130.

14. Gandhi MS, Stringer JR, Nikiforova MN, Medvedovic M, Nikiforov YE. Gene position within chromosome territories correlates with their involvement in distinct rearrangement types in thyroid cancer cells. Genes Chromosomes Cancer. 2009;48:222-228.

15. Neves H, Ramos C, da Silva MG, Parreira A, Parreira L. The nuclear topography of ABL, BCR, PML, and RARalpha genes: evidence for gene proximity in specific phases of the cell cycle and stages of hematopoietic differentiation. Blood. 1999;93:1197-1207.

16. Nikiforova MN, Stringer JR, Blough R, Medvedovic M, Fagin JA, Nikiforov YE. Proximity of chromosomal loci that participate in radiation-induced rearrangements in human cells. Science. 2000;290:138-141.

17. Gabrea A, Leif Bergsagel P, Michael Kuehl W. Distinguishing primary and secondary translocations in multiple myeloma. DNA Repair (Amst). 2006;5:1225-1233.

18. Szczepek AJ, Seeberger K, Wizniak J, Mant MJ, Belch AR, Pilarski LM. A high frequency of circulating B cells share clonotypic Ig heavy-chain VDJ rearrangements with autologous bone marrow plasma cells in multiple myeloma, as measured by single-cell and in situ reverse transcriptase-polymerase chain reaction. Blood. 1998;92:2844-2855.

19. Recommendations for FISH in multiple myeloma: http://www.cytogenetics.org.uk/prof_standards/myeloma.htm; Mar 11, 2005.

20. Fonseca R, Barlogie B, Bataille R, et al. Genetics and cytogenetics of multiple myeloma: a workshop report. Cancer Res. 2004;64:1546-1558.

21. Cremer M, Grasser F, Lanctot C, et al. Multicolor 3D Fluorescence In Situ Hybridization for Imaging Interphase Chromosomes. Methods Mol Biol. 2008;463:205-239.

22. Harizanova J, Taylor-Kashton C, Mai S. Summary of the quantitative analyses of the three-dimensional distribution of chromosomes in mouse cells. AACR; 2008.

23. Ridler TW CS. Picture thresholding using an iterative selection method. IEEE Trans on Systems, Man and Cybernetics 1978;SMC-8:630-632.

24. Sarkar R GA, Vermolen BJ, Garini Y, Mai S. . Alterations of Centromere Positions in Nuclei of Immortalized and Malignant Mouse Lymphocytes. Cytometry Part A 2007;71A:386-392.

25. Cremer M, von Hase J, Volm T, et al. Non-random radial higher-order chromatin arrangements in nuclei of diploid human cells. Chromosome Res. 2001;9:541-567.

26. Kosak ST, Skok JA, Medina KL, et al. Subnuclear compartmentalization of immunoglobulin loci during lymphocyte development. Science. 2002;296:158-162.

27. Ragoczy T, Bender MA, Telling A, Byron R, Groudine M. The locus control region is required for association of the murine beta-globin locus with engaged transcription factories during erythroid maturation. Genes Dev. 2006;20:1447-1457.

28. Williams RR, Azuara V, Perry P, et al. Neural induction promotes large-scale chromatin reorganisation of the Mash1 locus. J Cell Sci. 2006;119:132-140.

29. Dekker J. Gene regulation in the third dimension. Science. 2008;319:1793-1794.

30. Soutoglou E, Dorn JF, Sengupta K, et al. Positional stability of single double-strand breaks in mammalian cells. Nat Cell Biol. 2007;9:675-682.

31. Chuang CH, Carpenter AE, Fuchsova B, Johnson T, de Lanerolle P, Belmont AS. Long-range directional movement of an interphase chromosome site. Curr Biol. 2006;16:825-831.

32. Dundr M, Ospina JK, Sung MH, et al. Actin-dependent intranuclear repositioning of an active gene locus in vivo. J Cell Biol. 2007;179:1095-1103.

Chapter Five: Discussion

5.1 SIGNIFICANCE OF THIS WORK

Based on experimental evidence that maps the *IGH* breakpoints on derivative chromosomes to areas specific to the generation of DNA DSBs during *IGH* recombination, and that *IGH* recombination enzymes can create DSBs in "off-target" oncogenes, we and others have speculated that *IGH* diversification enzymes are responsible for the DNA DSBs generated in the potential translocation partner loci (Introduction) (reviewed by[1]). Most recently, it has been shown that AID induces DSBs at non-Ig loci in activated B-cells, at sites syntenic with sites of translocations[2], providing evidence that AID can produce DSBs in "off-target" genes. The mechanisms involving the selection of a partner in MM, however, have not previously been explored.

Although the involvement of B-cells in MM evolution has been documented by molecular, phenotypic, and functional studies using the clonotypic *IGH* [V(D)J] gene rearrangement to identify a proportion of these cells as components of the malignant clone[3-7], a significant subset of

small B-lymphocytes in the blood of MM patients are polyclonal and hence non-malignant[8]. Here, utilizing 3D FISH and 3D analysis software, we have characterized the genome organization of the TPGL, *IGH*, *FGFR3*, *CCND1*, and *c-MAF* in the interphase nucleus using purified populations of *ex-vivo* CD34+ HPC and B-cells from MM patients or from HD as our model. We used non-malignant patient subsets for our investigation to characterize genome organization in cells that were not malignantly transformed; the assumption being that genome positioning of TPGL in patient-derived normal cells may closely reflect loci positioning present in the original cell in which the translocation initially formed, and may favour translocations between proximal loci in a patient-specific manner. The observation that none of the patients subsets displayed translocations validates their status as non-malignant. We compared the positioning of TPGL in patient subsets to HD subsets, speculating that genome organization may differ in presumptively healthy cells from cancer patients as compared to their counterparts from HD. Characterization of TPGL positioning in HPC characterizes genome organization in the earliest stage of hematopoietic cell lineage; subsequent analysis in purified non-malignant B-cells provides information regarding the lineage that gives rise to MM, and allows for the comparison of positioning patterns of

hematopoietic cells at sequential stages contributing to normal B lineage differentiation. Specifically, we investigated the influence of three parameters on translocation potential: (i) the average radial position of the TPGL in the nucleus, (ii) the relative position of *IGH* and its potential partners *FGFR3*, *CCND1*, and *c-MAF* in the nucleus, and (iii) the physical relationship between *IGH*, TPGL and a control gene *TGFBR2*. *Ex-vivo* cells from MM patients provided an ideal model for study because *FGFR3* and *CCND1* participate in translocations with *IGH* at a much higher clinical frequency than does *c-MAF*. In previous studies using other model systems, genomic regions that participate in translocations have been shown to be spatially proximal in the nucleus.

Our working hypothesis was that the organization of *IGH* and the other TPGL in the nucleus of non-malignant cells from MM patients would influence the selection of an *IGH* translocation partner, thereby providing a window into the original events that led to MM. In addition, we wanted to determine whether the positioning of TPGL in cells from MM patients would be different from their positioning in HD.

We initially investigated the relative and radial positioning of *IGH*, *FGFR3*, *CCND1* and a negative control locus, *TGFBR2* in the interphase nucleus of HPC and B-cells from HD or MM patients with t(4;14) and t(11;14). We determined that the average radial position in nuclear "shells" of each of the TPGL (*IGH*, *FGFR3*, and *CCND1)* was not significantly different in HPC from MM patients as compared to HPC from HD. This indicated that the radial positioning of each individual locus was not different prior to B lineage commitment. In contrast, we found that the average radial positions of *IGH*, *FGFR3*, and *CCND1* in mature B-cells from t(4;14) and t(11;14) patients were significantly more central in the nucleus as compared to the radial position of the same loci in HD B-cells or HPC from MM patients. The average radial positions of *IGH*, *FGFR3*, and *CCND1* were not different in B-cells from t(4;14) or t(11;14) patients, suggesting that there is no difference in the radial positioning pattern of TPGL based on the patient translocation type. The average radial position of the control locus, *TGFBR2* was not significantly different in any of the cell subsets, providing an internal control. This is the first report of patient-specific positioning of TPGL, and supports the novel suggestion that the significantly more central radial position of *IGH*, *FGFR3*, and *CCND1* in

the interphase nucleus is restricted to patient B-cells and may influence translocation potential in these cells.

We next determined that *IGH* and *FGFR3* in patients with t(4;14) or *IGH* and *CCND1* in patients with t(11;14) are closer together in the nucleus than *IGH* and the control locus, *TGFBR2*; and closer together than in HD B-cells and in HPC from HD and patients. This suggests that there may be a bias towards the selection of *FGFR3* and *CCND1* as translocation partners for *IGH* in B-cells from patients with t(4;14) and t(11;14) myelomas that is not observed in the other cell subsets tested here. Extrapolating backwards to the original parent B cell that gave rise to MM, the loci involved in the initial translocation event are likely to have participated in favoured pairing during aberrant break and rejoining events. These data maintain the principle of the "contact-first" model of chromosomal translocations, and suggest that intergene proximity of TPGL influences the selection of an *IGH* translocation partner in B-cells from t(4;14) and t(11;14) patients.

To the best of our knowledge, *IGH* translocations have not been reported in HPC, and those analyzed here did not exhibit translocations. Having

determined that the radial and relative positioning of *IGH*, *FGFR3*, and *CCND1* in HPC was not significantly different among HPC from MM patients and HD cells, we continued the investigation of genome organization and translocation potential only in B-cell subsets. No translocations were observed in the B-cells analyzed. We expanded the study of TPGL positioning in the interphase nucleus to include the *IGH* translocation-prone gene locus, *c-MAF*, and B-cells from t(14;16) patients. We compared the average radial positioning of *IGH*, *FGFR3*, and *CCND1* in B-cells from t(14;16) patients to HD B-cells. Unlike their positioning in B-cells from t(4;14) and t(11;14) patients, *IGH*, *FGFR3*, and *CCND1* in B-cells from t(14;16) patients were located significantly further from the nuclear center towards the periphery, and the positions were not different from the positioning in HD B-cells. In comparison, the position of *c-MAF* and that of the control locus *TGFBR2* were consistently located in the periphery in all patient groups analyzed as well as in HD B-cells. In addition, we determined that *c-MAF* maintained an average radial position in the cell nucleus that was significantly more peripheral than *IGH*, but not significantly different from the control locus, *TGFBR2*. In t(14;16) patients, B-cells showed no significant differences in the average intergene distances between *IGH* and *FGFR3*, *CCND1*, *c-MAF* or the control locus,

TGFBR2. Overall, this work suggests that selection of an *IGH* translocation partner does not seem to be based on spatial proximity in B-cells from t(14;16) patients as much as in B-cells from the other two translocation groups. In contrast, we found that *IGH* and *FGFR3* in B-cells from t(4;14) patients or *IGH* and *CCND1* in t(11;14) patients were closer together than were *IGH* and *c-MAF* in the same B-cell subsets, providing additional evidence for the favoured selection of *FGFR3* and *CCND1* as potential *IGH* translocation partners in these B-cells. These observations demonstrate that *c-MAF* is not a spatially favoured *IGH* translocation partner in any of the patient B-cell subsets, which may provide a partial explanation for the low clinical frequency of translocations involving *IGH* and *c-MAF* in MM patients (5%). These data provide the first evidence to suggest that organization of *FGFR3* and *CCND1* in B-cells from MM patients is different among the three translocation types, and suggests that the events promoting recurrent translocations in t(4;14) and t(11;14) patients may be different than those promoting translocations involving *IGH* and *c-MAF* in t(14;16) patients.

Lastly, we investigated the hypothesis that extra-territorial positioning (ETP) of the translocation-prone gene loci, *FGFR3*, *CCND1*, and *c-MAF*

may influence translocation potential in B-cells from patients with MM and from HD. To initiate an investigation of the relationship between TPGL and their respective CTs, we first determined the average radial positions of *FGFR3*, *CCND1*, *c-MAF* and the average radial positions of the centers of mass of their respective CTs, Ch4, Ch11, and Ch16. In patient B-cells, we observed that the average radial positions of *FGFR3* and *CCND1* are significantly more central in the nucleus than the radial positions of their respective CTs. Conversely, the average radial position of *c-MAF* and of the control locus *TGFBR2* were more peripheral in the nucleus than the center of mass of their CTs, although this difference in positioning was not significant. This directional radial positioning of loci in the nucleus may have a function in gene regulation, although this premise is controversial. Specific genes (*β-globin*, *IGH* and *IGK)* have been shown to move from a peripheral position to an interior position upon activation[9-11], however, other genes remain static when activated[12,13], or move to the periphery with no change in expression[13]. It appears that different genes possess specific positioning patterns upon activation (reviewed by[14]). Regardless, this observation further supports the hypothesis that a central radial position of TPGL enhances translocation potential in B-cells from MM patients, as the two loci that participate in translocations most frequently

with *IGH* are also those positioned most centrally in the nucleus. This may or may not signal the movement of these two loci to a more transcriptionally active location in the cell nucleus.

Through analysis of ETP of *FGFR3*, *CCND1*, and *c-MAF* in the interphase nucleus of B-cells from MM patients and from HD, we observed that *FGFR3* and *CCND1* position outside of CT4 and CT11 respectively, at a significantly higher frequency than *c-MAF* positions outside of CT16. This pattern of ETP reflects the pattern of clinical frequencies in MM and suggests that the ETP of *FGFR3*, *CCND1*, and *c-MAF* may influence their potential for translocation with *IGH*. Although it has been shown that the degree to which specific chromosome pairs intermingle correlates with their translocation frequencies[15], these findings show that some TPGL frequently extend beyond their CTs and occasionally co-localize with *IGH*. These observations provide evidence for a previously undocumented mechanism that brings translocation-prone gene loci from different chromosomes into spatial proximity with one another.

c-MAF, however, rarely extends outside of CT16 in B-cells. In thyroid cells, specific loci that participate in interchromosomal translocations are

positioned at their respective CT periphery more frequently than loci that participate in intrachromosomal inversions[16]. Localization of *c-MAF* at the edge of its CT may facilitate its participation in translocations with *IGH*, however, additional experimentation to determine the location of *c-MAF* with respect to the edge of CT16 will be necessary.

As discussed in Chapter 3, events promoting recurrent t(14;16) translocations in MM patients may be significantly different from those promoting t(4;14) or t(11;14) translocations. We observed that *IGH*, *FGFR3*, and *CCND1* position more centrally in the nucleus and are closer together in normal B-cells from t(4;14) and t(11;14) patients than in cells from patients with t(14;16). Furthermore, in t(4;14) and t(11;14) patients, *IGH* and *FGFR3* or *IGH* and *CCND1* are closer together than are *IGH* and *c-MAF*. In B-cells from t(14;16) patients, *IGH* is equivalently distal to *FGFR3*, *CCND1*, *c-MAF*, and the control locus, *TGFBR2*. In all translocation types, *c-MAF* occupies a peripheral position in the nucleus that is significantly different than *IGH*, but not different from *TGFBR2*. *c-MAF* rarely extends outside of CT16 in B-cells from t(14;16) patients or HD, while *FGFR3* and *CCND1* frequently extend beyond their respective CTs. Extra-territorial *FGFR3* and *CCND1* were shown to co-localize with

IGH, whereas extra-territorial *c-MAF* did not. The radial and relative positioning of the TPGL in cells from t(14;16) patients does not differ from HD B-cells: B-cells from t(14;16) patients model the behaviour of HD B-cells. Collectively, these data strongly suggest that the selection of *c-MAF* as a translocation partner for *IGH* proceeds through a different mechanism than does the selection of *FGFR3* and *CCND1*. In patients with t(4;14) and t(11;14) myelomas, *IGH* translocation partner selection in the original parent cell may be heavily influenced by spatial proximity and central position in the nucleus. In t(4;14) and t(11;14) patients, there may be a bias against selection of *c-MAF* as an *IGH* translocation partner based on spatial proximity, however in t(14;16) patients and in HD, *IGH* is equivalently proximal to *FGFR3*, *CCND1*, and *c-MAF*. Viewed this way, *c-MAF* has the same potential for translocation with *IGH* as *FGFR3* or *CCND1* in patients with t(14;16), which extrapolates to an increased potential for selection of *c-MAF* as compared to t(4;14) or t(11;14) patients. The impetus for t(14;16) may be the location of FRA16 fragile site located centromeric to the *c-MAF* locus. If this is the case, we might expect to observe t(14;16) translocations in B-cells from HD, however, this has not been documented. This implies a role for additional factors in the

genesis of t(14;16) translocations, such as aberrant repair mechanisms (discussed later).

5.2 POTENTIAL ROLE OF TRANSCRIPTION FACTORIES IN THE GENERATION OF *IGH* TRANSLOCATIONS

Utilizing RNA immuno-FISH, it has been shown that active genes associate with transcription factories in the interphase cell nucleus[17,18]. This is a dynamic association, switching transcription on when the genes move into the factory, and off when they dissociate[17]. There are exceptions, however, as some single copy genes, aptly named "supergenes", are transcribed almost continuously. *IGH* is one of the few genes to be classified as a supergene[19]. In pro-B-cells, it undergoes both genic and intergenic transcription during V(D)J recombination[20]. In activated mature B-cells, ~ 90% of *IGH* alleles are actively transcribed and appear to be associated with transcription factories[18]. In 80% of these activated B-cells both alleles are transcribed[18]. Ongoing transcription is necessary for the functional activity of *IGH* diversification enzymes[21-23], and several reports indicate that that these same enzymes have off-target

effects on proximal genes[24-27]. The *IGH* breakpoints detected in each of the recurrent *IGH* translocations in MM point to the involvement of specific *IGH* modification enzymes with specific translocation types.

Within this work, we have suggested that *IGH* and TPGL may co-localize in transcription factories, and that during active transcription, "off-target" activities of AID, RAG, or SHM (Figure 1-2) result in DSBs in DNA from two gene loci simultaneously. The classification of *IGH* as a supergene suggests that it is consistently associated with transcription factories. If this is the case, it is highly probable that, in order to co-localize with *IGH*, its potential partners, *FGFR3*, *CCND1*, and *c-MAF* would come into contact with *IGH* within a transcription factory. It has been shown that when *MYC*, a frequent translocation partner with *IGH*, is activated, alleles moved to a factory occupied by *IGH*[18]. Moreover, the frequency of transcriptional co-localization of specific genes with *IGH* in transcription factories mirrors the clinical frequencies of the corresponding translocations. Co-localization of *IGH* and the TPGL, *FGFR3*, *CCND1*, and *c-MAF* in a transcription factory could provide a physical location of ongoing transcription that is necessary for the "off-target" effects of the *IGH* diversification enzymes. Transcription factories are distributed

uniformly throughout the nucleus[28], so despite the observation that *c- MAF* occupies a more peripheral location than *FGFR3* and *CCND1*, it may still localize with *IGH* in a transcription factory. Alternatively, the physical location for *IGH* interaction with *c-MAF* may not be in a transcription factory. As determined in murine B-cells, AID is capable of inducing DSBs within the fragile site specific to *WWOX* (FRA16 in humans), but not all of the DSBs induced by AID were restricted to transcribed regions within the genome[2], suggesting that active transcription may not be essential for the "off-target" activities of AID.

To better understand the functional aspects of the genome organization of *IGH* and the TPGL, future work will validate the localization of these loci to areas of transcription. This will require a triple-label RNA immuno-FISH approach to detect transcriptionally active TPGL alleles and RNA polymerase II (RNA pol II)[18]. *IGH* and each of *FGFR3*, *CCND1*, and *c-MAF* would need to be hybridized on separate slides. As indicated above, we have observed ETP of *FGFR3*, *CCND1*, and *c-MAF*, and the co-localization of extra-territorial *FGFR3* and *CCND1* with *IGH.* In this context it becomes conceptually important to determine whether the extra-territorial loci that co-localize with *IGH* do so in transcription factories. This

is a complex approach, which may be hindered by the transient nature of loci interactions. Future work will involve a combination of RNA and DNA immuno-FISH requiring quadruple labeling. Immunolabeling of RNA pol II to detect the transcription factories would precede RNA FISH to detect the active *IGH* and TPGL alleles, followed by DNA FISH to delineate the chromosome territories. This type of approach may aid in clarifying the functionality of ETP.

As outlined in the introduction to this thesis, a growing body of work implicates the "off-target" effects of *IGH* diversification enzymes on oncogenes. Most recently, it has been demonstrated that AID is necessary for DSBs that form in *MYC/IGH* translocations seen in activated B-cells[25], and that AID is capable of inducing DSBs within the fragile site specific to *WWOX* (FRA16 in humans) in murine B-cells[2]. It has been suggested that the simultaneous expression of RAG and AID results in DSBs in *CCND1*[27]. Similar studies may identify the diversification mechanisms responsible for DNA DSB in *FGFR3 /MMSET.*

In addition, the temporal component of the "off-target effects" of *IGH* diversification enzymes is not clear. Han *et al.* have shown that AID is

expressed in pre-B and immature B cells of normal wild type mice, resulting in active SHM and CSR [29]. More recently, Wang *et al.* have demonstrated that a subset of activated peripheral B-cells with defective NHEJ simultaneously harbor DSBs in the *IGL* and *IGH* loci associated with V(D)J recombination and CSR, respectively[30]. Hybrid switch regions are present in the three most frequent *IGH* translocations in MM. This suggests that illegitimate switch region translocations may occur in B-cells that have already undergone legitimate CSR, perhaps involving secondary CSR at a later stage or outside of the GC. Sequencing studies done in plasma cells by Taylor *et al.* demonstrate ongoing mutation in the *IGH* locus in the area between J_H and $S\mu$[31]. This suggests that SHM is occurring outside of the germinal center as a continuing process in mature B-cells, as reflected in end stage plasma cells. Collectively, these studies provide evidence to refute the long-held dogma that V(D)J recombination, SHM, and CSR are restricted to specific stages of B-cell development within specific areas of immune tissue. It is seemingly apparent that the translocation breakpoints seen in the *IGH* locus are generated at different time points in the B lineage-pathway, and involve different mechanisms. This may contribute to the selection of an *IGH* translocation partner, as physical proximity to *IGH* in the interphase nucleus may be temporal. To

clarify this issue, it may be necessary to more precisely investigate factors such as radial positioning and spatial proximity in cells of the B-lineage cells at other stages of differentiation.

5.3 POTENTIAL ROLE OF ABERRANT REPAIR MECHANISMS IN THE GENERATION OF *IGH* TRANSLOCATIONS

Finally, following the generation of DSBs on potential partner loci, aberrant repair mechanisms may be contributing to the promiscuity of translocation partners seen in MM. Fifty per cent of myeloma cases have loss of *hMLH1*, a protein necessary for the MMR repair[32], one of the pathways involved in resolution of DSBs generated by SHM. Two myeloma cell lines demonstrate an impairment of the capacity to repair DSBs via the NHEJ pathway in response to radiation, providing evidence of impaired NHEJ in HMCLs[33].

For successful repair to occur, the DNA at the site of DSBs on chromosomes must be held 'stable' while the NHEJ machinery repairs the break. Soutoglou et al. have demonstrated that Ku86 is necessary for the

positional stability of single double strand breaks, and that in the absence of Ku, there is an increased frequency of cells displaying clearly separated broken ends (>500nm) at artificially generated DSBs. The broken ends of DNA in the Ku86 knockdown cells display increased ability to locally diffuse, with the cells showing an increased occurrence of translocations[34]. The latter point indicates that DSB repair (albeit aberrant in the case of translocations) is still able to proceed in the absence of Ku, perhaps via the alternative end-joining pathway. It is interesting to note that Ku86 is also associated with transcription factories[35]. This would suggest that the generation and repair of DNA DSBs in transcription factories is not a rare event.

Although the expression of the Ku variant in myeloma is controversial, it is tempting to speculate on the potential role of Ku86v in the promiscuity of translocation partners seen in myeloma. It is not known whether the expression of Ku86v affects positional stability of DSBs. This variant is capable of binding to DNA ends, but does not appear to bind DNA-PKcs. The kinase activity of DNA-PKcs is reduced in patient cells expressing both Ku86 and the variant, and is absent in cells expressing only Ku86v[36]. It has been shown that Ku86 is essential for the recruitment of DNA-PKcs

at DSBs[37], and it would appear that Ku86v is not able to recruit the kinase in the absence of its C-terminal arm. If the ability of DNA-PKcs to interact in *trans* does indeed contribute to positional stability of DSBs, stability of the DSB ends could be compromised in the presence of the Ku86 variant. This would increase the probability that the chromosome break could diffuse to the site of another DSB in a proximal heterologous chromosome. Ku86v may retain its ability to recruit the other members of the NHEJ, allowing NHEJ to proceed, albeit with a non-homologous chromosome. Or, in the absence of DNA-PKcs and its kinase activity, the alternative end-joining pathway could be activated. Alternatively, the expression of both Ku86 and Ku86v may result in a simple competition between the two proteins for binding at DSBs, resulting in a decreased capacity for full-length Ku86 binding. This in turn could result in decreased DNA-PKcs recruitment which could impair the NHEJ process. Further experimentation is necessary to definitively determine the presence or absence of the Ku86v in the cells from patients with MM, particularly in B-cells, where translocations initially arise

5.4 CONCLUSION

Excluding this work, studies on genome organization with respect to translocation potential have utilized normal cells from HD, heterogeneous cell populations from patients, murine models, and cell lines. From work with these model systems, it was shown that translocation-prone genome regions are in close proximity in the interphase nucleus, and that spatial proximity in a normal cell line correlates with translocation frequency in patients. This is the first study of genome organization in purified subpopulations of normal cells from affected patients, and the first comparison to purified subsets from healthy donors with the object of determining whether gene loci positioning differs between patients and healthy individuals. Prior to this work, it was not known which factors influenced the selection of a translocation partner with *IGH* in patients with MM. This work has shown that spatial proximity of gene loci and radial positioning in the interphase nucleus appears to influence translocation potential in B-cells from MM patients, and appears to be patient-specific for some subtypes of MM patients. Furthermore, we show that TPGL position outside of their chromosome territories and co-localize with *IGH*,

presenting a novel mechanism whereby TPGL are brought into close spatial proximity. The work presented here demonstrates that the positioning of TPGL in the nucleus of non-malignant cells from MM patients places potential translocation partners in distinct and preferential proximities that appear to promote their participation in *IGH* translocation events.

5.5 REFERENCES

1. Mahowald GK, Baron JM, Sleckman BP. Collateral damage from antigen receptor gene diversification. Cell. 2008;135:1009-1012.
2. Staszewski O, Baker RE, Ucher AJ, Martier R, Stavnezer J, Guikema JE. Activation-induced cytidine deaminase induces reproducible DNA breaks at many non-Ig Loci in activated B cells. Mol Cell;41:232-242.
3. Reiman T, Seeberger K, Taylor BJ, et al. Persistent preswitch clonotypic myeloma cells correlate with decreased survival: evidence for isotype switching within the myeloma clone. Blood. 2001;98:2791-2799.
4. Pilarski LM, E. B, M.J. M, et al. Multiple myeloma includes CD20+ B and plasma cells that persist in patients treated with rituximab. Clinical Medicine: Oncology. 2008;2:275-281.
5. Sahota SS, Garand R, Mahroof R, et al. V(H) gene analysis of IgM-secreting myeloma indicates an origin from a memory cell undergoing isotype switch events. Blood. 1999;94:1070-1076.
6. Pilarski LM, Seeberger K, Coupland RW, et al. Leukemic B cells clonally identical to myeloma plasma cells are myelomagenic in NOD/SCID mice. Exp Hematol. 2002;30:221-228.
7. Kirshner J, Thulien KJ, Martin LD, et al. A unique three-dimensional model for evaluating the impact of therapy on multiple myeloma. Blood. 2008;112:2935-2945.
8. Pilarski LM, Baigorri E, Mant MJ, et al. Multiple myeloma includes CD20+ B and plasma cells that persist in patients treated with rituximab. Clinical Medicine:Oncology. 2008;2:275-281.
9. Kosak ST, Skok JA, Medina KL, et al. Subnuclear compartmentalization of immunoglobulin loci during lymphocyte development. Science. 2002;296:158-162.

10. Ragoczy T, Bender MA, Telling A, Byron R, Groudine M. The locus control region is required for association of the murine beta-globin locus with engaged transcription factories during erythroid maturation. Genes Dev. 2006;20:1447-1457.

11. Williams RR, Azuara V, Perry P, et al. Neural induction promotes large-scale chromatin reorganisation of the Mash1 locus. J Cell Sci. 2006;119:132-140.

12. Hewitt SL, High FA, Reiner SL, Fisher AG, Merkenschlager M. Nuclear repositioning marks the selective exclusion of lineage-inappropriate transcription factor loci during T helper cell differentiation. Eur J Immunol. 2004;34:3604-3613.

13. Meaburn KJ, Misteli T. Locus-specific and activity-independent gene repositioning during early tumorigenesis. J Cell Biol. 2008;180:39-50.

14. Takizawa T, Meaburn KJ, Misteli T. The meaning of gene positioning. Cell. 2008;135:9-13.

15. Branco MR, Pombo A. Intermingling of chromosome territories in interphase suggests role in translocations and transcription-dependent associations. PLoS Biol. 2006;4:e138.

16. Gandhi MS, Stringer JR, Nikiforova MN, Medvedovic M, Nikiforov YE. Gene position within chromosome territories correlates with their involvement in distinct rearrangement types in thyroid cancer cells. Genes Chromosomes Cancer. 2009;48:222-228.

17. Osborne CS, Chakalova L, Brown KE, et al. Active genes dynamically colocalize to shared sites of ongoing transcription. Nat Genet. 2004;36:1065-1071.

18. Osborne CS, Chakalova L, Mitchell JA, et al. Myc dynamically and preferentially relocates to a transcription factory occupied by Igh. PLoS Biol. 2007;5:e192.

19. Fraser P. Transcriptional control thrown for a loop. Curr Opin Genet Dev. 2006;16:490-495.

20. Bolland DJ, Wood AL, Johnston CM, et al. Antisense intergenic transcription in V(D)J recombination. Nat Immunol. 2004;5:630-637.

21. Peters A, Storb U. Somatic hypermutation of immunoglobulin genes is linked to transcription initiation. Immunity. 1996;4:57-65.

22. Fukita Y, Jacobs H, Rajewsky K. Somatic hypermutation in the heavy chain locus correlates with transcription. Immunity. 1998;9:105-114.

23. Schrader CE, Guikema JE, Linehan EK, Selsing E, Stavnezer J. Activation-induced cytidine deaminase-dependent DNA breaks in class switch recombination occur during G1 phase of the cell cycle and depend upon mismatch repair. J Immunol. 2007;179:6064-6071.

24. Pasqualucci L, Neumeister P, Goossens T, et al. Hypermutation of multiple proto-oncogenes in B-cell diffuse large-cell lymphomas. Nature. 2001;412:341-346.

25. Robbiani DF, Bothmer A, Callen E, et al. AID is required for the chromosomal breaks in c-myc that lead to c-myc/IgH translocations. Cell. 2008;135:1028-1038.

26. Liu M, Duke JL, Richter DJ, et al. Two levels of protection for the B cell genome during somatic hypermutation. Nature. 2008;451:841-845.

27. Tsai AG, Lu H, Raghavan SC, Muschen M, Hsieh CL, Lieber MR. Human chromosomal translocations at CpG sites and a theoretical basis for their lineage and stage specificity. Cell. 2008;135:1130-1142.

28. Wansink DG, Schul W, van der Kraan I, van Steensel B, van Driel R, de Jong L. Fluorescent labeling of nascent RNA reveals transcription by RNA polymerase II in domains scattered throughout the nucleus. J Cell Biol. 1993;122:283-293.

29. Han JH, Akira S, Calame K, Beutler B, Selsing E, Imanishi-Kari T. Class switch recombination and somatic hypermutation in early mouse B

cells are mediated by B cell and Toll-like receptors. Immunity. 2007;27:64-75.

30. Wang JH, Gostissa M, Yan CT, et al. Mechanisms promoting translocations in editing and switching peripheral B cells. Nature. 2009;460:231-236.

31. Taylor BJ, Kriangkum J, Pittman JA, et al. Analysis of clonotypic switch junctions reveals multiple myeloma originates from a single class switch event with ongoing mutation in the isotype-switched progeny. Blood. 2008;112:1894-1903.

32. Martin P, Santon A, Garcia-Cosio M, Bellas C. hMLH1 and MGMT inactivation as a mechanism of tumorigenesis in monoclonal gammopathies. Mod Pathol. 2006;19:914-921.

33. Yang C, Betti C, Singh S, Toor A, Vaughan A. Impaired NHEJ function in multiple myeloma. Mutat Res. 2009;660:66-73.

34. Soutoglou E, Dorn JF, Sengupta K, et al. Positional stability of single double-strand breaks in mammalian cells. Nat Cell Biol. 2007;9:675-682.

35. Mo X, Dynan WS. Subnuclear localization of Ku protein: functional association with RNA polymerase II elongation sites. Mol Cell Biol. 2002;22:8088-8099.

36. Tai YT, Teoh G, Lin B, et al. Ku86 variant expression and function in multiple myeloma cells is associated with increased sensitivity to DNA damage. J Immunol. 2000;165:6347-6355.

37. Uematsu N, Weterings E, Yano K, et al. Autophosphorylation of DNA-PKCS regulates its dynamics at DNA double-strand breaks. J Cell Biol. 2007;177:219-229.